Nagoya University

Graduate School of Engineering

Manipulation of Oocytes by Magnetically Driven Microrobot on a Chip

A dissertation submitted for the degree of Doctor of Philosophy

Department of Micro-Nano Systems Engineering

Lin FENG

Acknowledgements

It is my great pleasure to acknowledge all people who concern this work.

First I would like to express gratitude to Professor Fumihito Arai, Department of Micro-Nano Systems Engineering, Nagoya University, Japan, for his constant support, guidance, encouragement, patience, and giving me a chance to study in Arai lab and learn how to be a good researcher. And also, as a foreign student, studying abroad has a lot of troubles in daily life. Professor Arai shows great loving care even for my daily life.

I would like to extend my sincere to Professor Seiichi Hata in Department of Micro-Nano Systems Engineering, Professor Masahiro Ohka in Department of Complex Systems Science, Associate Professor Hisataka Maruyama in Department of Micro-Nano Systems Engineering, Associate Professor Kousuke Sekiyama in Department of Micro-Nano Systems Engineering for kind agreement with being my doctoral committee members.

I would also like to personally thank to Associate Professor Yoko Yamanishi, Dr. Masaya Hagiwara, Associate Professor Akihiko Ichikawa, Associate Professor Tomohiro Kawahara, Assistant Professor Taisuke Masuda, Assistant Professor Kosuke Nogawa for their constant support not only for the research aspect but also personal as well. And also Ms. Tsukamoto, and Ms. Ohsumi for their kind help for my study abroad in Japan. I would like to extend my thanks to the entire lab members to share the precious time in my doctoral course.

Finally, I would like to express my deepest gratitude to my parents Yinglan Xue and Runtang Feng, my sister Xue Feng and my girlfriend for their encouragement and support.

2014 *Lin Feng*

Manipulation of Oocytes by Magnetically Driven Microrobot on a Chip

Lin Feng

Abstract

This thesis presents on-chip various manipulations of oocyte, in order to improve the controllability of a single cell in the biotechnology, this thesis introduces four different approaches for a single oocyte manipulation. It includes microbeads loading for potential usage of oocytes loading, oocyte enucleation in high-speed with cutting accuracy control, single oocytes dispensing system, and also, finally to increase the cutting accuracy and investigate the oocyte properties, the orientation control by using Magnetically Driven Microtool (MMT) will also be briefly discussed. These methods make the single cell manipulation much easier and faster, allow the single cell analysis doing in an easier way and could reduce the burden of the operator.

First, cultivating the cells on the surface of microbead has been widely used as temporal scaffolds for cell culture engineering, here, we succeeded in demonstration of the delivery of polystyrene beads (100 μm) with the flow velocity of from 0.02 ml/h to 0.04 ml/h and MMT frequency from 1 Hz to 6 Hz to adjust the pitch of each micro-bead. The spacing interval of microbeads could be mainly adjusted by changing of MMT frequency and the flow velocity of output stream. This technique shows the potential usage on on-demand delivery of oocytes. As the oocytes is viscoelasticity, which is different from polymer beads, thus further works should be studied on this topic.

Second, since the delivery of the microbeads and oocytes has been studied, next, a microfluidic chip with an MMT for oocyte enucleation is proposed. A microfluidic system was specially designed for enucleation, and the microrobot actively controls the local flow-speed distribution in the microfluidic chip. The microrobot can adjust fluid resistances in a channel and can open or close the channel to control the flow distribution. Analytical modeling was conducted to control the fluid speed distribution using the microrobot, and the model was experimentally validated. The novelties of the developed microfluidic system are as follows: (1) the cutting speed is improved significantly owing to the local fluid flow control; (2) the cutting volume of the oocyte can be adjusted so that the oocyte undergoes less damage; and (3) the nucleus can be removed properly using the combination of a microrobot and hydrodynamic force. Using this device, a minimally invasive enucleation process has been achieved. The average enucleation time was 2.5 s and the average removal volume ratio was 20%. The proposed new system has the advantages of faster operation speed, higher cutting precision, and potential for repeatable enucleation.

Third, after the enucleation process, enucleated oocytes are dispensed in sequent from the microfluidic chip. A pair of capacitance sensors has been placed in a microfluidic chip to detect the oocyte, and custom-designed a special buffer zone in the microchannel to decelerate the flow velocity and reduce the hydraulic pressure acting on the oocyte. In the buffer zone, a semicircular bay, formed by equally spaced micropillars, is used to stop the oocyte at the dispensing nozzle hole. Finally, the oocyte is ejected by airflow to the culture array. The novel feature of the developed microfluidic system is that the extraordinary improvement in success rate is accompanied by a lack of change in oocyte survival rate (as assessed by a comparison of survival rates before and after the dispensing procedure). By using this device, we achieved a

highly accurate single-oocyte dispensing process with a success rate of 100%. The oocyte survival rate is approximately 70%, regardless of whether or not the oocyte is dispensed. The newly proposed system has the advantages of high operation speed and potential usage for two-dimensional micropatterning. In order to achieve continuous oocyte manipulations, all of these modules could be considerably consisted into one microfluidic chip.

Finally, in the study of the oocytes/embryos, as I discussed before like enucleation, microinjection in order to increase the success ratio of the fertilization and characteristics study of the oocytes, all of these research and clinical applications involve 3-D rotation of mammalian oocytes. The gesture or the orientation of the oocyte is critical for improving the enucleation success rate, and characteristics investigation of the oocyte. Cell rotation in conventional approaches mainly are electrorotation or manual operation by skilled professionals based on trial-and-error, repeating the vacuum aspiration and release. The poor reproducibility and inconsistency entail a simple and convenient approach for single oocyte rotation. This paper reports a 3-D rotational control of bovine oocyte. By using customer designed magnetically driven microtool (MMT), the oocyte orientation control could be achieved. Comparing with the conventional works, rotation control by using MMT shows great advantage in control accuracy and the rotation speed. Orientation with an accuracy of 7 °, and the average rotation velocity of 3 rad/s have been achieved. Rotation by utilizing MMT demonstrated overall out-of-plane and in-plane in a quite simple way. And by utilizing this approach, the cell manipulation for cell study becomes much easier on investigating single cell characteristics and analysis mechanism properties.

Contents

List of Figures

List of Tables

Chapter 1.

Introduction

1.1 Cell Manipulations

1.1.1 General cell manipulations

In the last century, the Industrial Revolution was the transition to the new manufacturing processes, which is a major turning point in history; almost every aspect of daily life was influenced in some way. In particular, average income and population began to exhibit unprecedented sustained growth. In this century, people predicted that a new round of technique

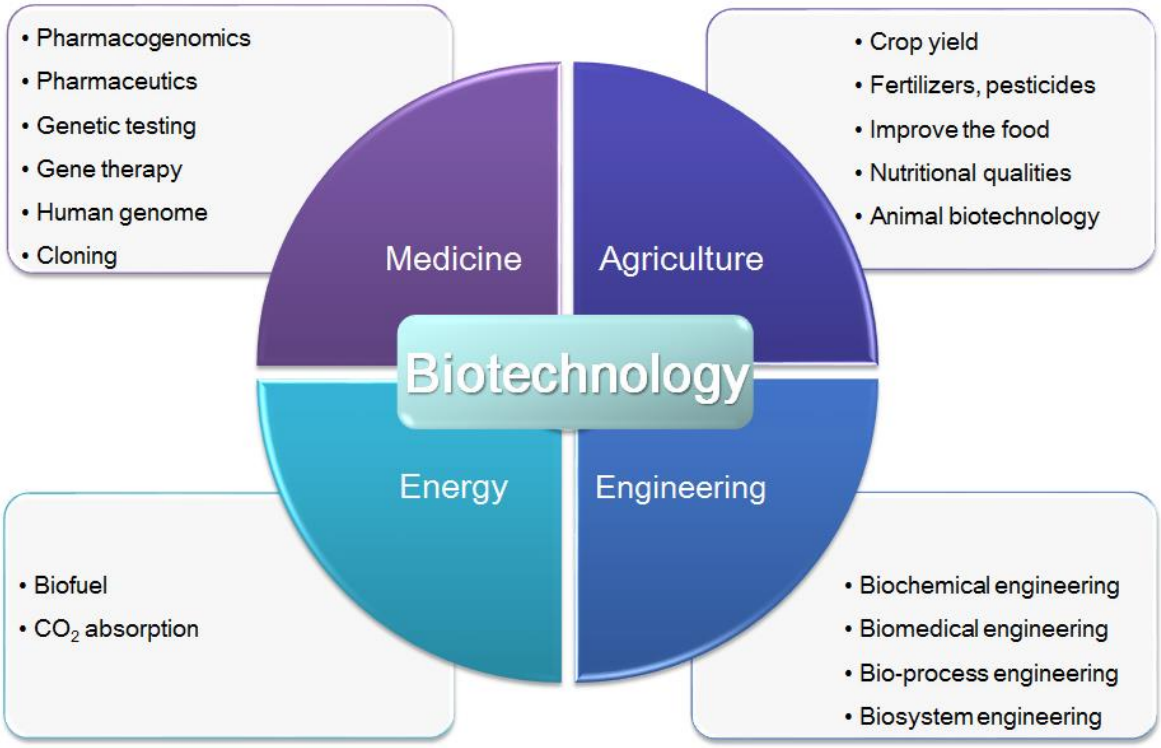

Figure 1.1 Applications of biotechnology in various fields.

revolution would be the biology revolution. Biologically inspired engineering is a new scientific discipline that applies biological principles to develop new engineering solutions for medicine, industry, the environment, and many other fields that have previously not been touched. Figure 1.1 shows the applications of biotechnology in various fields.

In biology, the study of cell attracted the most attentions, since the cell is the basic structural, functional and biological unit of all known living organisms. Cells are the smallest unit of life that is classified as a living thing, and are often called the "building blocks of life". Therefore, understanding the functions of cells in order to investigate and apply it to enrich human life becomes essential. The importance of cell manipulation and cultivation are growing rapidly in recent years for various fields, such as drug discovery, regenerative medicine, investigation of

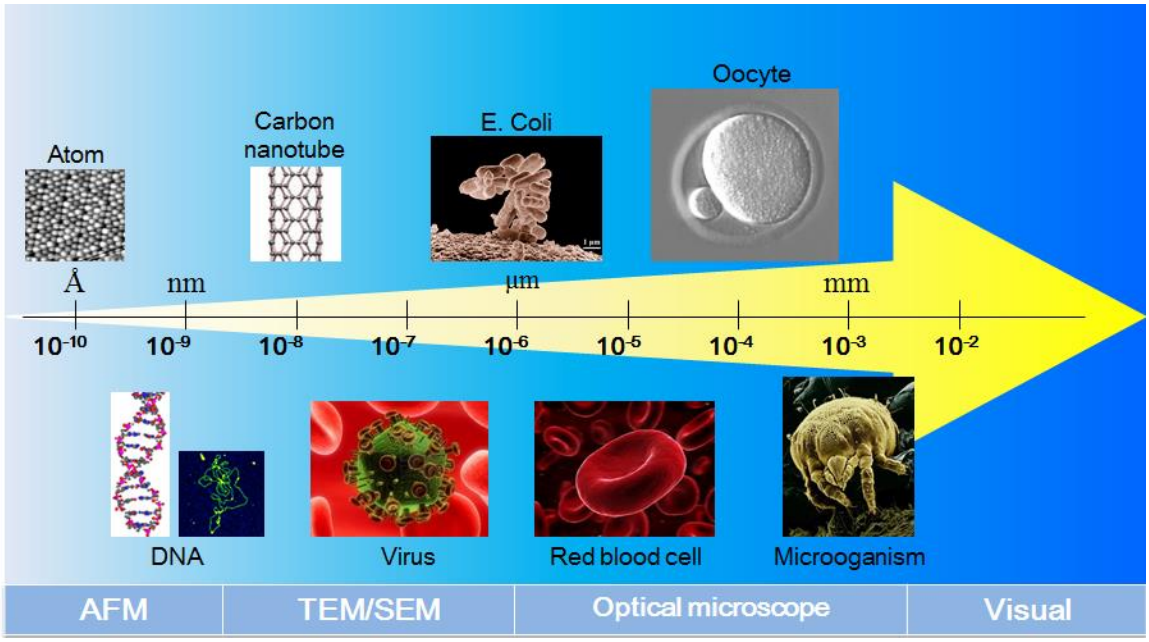

Figure 1.2 Classifications of micro / nano world [1]–[7].

and so on [8]–[12]. Biomanipulations widely used in many applications shows great commercial value, over tens of billions of dollars pumped into this field all whole the world. Therefore, many researches focus on the methodology to manipulate cells precisely, effectively and with high throughput. However, mainly in the cell manipulation world, the dominant factor of the conventional Newton equation is totally different in such a small scale from macro-scale world since the sizes of the cells are micro/nanometer order. In micro/nanometer size world, the volume force such as gravity force and inertia force does not have impact on the actuator, while the friction force, adhesion force, viscous force and any other surface forces, which is not major force in macro scale world, are emerging more. In order to achieve precise cell manipulation, these factors have to be considered carefully. Figure 1.2 shows the size classification of micro/nano-world [1]–[7].

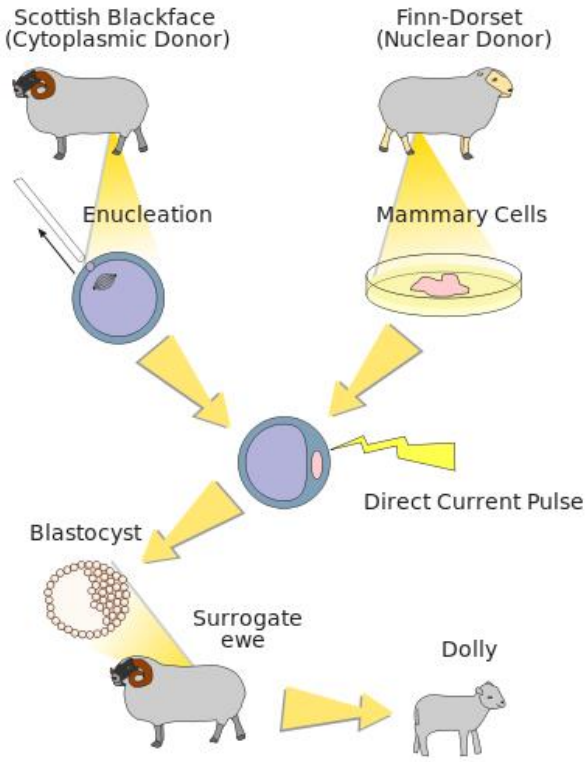

Figure 1.3 Cloning process of the sheep “Dolly” [13].

1.1.2 Cloning technique

Among the applications of biotechnology, the cloning attracted the most attention. Definition of clone in British and World English in Oxford dictionary is biology an organism or cell, or group of organisms or cells, produced asexually from one ancestor or stock, to which they are genetically identical [14]. Currently, some researches have reached the practical level such as a production of monozygotic multiples or clone livestock by splitting of the fertilized oocyte, a sexing of fertilized oocyte, and a microinsemination. Moreover, somatic cell cloning technologies have been focused on since the development of the sheep “Dolly” made an impact on all over the world [13]. Figure 1.3 shows the cloning process of the sheep “Dolly”. These researches have been achieved in production of clone animals such as, sheep [15], cattle [16],

and pig [17]. The technologies have been attracting attention as an efficient breeding of livestock. Additionally, it is possible to produce transgenic livestock effectively by genetic manipulation on somatic cells used as donor cells. However the technique used in the cloning process has only a limited improvement. Therefore, in this thesis, many new approaches proposed to improve the success rate of enucleation process, and complimentary methods like, cell loading, cell dispensing, cell orientation control can make the cloning process easier during the manipulations.

1.2 Manipulation Approaches

1.2.1 Contact manipulation

As mentioned before, in order to achieve the cell manipulation, generally the cell is in micron order, therefore complex procedures under the microscopic manipulation is required in biotechnology. A micromechanical manipulator with 6-freedom control (Figure 1.4) is widely used for medical and life science applications because of its capability of high accuracy, high power output, and flexibility of the manipulation. In particular, for oocyte enucleation process, a glass capillary is attached onto the micromanipulator, which is commonly carried out manually [18]–[21]. The cloning process contains the complex procedures; enucleation, donor cell injection, fusion of the original oocyte and the injected donor cell. Such kind of operation technique has been used almost 20 years with quite limited improvement. Because the manipulators are placed outside of the cell culture environment, letting operation arms inserted into the cell operation environment that leads to the cell contamination issues. In addition, there are many potential disturbances such as unexpected fluid flow due to the open space and it encumbers precise motion. In recent years, researchers achieved cell manipulation in the size

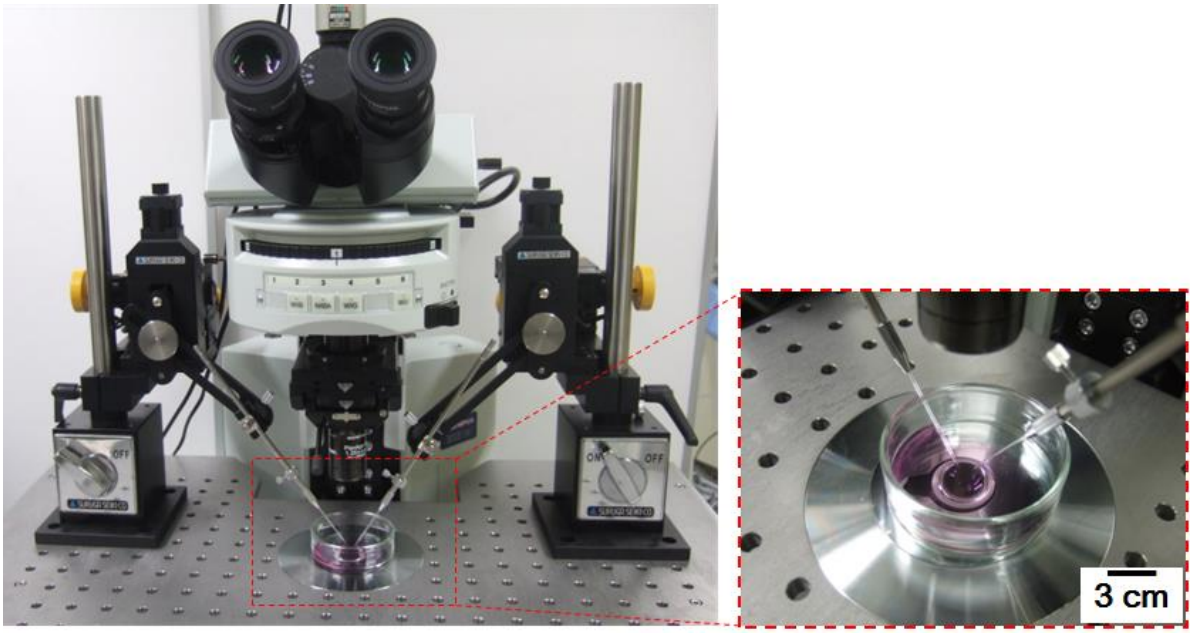

Figure 1.4 Conventional mechanical micromanipulator.

of nanometer order by inserting mechanical manipulator into E-SEM environment [22]–[24]. The approach allows precise and powerful cell manipulation, even it is used in cutting yeast cell. However the operation speed takes time because it effected by the scanning time of ESEM system, and also the viability of cell might be significantly affected by harsh environment. Meanwhile, such kind precise operation only can be taken a high skilled operator because the manipulator has to be controlled in 6 degrees of freedom for micron scale operation. Therefore, the success rate, repeatability and productivity tend to depend on the operator's skill, especially for the skilled job like enucleation of oocyte.

1.2.2 Noncontact manipulator

In order to achieve much more flexible actuation in a closed space, researchers, recently, are interesting in the noncontact manipulation of robot, especially for the biology applications.

Noncontact methods shows great merits on non-contaminations and remote control. Even like doing the surgery, doctor tried to reduce the harm to the human body, and also alleviate the suffering of patients. Like that, to study of the cell or the microorganism, researchers are also want to reduce the side effects on them. Therefore, many optional methods without contact, such as electric force, optical force, acoustic force, and magnetic force have been well studied. The actuation principles and related researches are discussed in the following sections.

1.2.2.1 Electrophoresis and dielectrophoresis

When putting a microparticle or a cell in an electric filed, a force is applied on the particle. The force could be Electrophoresis (EP) or Dielectrophoresis (DEP). EP Electrophoresis is the motion of dispersed particles relative to a fluid under the influence of a spatially uniform electric field [25], [26]. Whereas, DEP is a phenomenon in which a force is exerted on a dielectric particle when it is subjected to a non-uniform electric field [27], [28]. Both forces are produced by the electrodes fabricated in a microfluidic chip for microparticle or cell manipulations. However, the DEP force does not require the particle to be charged. All particles exhibit dielectrophoretic activity in the presence of electric fields. Based on the balance of permittivity between the particle and medium, the direction of the force on the microparticle is determined, and it moves toward high or low field gradient. Therefore, DEP was more widely used for microparticle or cell manipulations. The DEP force amount is depend on the balance of permittivity of the medium surrounding the microparticle (ε_m), the electric field (E_{rms}), the radius of the particle (r). For a homogeneous sphere of radius and complex permittivity in a medium with complex permittivity the (time-averaged) DEP force is [29], [30]:

$$\vec{F}_{DEP} = 2\pi r^3 \varepsilon_m \,\mathrm{Re}\{\frac{\varepsilon_p^* - \varepsilon_m^*}{\varepsilon_p^* + 2\varepsilon_m^*}\} (\nabla \vec{E}_{rms}{}^2) \quad (1.1)$$

The factor in curly brackets is known as the complex Clausius-Mossotti function [29], [31] and contains all the frequency dependence of the DEP force.

Dielectrophoresis has been successfully demonstrated in the separation [28], [32]–[34], transportation [35], trapping[36]–[39], and sorting of various biological particles[40]–[45]. Pohl describes the use of wire electrodes, applied with 11 kV voltages, to separate various types of particles in mixtures [32]. The castellated geometry shown in Figure 1.5 (a) was chosen because it provides a large value for attenuation of the electric field using modest values of applied voltage [45]. The characteristic dimension ranges from 10 to 120 μm defining the planar geometry typically, selected to be 5–10 times the diameter of the particles to be manipulated by DEP. As depicted in Fig. 1.5(b), this electrode geometry can be used to simultaneously observe both positive and negative DEP of cells across an array of microelectrodes [46].

Morgan et al. also succeeded in separating submicron particles by arraying the electrode on the microchannel and making use of the permittivity differences between cells [33] shown in Figure 1.5. Asbury et al. achieved to trap DNA molecules at the edges of the electrodes [47]. They also succeeded in moving the trapped DNA from one edge to another by mixing static and oscillating electric fields. Durr et al. comprehensively analyzed DEP force and experimentally measured DEP force, which was 50 fN to 1 pN [48]. Currently, most efforts are directed towards biomedical applications, such as selective separation/enrichment of target cells or bacteria, the spatial manipulation, high-throughput molecular screening, biosensors, immunoassays, and the three-dimensional cell constructs. DEP doesn't need to label the cells or the particles, and without contact to any surfaces. This opens up potentially important applications of DEP

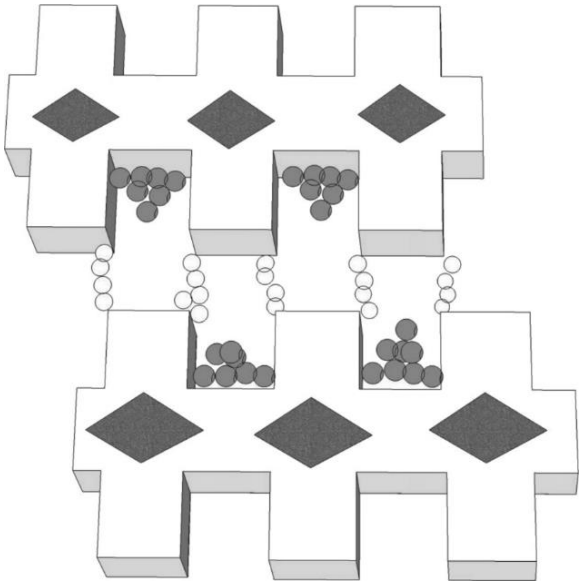

(a)

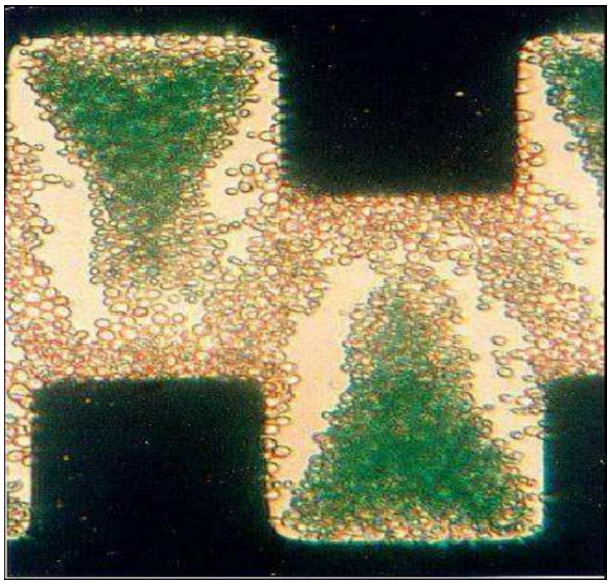

(b)

Figure 1.5 Particles collection by using DEP. (a) The castelled electrode design for observing both positive and negative DEP collection of particles. Particles collecting in the diamond-shaped areas on the electrodes are driven there by hydrodynamic fluid flow [46]. (b) Viable yeast cells collecting by positive DEP into pearl chains, and (stained) nonviable cells collecting by negative DEP into triangular aggregations levitated above the electrode plane [49].

as a tool to address an unmet need in stem cell research and therapy.

As the discussion above, DEP force can be suitable power source to migrate or accumulate selective cells on the particular place but it is controllable only in the limited region adjacent to the electrodes, and thus it is difficult to apply any other cell manipulation such as cutting and mechanical stimulations.

1.2.2.2 Optical tweezers

Optical tweezers (originally called "single-beam gradient force trap") are instruments that use a highly focused laser beam to provide an attractive or repulsive force (typically on the order of piconewtons), depending on the refractive index mismatch to physically hold and move microscopic dielectric objects. A dielectric particle near the focus will experience a force due to the transfer of momentum from the scattering of incident photons. Arthur Ashkin first developed the field of laser-based optical trapping, “optical tweezers” [50], [51]. Ashkin et al. employed optical tweezers in a wide range of experiments to manipulate live bacteria or virus [51], and trapping of neutral atom [52].

Many works have been conducted in optical trapping technique. Glückstad et al. developed computer generated hologram (CGH) approach, by using a direct imaging operation between the spatial light modulator and the intensity profile in the tweezers plane [53]. Glückstad et al. also developed generalized phase-contrast (GPC) method to the implementation of a multi-beam optical tweezers system [54]. They achieved to generate four optical tweezers from a fixed phase mask in conjunction with a GPC system to trap and hold micron size polystyrene beads in solution. Arai et al. developed a Time-shared scanning (TSS) synchronized laser micromanipulation, which allowed manipulating multiple targets independently using the

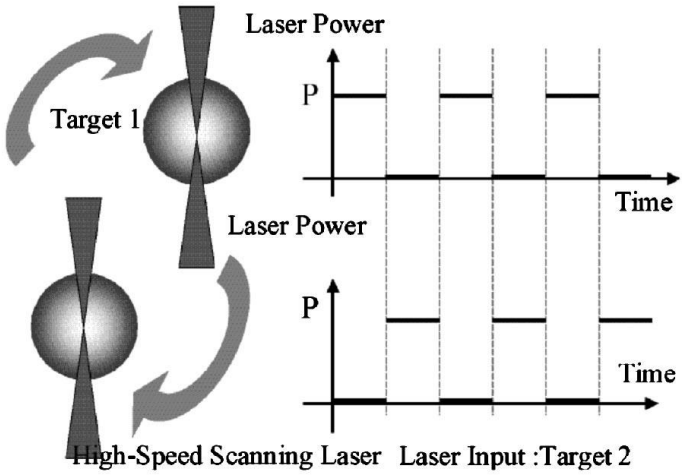

Figure 1.6 Principle of Time-shared Scanning: TSS [55].

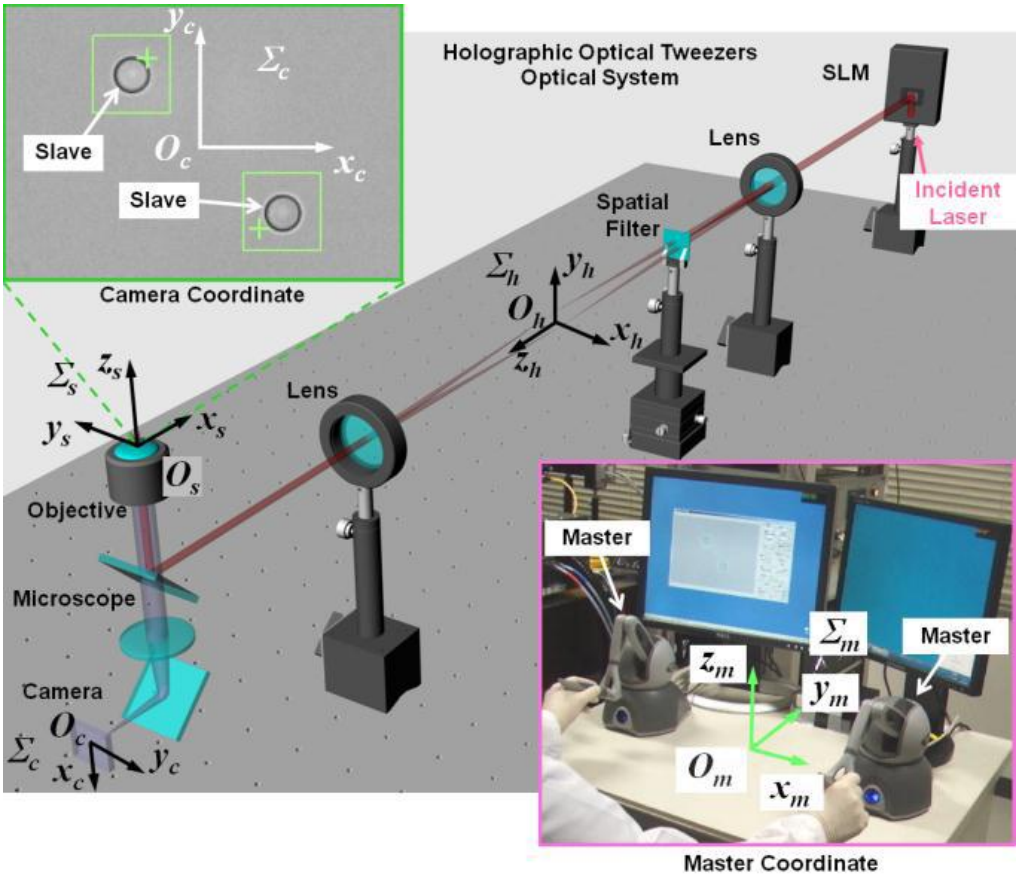

Figure 1.7 Schematic diagram of the teleoperation system using holographic optical tweezers [56].

single laser by changing discrete laser scanning pattern (Figure 1.6) [55]. Lately, Onda et al, has demonstrated a multi-beam bilateral teleoperation of holographic optical tweezers accelerated by a GPU. By using this system, multi-trapping and multi-force-sensing have been achieved, it is possible to squeeze or strain micro-scale objects dexterously with measuring forces at multiple points [56] (Figure 1.7).

The ability of applying pico-neweton order forces to micrometer objects with nanometer precision is widely applied to the researches. For instance, single molecular applications [57]–[60], single cell analysis [61]–[64] and virus separation [65]. Wener et al. succeeded in immobilization of more than 200 yeast cells into a high-density array of optical traps and the cell array could be moved to specific locations in a controlled manner to expose the cells to reagents and to analyze the responses of individual cells. Maruyama et al. developed the device to separate ϕ 100 nm virus by employing optical tweezers and DEP and achieved to infect a specific cell with an influenza virus in order to analyze the mechanism of the infection.

As shown above, the optical tweezers are now one of the most successful tools to manipulate single cell and it has ability to manipulate cells of nm to μm size with nm order resolution. However, the weakness of the optical tweezers is its small amount of output force and thus the application is limited to trapping or migration of small size of cells.

1.2.2.3 Optically-induced dielectrophoresis

Chiou et al. [66] reported a novel manipulation tool in 2005, they called this technique optoelectronic tweezers (OET) (Figure 1.8), and which combines the both of the merits of optical tweezers and dielectrophoresis (DEP) as introduced in the previous chapters. OET just using ~100,000 times less optical power than laser-based optical tweezers. The reducing of

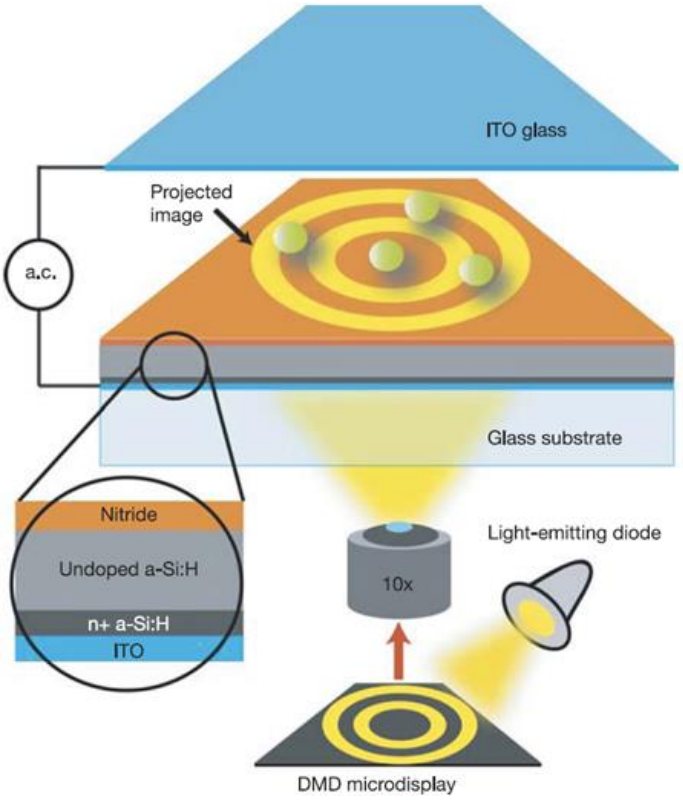

Figure 1.8 Device structure used in optoelectronic tweezers.

optical power requirement which is a great advantage in terms of avoiding damage to live cells during the manipulations. OET devices are based on optically-induced DEP force (ODEP), which is induced by illuminated optical images onto an hydrogenated amorphous silicon (a-Si:H) surface, for instance, the a-Si:H is used as the photoconductive material surface of substrate. This technique enable massively parallel manipulation, concentration, transportation, and separation of micro/nano entities by the virtual electrodes induced by the incident light with any desired geometric pattern. Wen J. Li et al. investigate the importance factors that affect the magnitude of the DEP force generated in an ODEP chip [67]. The effects of AC potential waveforms across the liquid medium, and another factor is optical spectrum of the projected image on the a-SI:H layer on an ODEP chip.

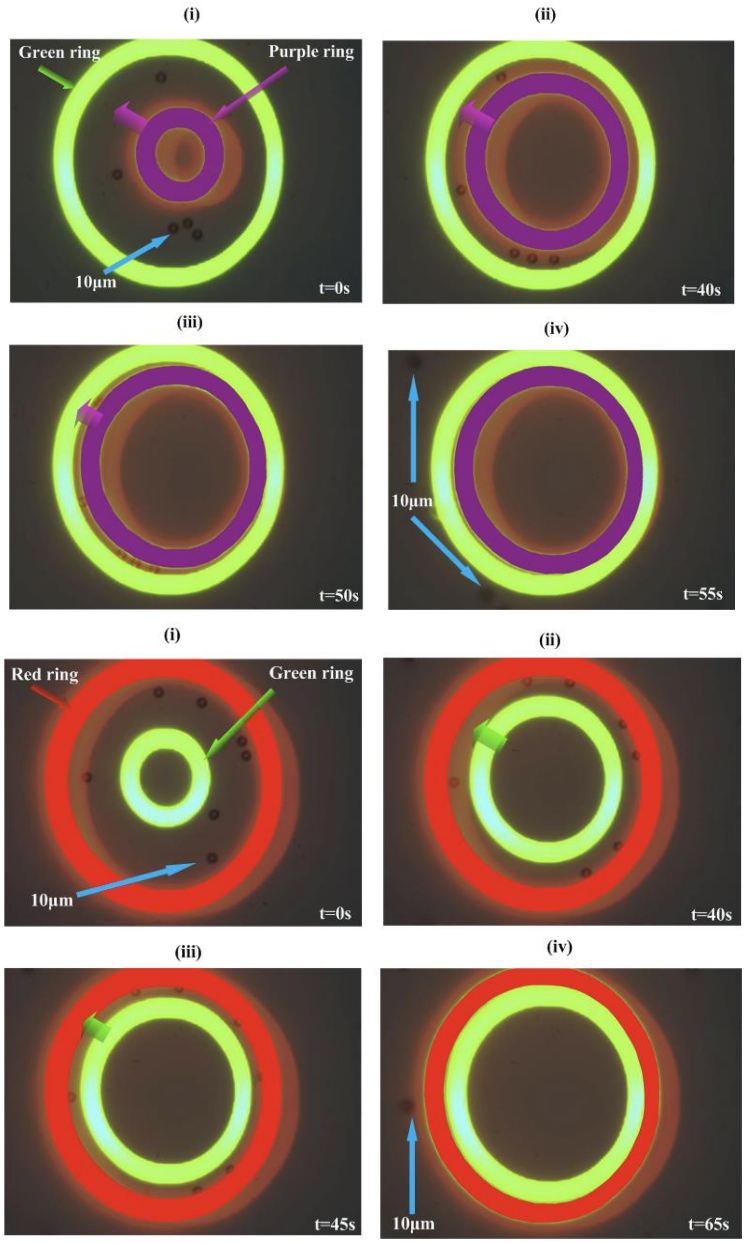

Figure 1.9 Experimental results which confirm the theoretical prediction that higher ODEP force in an ODEP chip

As shown above, the ODEP can achieve both in the mass manipulation and a single cell manipulation. However, the weakness of the ODEP still is its small amount of output force and thus the application is limited to trapping or migration of small size of cells.

1.2.2.4 Acoustic radiation force

Acoustic radiation force is a physical phenomenon resulting from the interaction of an acoustic wave with an obstacle placed along its path. Generally, the force exerted on the obstacle is evaluated by integrating the acoustic radiation pressure (due to the presence of the sonic wave) over its time-varying surface. The acoustic radiation force has been derived by Yeo et al. as follows;

$$F_{AR,L} = 2\pi\rho\left(\frac{2\pi f}{c_f}\right)R^6\left|\xi\right|^2 \frac{1+\frac{2}{9}\left(1-\frac{\rho}{\rho_p}\right)^2}{\left(2+\frac{\rho}{\rho_p}\right)^2} \tag{1.3}$$

where ξ is the fluid particle velocity, ρ is the fluid density, ρ_p is the particle density, f is the frequency of the incident sound field and c_f is the sound speed in the fluid medium.

Recently surface acoustic waves (SAW), generated by interdigital transducers (IDT) on a piezoelectric substrate, has been employed to focus [68], separate [69], [70], align [71]–[74], direct micro particles [71], [75], [76] and to manipulate the fluid droplets [70], [76], [77](Figure 1.10). Shi et al. developed a microfluidic particle focusing device using standing surface acoustic wave (SSAW) [69]. They also demonstrated to manipulate multiple particles both in 1-D and in 2-D by designing pairs of IDT in different direction (Figure 1.11) [78]. Cecchi et al. developed PDMS and $LiNBO_3$ devices for droplet control in microfluidic chip by SAW [79]. They succeeded in transporting the droplet though a microchannels (Figure 1.12).

The advantage of the SAW is that it can manipulate multiple particles at one time, and it can conduct multi-DOF manipulation by combining multiple IDT electrodes. On the other hand, it is difficult to manipulate single particle or cell from the mixture and achieve precise positioning control due to reflection and interference of the acoustic wave. It will be stronger

device if it is combined with any other noncontact actuation such as optical tweezers and magnetic force.

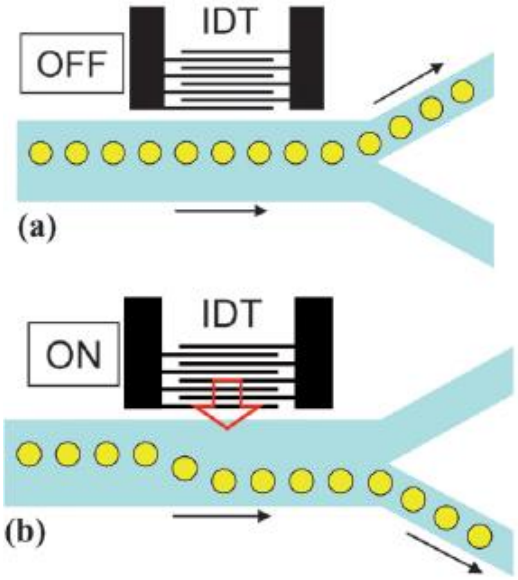

Figure 1.10 Particle sorting by SAW [68].

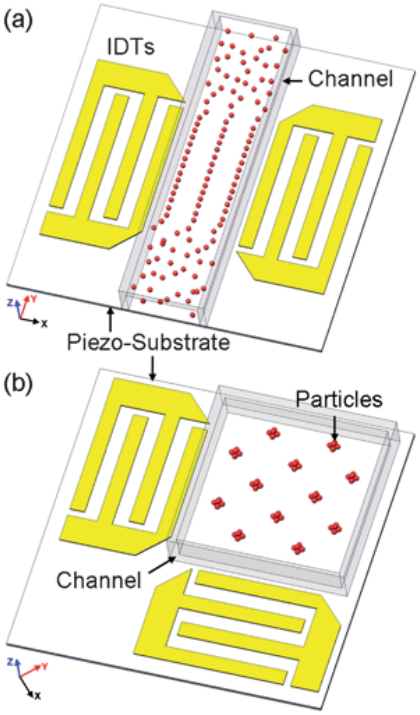

Figure 1.11 Schematic of the SSAW-based patterning devices [69].

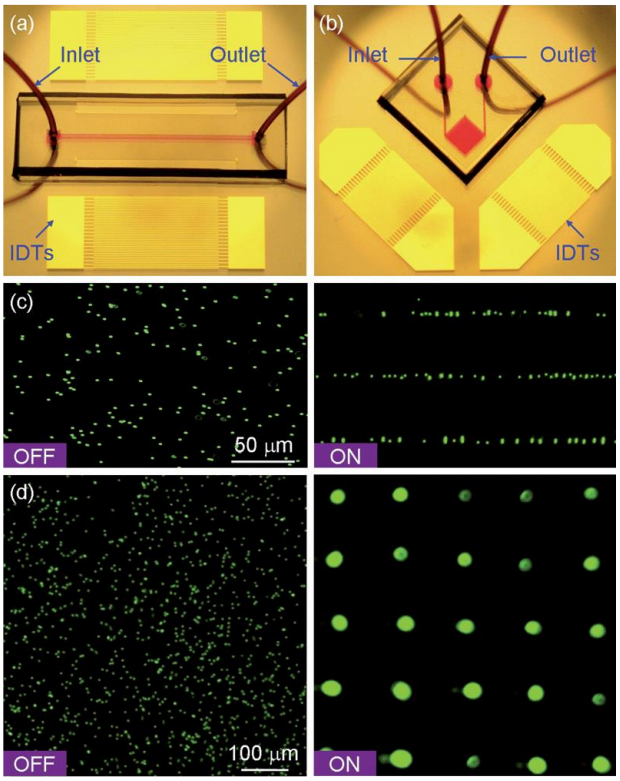

Figure 1.12 Cell alignment by SSAW [78].

1.2.2.5 Magnetic force

One of the most promising actuation methods at the microscale is magnetic force which is generated by permanent magnet or electromagnetic coils. The magnetic force can be calculated as follows;

$$F_{mag} = \mu_0 v(M \cdot \nabla)H \tag{1.4}$$

where μ_0 is magnetic permeability in vacuum, v is volume of magnetic body, M is magnetization of the material, H is magnetic field intensity, ∇ is gradient operator, which is expressed as

$$\nabla = \left[\frac{\partial}{\partial x} \quad \frac{\partial}{\partial y} \quad \frac{\partial}{\partial z}\right]^T \tag{1.5}$$

Cugat et al. comprehensively analyzed effect of magnetic force on the magnetic body in

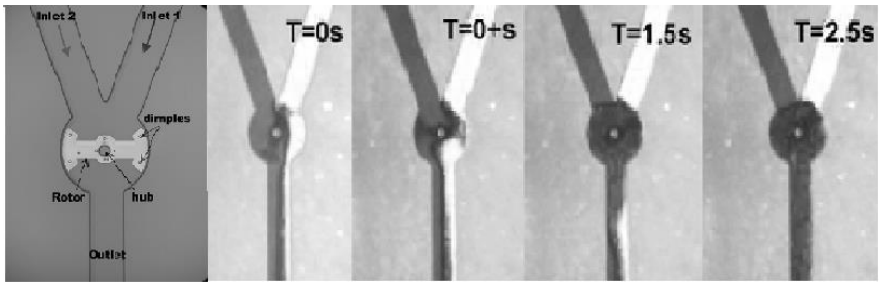

Figure 1.13 Sequential shots of the mixing operation of a micro stir-bar in a Parylene micromachined channel (stir-bar rotating at 150 rpm) at different time lapses [80].

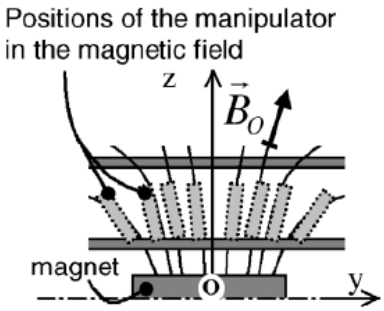

Figure 1.14 Manipulator control of permanent magnet actuation [82].

size and distance from the magnet and proved that magnetic force was strong power source for microactuator [81]. Barbic et al. actuated magnetic object in a microfluidic chip by magnetic fields generated by three electromagnetic coils set on the XYZ linear stages and they achieved to 3-DOF actuation, *x*-*y*-θ [80]. Rotation of magnetic material inside a microchannel was achieved by a rotating external magnet with a conventional stirrer plate [80] (Figure 1.13). Mensing et al. fabricated a magnetic driven microstrirrer [82]. Gauthier et al. analyzed the magnetic fields on the permanent magnet and controlled magnetic object position and its posture. They achieved strong output force from permanent magnet and precise positioning accuracy, but it was only available on the large magnet, thus, it could not operate multiple microrobot at a time and the application was limited since the posture was changing by

changing positions [83] (Figure 1.14).

Helmholtz coil, which is composed of pairs of electromagnetic coils with concentric circle, is widely used for the cell manipulation in recent years. It can generate uniform magnetic fields in multiple axes by combining two or three Helmholtz coils and it enables multi-DOF actuation of on-chip robot [84]. Kummer et al. investigates fundamental design, modeling, and control issues related to untethered biomedical microrobots guided inside the human body through external magnetic fields [85]. Nelson et al. was researching on magnetic actuators operated by pairs of Helmholtz coils [86], [87]. They fabricated spiral shape microrobot using MEMS technology and the microrobot could swim in liquid environment with 6-DOF precise actuation (Figure 1.15). The final goal of this research is a microrobot consisting of a polymer binded aggregate of ferromagnetic particles is controlled using a Magnetic Resonance Imaging (MRI) device in order to achieve targeted therapy [87]. Sitti et al. also applied pairs of Helmholtz coils for microrobot actuation [88], [89]. They actively employed stick-slip effects on the sliding magnetic object by switching the magnetic fields of vertical direction and horizontal direction (Figure 1.16). They recently achieved to assemble microobjects by manipulating hexahedron posture. Kumar et al. also employed Helmholtz coils to obtain precise control of microtransporter [90], [91]. By integrated the magnetic actuation with vision feedback control, the delivery of microgel to neuron has been achieved.

As described above, Helmholtz coils is a great tool to achieve precise accuracy of actuation in multi-DOF. However, it requires to modify the structure of the microscope. And also, the limitation of this method is Helmholtz coil only can generate micronewtons order force from electromagnetic coils. This is not suitable on operating bigger size of cell, like oocyte, and more than tens of micron size microrobot.

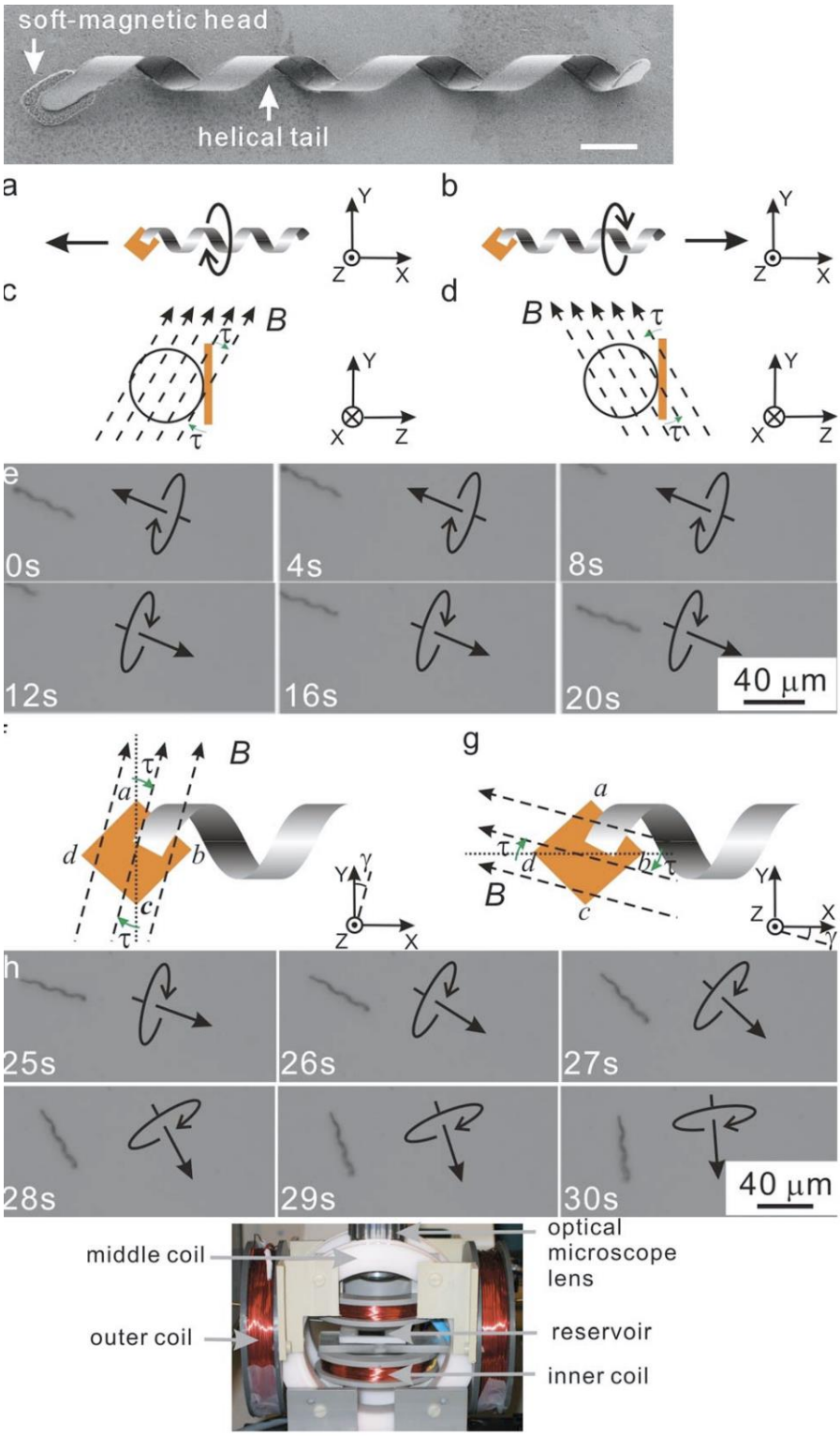

Figure 1.15 Artificial bacterial flagella: Fabrication and magnetic control [87].

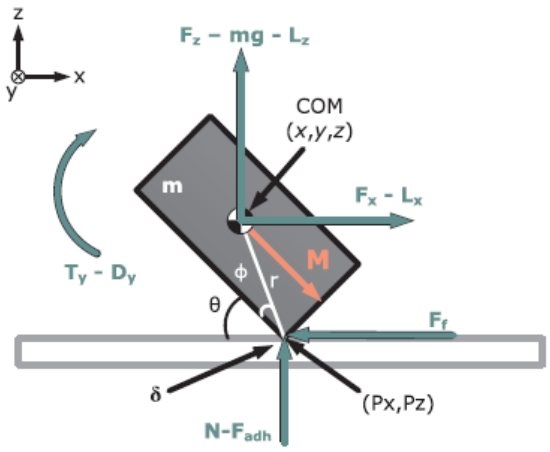

Figure 1.16 Stick-slip motion model actuated by Helmholtz coils [88].

1.2.3 Microfluidics

Microfluidics is mainly started from 1980s and widely used in the development of DNA chips, inkjet print heads, micro-propulsion, and micro-thermal technologies, especially lab-on-a-chip technology. Microfluidics is a multidisciplinary field intersecting engineering, physics, chemistry, nanotechnology and biotechnology, with practical applications to the design of systems in which small volumes of fluids will be handled. Meanwhile, it deals with the behavior, precise control and manipulation of fluids that are geometrically constrained to a small, typically sub-millimeter. Typically, the merits of microfluidics' features: 1) small volumes (microliter, nanoliter, picoliter, femtoliter), 2) small size, 3) low energy consumption, and 4) effects of the micro domain. Figure 1.17 shows multi-functional chip made by polydimethylsiloxane (PDMS). By integrating various functions to imitate laboratory environment in a small size of the chip. Currently, being well studied, the microfluidics could achieve high throughput screening, separation, detection and reaction in a confined microfluidic chip with the ability to use very small quantities of samples and reagents, and to carry out

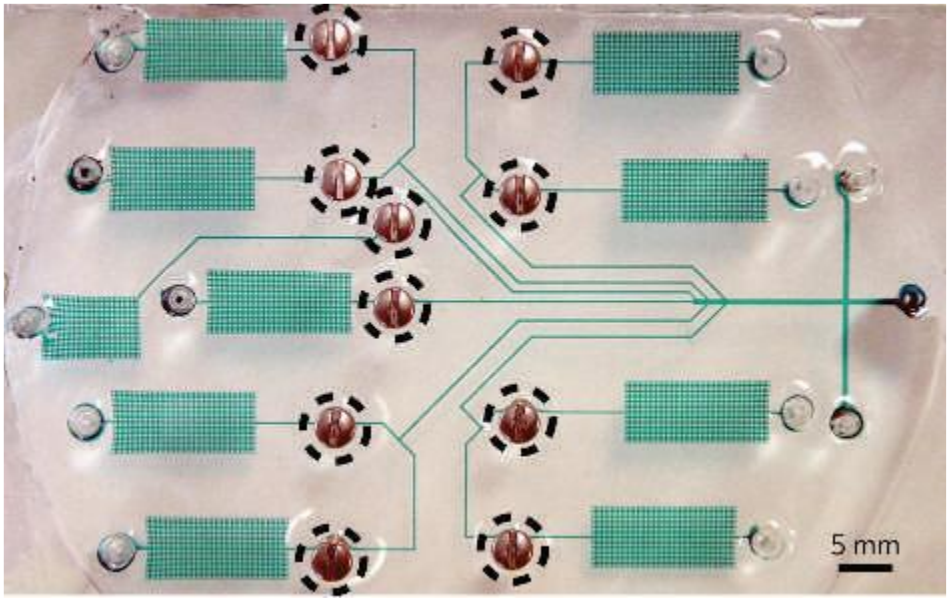

Figure 1.17 Microfluidic diagnostic device [92].

separations and detections with high resolution and sensitivity; low cost, short times for analysis; and small footprints for the analytical devices [92] (Figure 1.17). The applications of microfluidic chip are mainly separation [93]–[99], mixing [100]–[104], droplet generation [105]–[110], cultivation [111], [112] and so on.

Recently, researchers are interested in separate the target cells from the various cells, like Circulating Tumor Cells (CTC) from the human blood. Basing on the size difference of the cells, Stott et al. developed separation microfluidic chip for circulating tumor cells from blood by inertial microfluidics [113] (Figure 1.18). They focused attention on the fact that the tumor cell is relatively large in blood cells and designed microfluidic chip for tumor cell to get centered and for the other blood cell to flow along the PDMS wall.

The emulsification of liquids is an emerging technology [114], such as encapsulation of DNA [115], drug-delivery system for nanoparticles [116], and single-molecular enzyme analysis [117]. Since emulsification has become a crucial industrial technique, the quality of

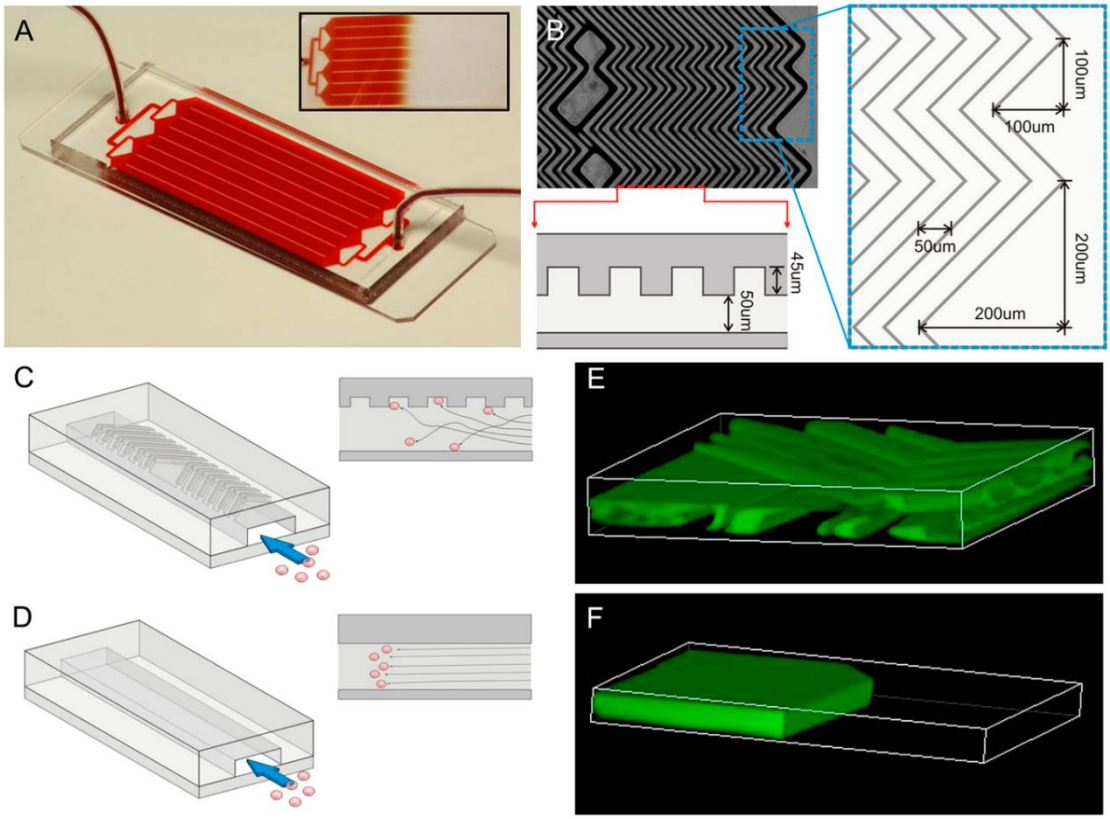

Figure 1.18 High throughput separation for circulating tumor cell from blood [113].

the emulsion droplets is significant, especially in biotechnology and nanomedicine applications [118]. In the last decade, droplets have been extensively used by various industries for plastic polymerization, drug development, and chemical processing. Recently, droplets have been enabled for microfluidic technologies to be used as liquid-reaction vessels for protein crystallization screening [119], as templates for providing self-assembly of materials [120], [121] as molds for forming polymeric microspheres [122], [123] and as components for microelectrical actuation [124]. Many researchers have already studied the highly efficient droplet generation, Yamanishi et al. successfully produced size-controlled emulsion droplets on a chip by adjusting the vibration frequency for Magnetically driven microtool [125] (Figure 1.19).

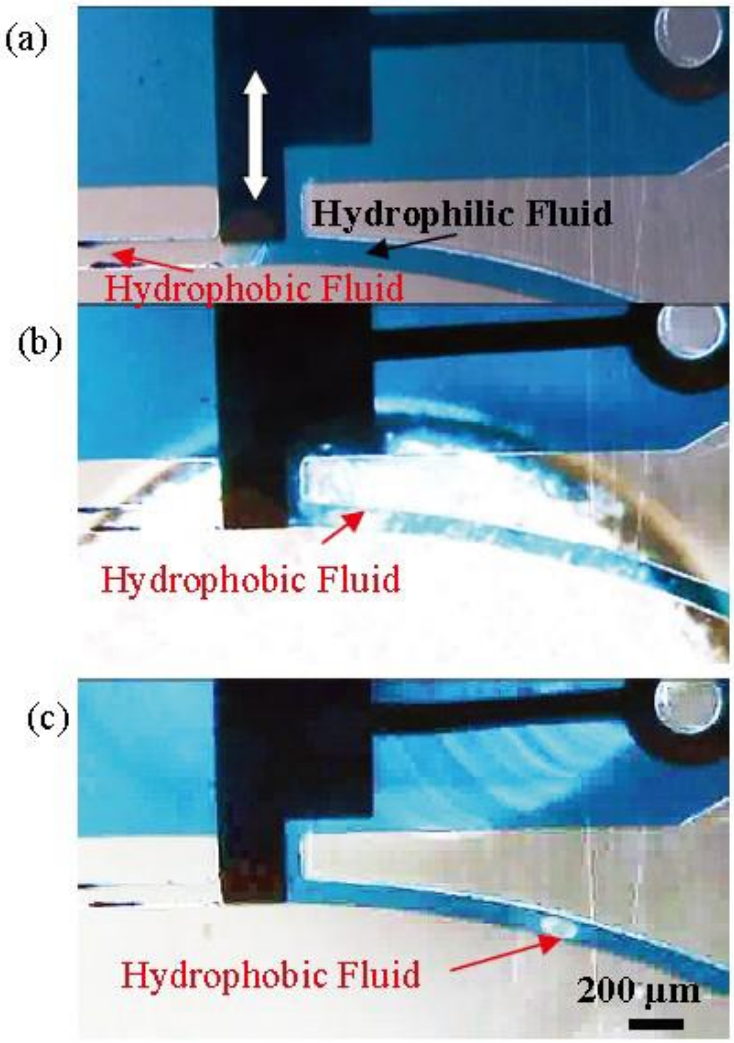

Figure 1.19 On-demand droplet generation [125].

1.3 Magnetically Driven Microtool (MMT)

Arai et al. continuously developed magnetically driven microtool (MMT) to manipulate biological cell in a microfluidic chip. Since a permanent magnet has a more than 10-100 times stronger magnetic field to drive a magnetic object than an electromagnetic coil of the same size. The novelty of the MMT is that powerful actuation by permanent magnet can be achieved and the shape and the materials are multiple choices for different applications. Figure 1.20 shows

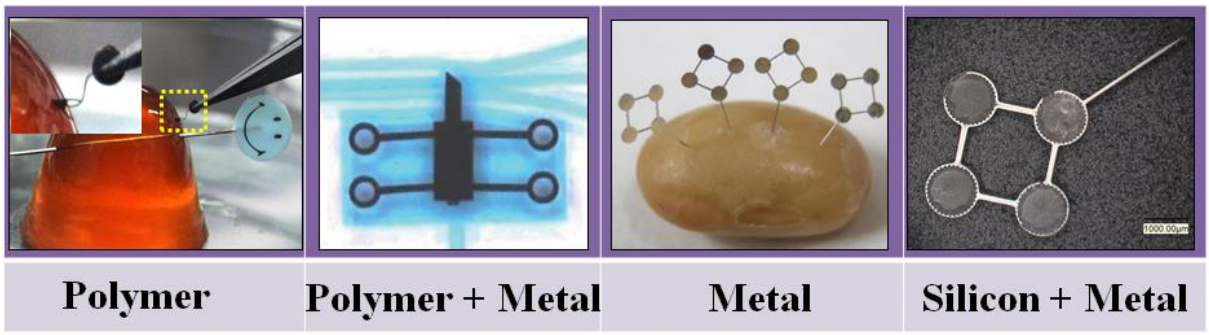

Figure 1.20 Classification of MMT based on material.

the classification of the MMT based on the composed material. Polymer MMT is fabricated by mixture of the polydimethylsiloxane (PDMS) and magnetite particles. This type of MMT can manipulate biological cells without damage since PDMS is soft and biocompatible material. Thereafter, a hybrid type, polymer inserted with a metal stick to increase the magnetic force has been developed. Then, Metal based MMT, which is fabricated by electroplating after photolithography, is hard material and it can receive strong magnetic force because of its ferromagnetism. Therefore, it can apply force required job, like cutting of oocyte. Finally hybrid of metal and silicon structure has both advantages of high force and well structure due to the silicon is hard to be deformed. And this thesis will finally discuss a new hybrid type of MMT, using permanent magnets and silicon. The force once again increased significantly. MMT can be used for various applications to relatively large cell / particle, whose size is 100 μm or more, manipulations such as particle sorter [126], loader [127], filtering [128], [129], droplet generation [130]–[133], and single cell manipulation[134].

1.4 Thesis Overview

1.4.1 Research aim and target

In order to understand the operating range of various manipulation approaches, Figure 1.21 shows comparison of various manipulation approaches according to the output force and general manipulation target, Although there are many novel noncontact actuators discussed above, however for the single oocyte manipulations, the output of the most of the noncontact actuators is less than μN orders, which has limitation on single oocyte manipulations. Especially, during the enucleation process, the oocyte must be cut and got the nucleus removed. Conventional techniques for the enucleation process mainly include the following: manual manipulator operation, microfluidic cutting methods in a microchip, and chemical treatment methods. However, as mentioned in the previous sections, these methods tend to have a long operation time, low success rate, contamination, and low repeatability. Therefore, the research aim is to integrate magnetically driven microtool to a microfluidic chip for a single cell manipulation. By custom-designed microfluidic chip, the single microbeads delivery, oocyte enucleation in high speed, single oocyte dispensing, retrieving and 3-D rotation are finally achieved.

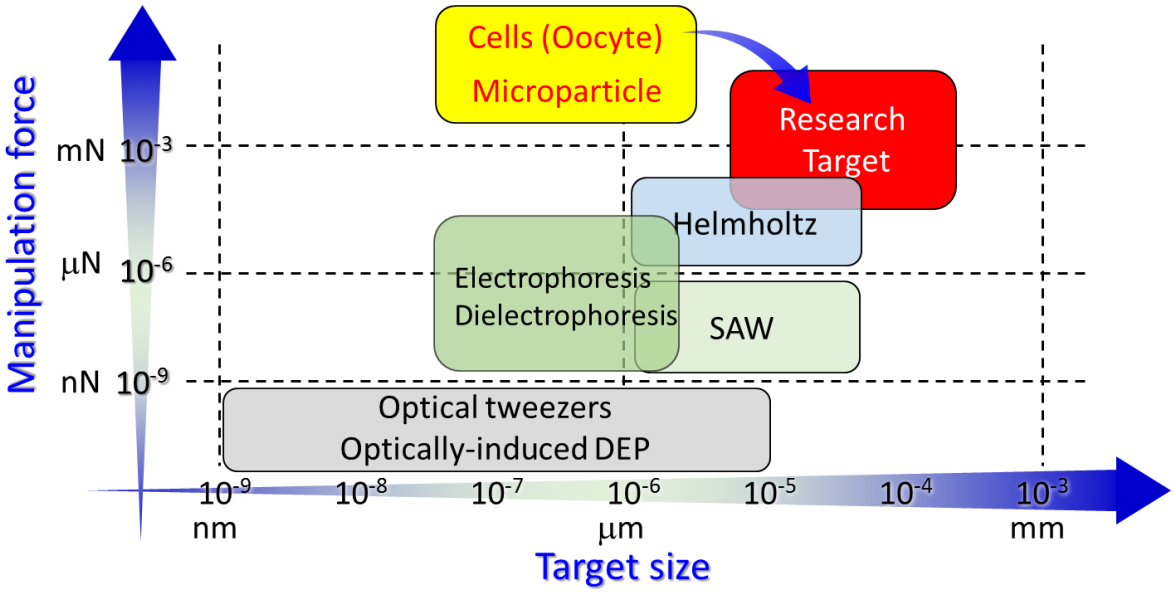

Figure 1.21 Comparison of various manipulation approaches and the target of our research.

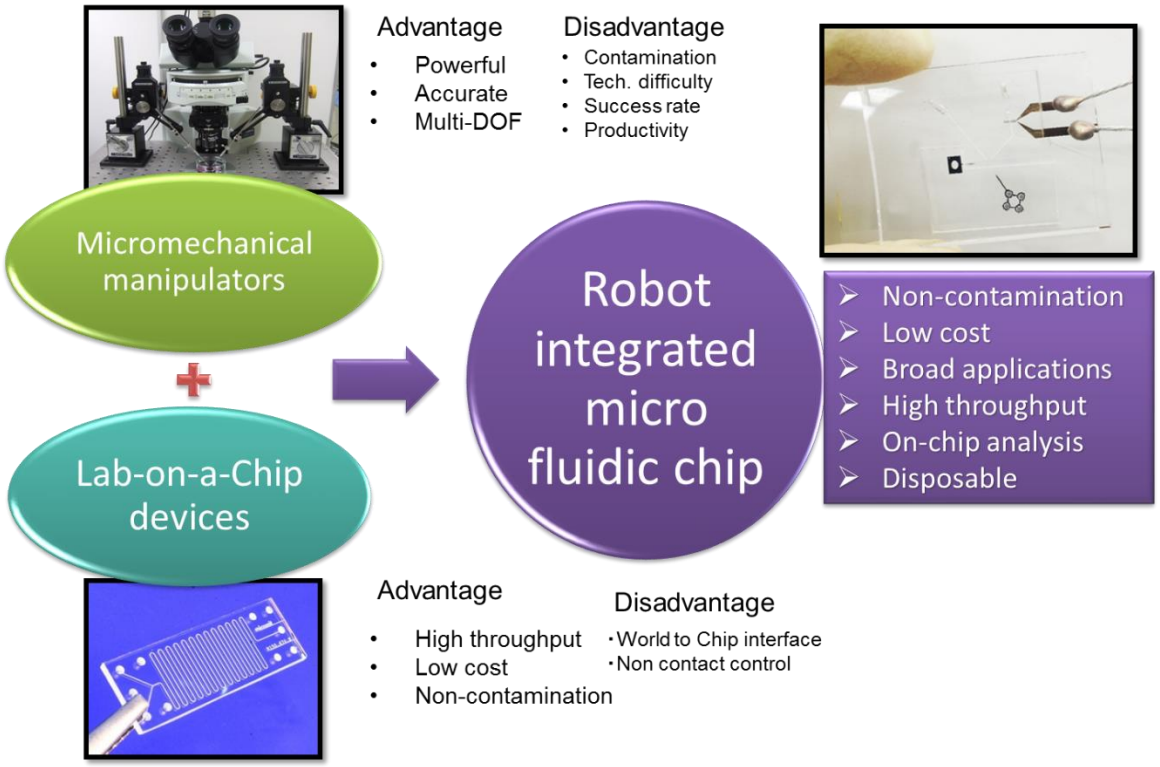

Figure 1.22 Concept of on-chip robot.

1.4.2 Robot on a chip

Cell manipulations in the closed space, a microfluidic chip, have great advantages in the field of biotechnology because of the low contamination capability, repeatability, and high throughput ability [135]–[137]. Figure 1.22 shows the concept of on-chip robot, which is taking advantages of both of manipulator and Lab-on-a-Chip devices. Under well studied of robot chip, on-chip robot have potential to achieve powerful and accurate actuation, and both mechanical approach and environmental approach for broad range of cell manipulations with high throughput can be achieved. In additions, the cost of on-chip robot is generally low thus it is disposable after the operation is conducted to prevent cell contaminations. Furthermore, closed environment of microfluidic chip also help to prevent cell contamination providing a stable environment for cell. Therefore, we are targeting in the improvement of the on-chip robotics techniques to achieve high efficiency, high speed, and high accuracy cell manipulations.

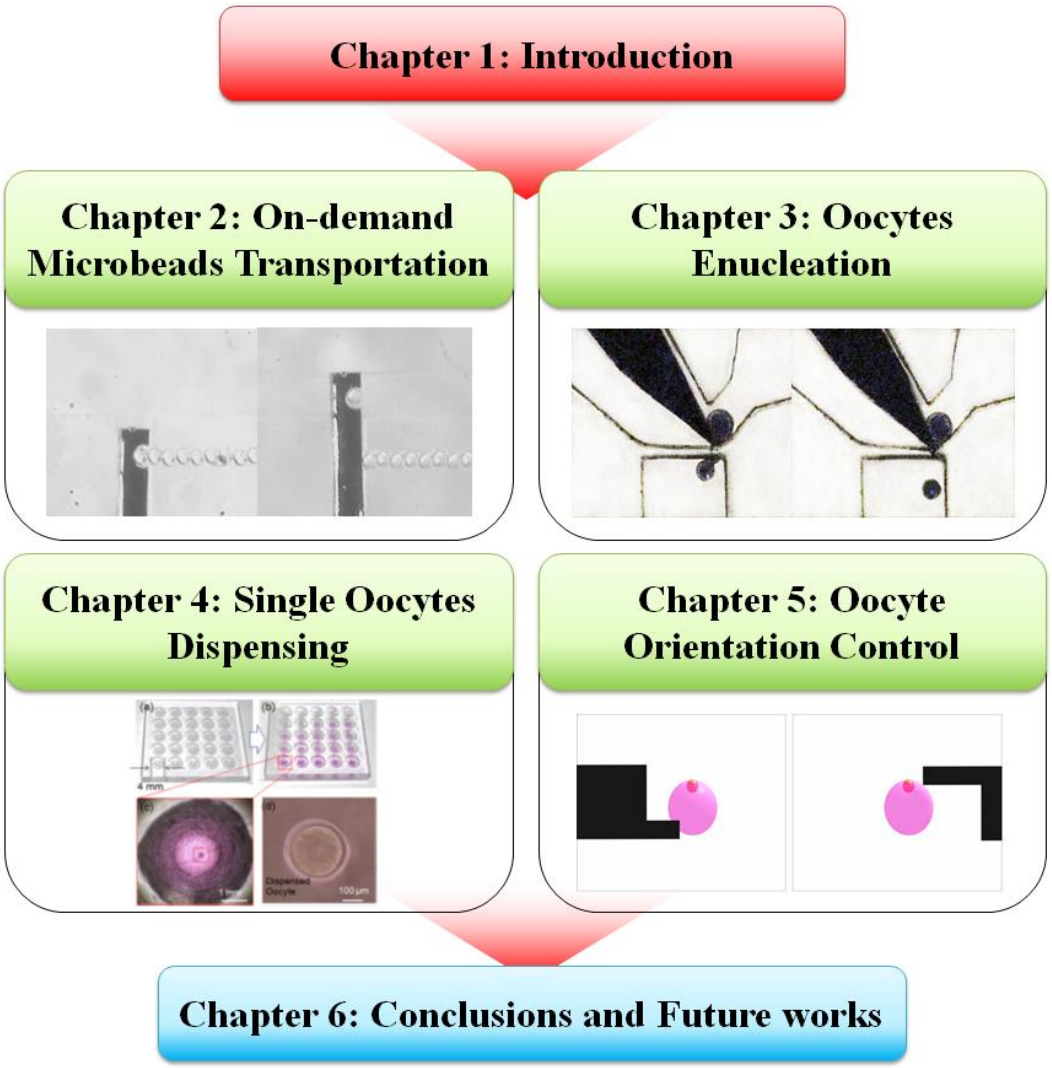

Figure 1.23 Outline of the dissertation.

1.4.2 Outline of dissertation

This dissertation consists of six chapters and proposes new methodologies for various single oocyte manipulations. The schematic diagram is shown in Figure 1.23. The novel methods are proposed from four different aspects, which are, 1. Microbeads delivery (Chapter 2), 2. Oocyte enucleation (Chapter 3), 3. Single oocytes dispensing (Chapter 4), and 4. Discuss the 3-D orientation control of a single oocyte (Chapter 5).

Chapter 2: On-demand microbeads delivery system will be proposed. In a microfluidic chip by using magnetically driven microtool (MMT), the spacing interval of microbeads could be mainly adjusted by changing of MMT frequency and the flow velocity of output stream. And approach shows the potential usage for single oocyte delivery, in order to supply oocytes one by one into the enucleation area.

Chapter 3: A new enucleation method will be proposed. A microfluidic system was specially designed for enucleation, and the microrobot actively controls the local flow-speed distribution in the microfluidic chip. And this microfluidic chip with a magnetically driven microrobot can achieve oocyte enucleation both in high speed and high accuracy.

Chapter 4: A new approach to increase the success rate of single oocyte dispensing and investigate the subsequent viability of the dispensed oocytes will be proposed. The integration of enucleation and dispensing system also will be discussed in this chapter.

Chapter 5: Orientation control of oocyte is critical issue, like stiffness of oocyte is unequable, and nucleus position is critical in the enucleation process. Therefore, by using MMT both in contact and non-contact ways for oocyte rotation will be discussed.

Chapter 6: Summary of the dissertation and future work will be discussed.

Chapter 2.

On-Demand Microbeads Transportation

2.1 Introduction

The recent advances in lab-on-chip systems have shown a great potential in biomedical applications. Microfluidic-based technology offers a convenient platform for cellular analyses of biological systems, as the small scale of micro-channels and devices allows producing scalable system architecture. Their inexpensive composition makes them a potential candidate for large scale production. Microfluidic technology covers not only the material phenomena but also the technology for manipulating and controlling the components as micro size particles in

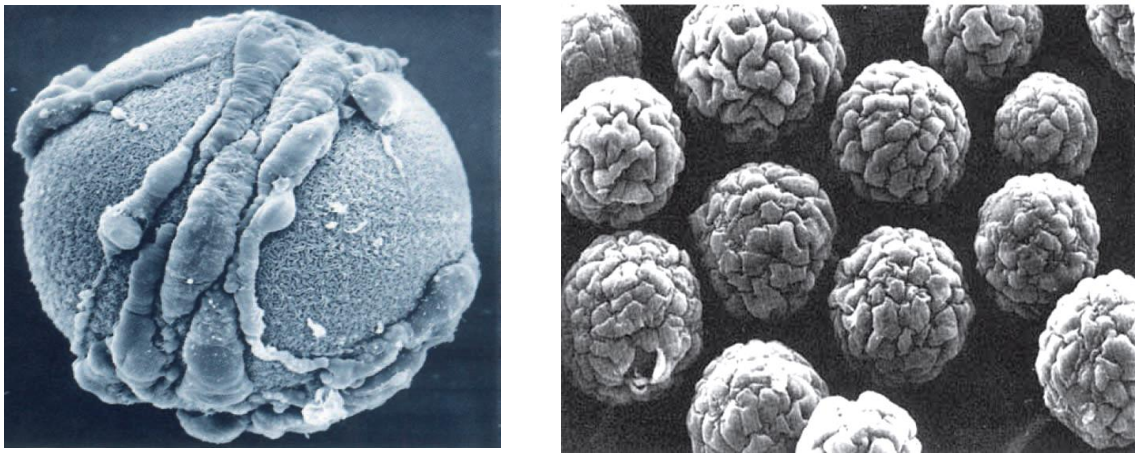

Figure 2.1 Microcarrier. (a) Chicken embryo myoblasts inoculation onto Cytodex. (b) Pig kidney cells (IBR-S2) growing on Cytodex [138].

microscopic-sized artificial capillaries. Therefore, the integration of these technologies with micro robotic applications could be useful in the automation of cell manipulation for important areas such as single cell analysis, manipulation and treatment.

Recently, cultivating the cells on the surface of micro-carrier, such as PLGA (polylactic-co-glycolic acid) microcarrier, has been widely used as temporal porous scaffolds for cell culture engineering because of its biocompatibility and controllable biodegradability. Zooblast culture on the microcarrier is critical to the study of cell culture, and differentiation. Additionally, it provides important biological contributions for the pharmaceutical industry, including enzymes, viral vaccines, hormones, and antibodies. In microcarrier cell culture technology, anchorage-dependent animal cells are grown on the surface of small (~150 μm) spheres which are maintained in stirred suspension cultures. Figure 2.1 shows the zooblast culture on a microcarrier. Because of their extremely high surface area to volume ratio, microcarrieres are more attractive and alternative than conventional monolayer cell culture methods, such as roller-bottle and stirred-tanks, perfusion, or air-lift methods. This technology

has been used successfully for: (1) routine and high density cell culture, (2) production culture volumes is over 1000 L, (3) reduction of costs and contamination, (4) efficient monitoring and culture control, in cell culture applications [139].

2.1.1 Conventional works on single cell sorting

An injectable cell delivery system using photo-crosslinkable biodegradable hydrogels has attracted much attention because the direct injection of cell into the defect site avoids an open surgery procedure[140],[141]. Therefore, precise assay becomes crucial, that means quantitative cell culture becomes urgent need.

In the biomedical field, automation of bio-manipulation by non-contact actuation is demanded using a disposable microfluidic chip. Conventional PDMS disposable microfluidic chip have many functions such as loading, cutting and so on [126], [142]–[144]. By using the PDMS disposable chips, on-chip particle manipulation has been studied with 3D magnetic particle loader to supply single particles to different microchannels or modules [128]. However limited study is available on retrieving particles after they are manipulated on a chip.

2.1.2 Our approach

Here, we describe an on-chip approach to achieve a certain amount of microbeads as a microcarrier loader, and finally loaded microcarrier could be dispensed out by using our dispensing system. It is important to transport the particles that are continuously manipulated from the microfluidic chip to the incubation atmosphere. The concept design of the entire system is illustrated in Figure 2.2. Actually, this system concludes three modules, microbeads loading, sensing, and dispensing. In this chapter, mainly the oocyte loading mechanism will be

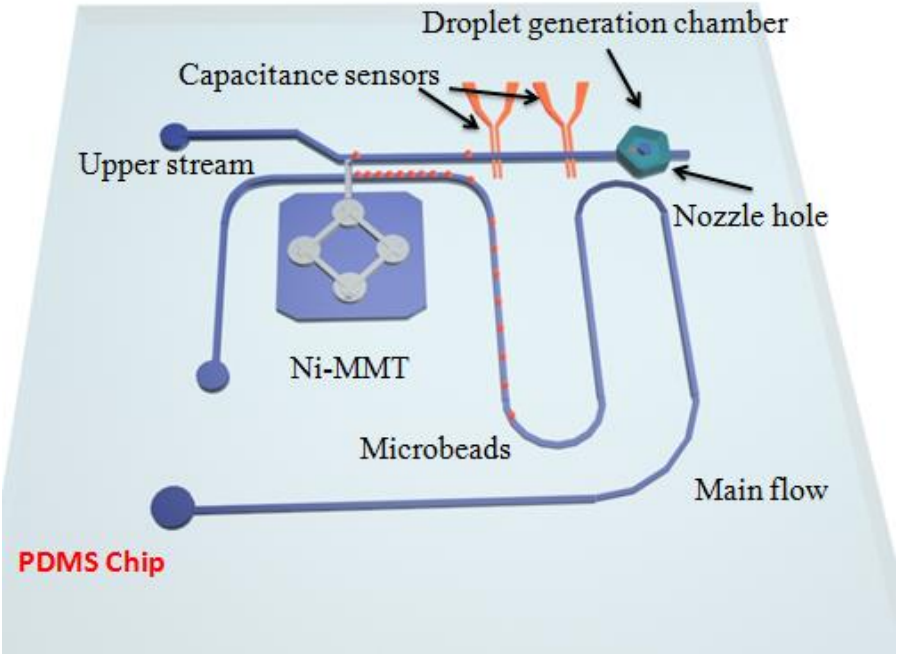

Figure 2.2 Concept view of microfluidic particle loading and dispensing chip.

introduced. The detailed principle of sensing and the dispensing will be discussed in the Chapter 4.

Figure 2.2 shows the top view of loading concept, the microbeads are injected from the inlet and delivered by flow to the hook of the tip of the MMT, by actuating the MMT's up and down movement, microbeads could be transported one by one. According to the concept, the rest of this chapter is divided into the three main sections, (1) methods and modules, (2) applications and experimental results (3) discussion and summary.

2.2 Methods and Modules

2.2.1 Methodology

The MMT particle loader is a non-contact magnetic loader module to manipulate particles in a microfluidic channel. It is capable to load micro-particles one-by-one by using its hook

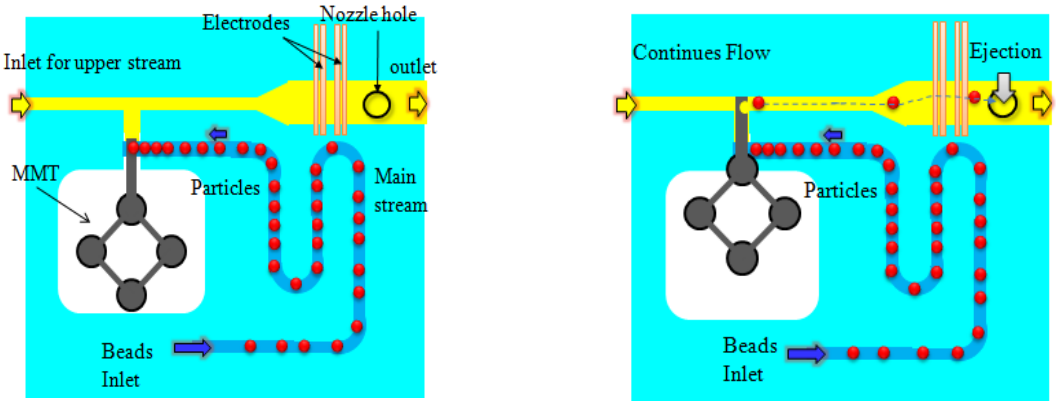

(a) (b)

Figure 2.3 Loading concept. (a) Schematic view of particle loading while transferring particles to loading area, (b) Particles are loaded to upper stream for dispensing hole.

shape handles while moving up and down as it is illustrated in Figure 2.3. It is controlled by magnetic actuator located outside of the microfluidic chip. Control system is accompanied by ultrasonic piezo vibrator drives magnets attached on a micro-stage [145]. The particle loader move up and down in terms of controlled magnet motion which is laid under a glass substrate.

The nickel-based magnetically driven microtool (Ni-MMT) is for making a disposable microchip with non-contact actuation. The main process of fabrication of Ni-MMT is the conventional electroplating technique that is a plating process in which metal ions, affected by electric field, move to metal surface of an electrode.

The design of MMT is shown in Figure 2.3; the MMT made of Ni is fabricated by electroplating after the photolithography. The MMT is actuated by horizontally arranged four permanent magnets and the permanent magnet is set on the 2-DOF linear stage. As a magnetic driving system, four neodymium (Nd2Fe14B) magnets (size: 1.0 × 1.0 × 1.0 mm, grade: N40) are used and for the MMT, Ni based multi-DOF MMT, which is illustrated in Figure 2.3 is employed.

2.2.2 Analysis

In the experiment, the Nickel MMT is actuated by HPD (horizontal polar drive). Figure 2.4 shows the concept and the FEM result of HPD [144] (magnet: ⏀ 1.0 × 1.0 mm neodymium, MMT: ⏀1.0 × 0.05 mm Ni MMT). The magnetic flux flows in a circular pattern through the MMT, and its direction is aligned to the driving direction. Magnetic power with a considerably high efficiency is applied to the MMT and the magnetic force on the MMT is much greater in the driving direction than in the vertical direction; therefore, the friction force is reduced by decreasing the vertical force on the MMT.

Figure 2.5 shows the frequency response characteristic of MMT. This figure is obtained experimentally of following response ability of the MMT against the linear stage with the permanent magnet. According to this investigation, in our experiments we set maximum actuation frequency of MMT to 6 Hz in the experiment, because of the tracking performance of MMT against permanent magnet is decreased significantly when actuation frequency beyond 6 Hz.

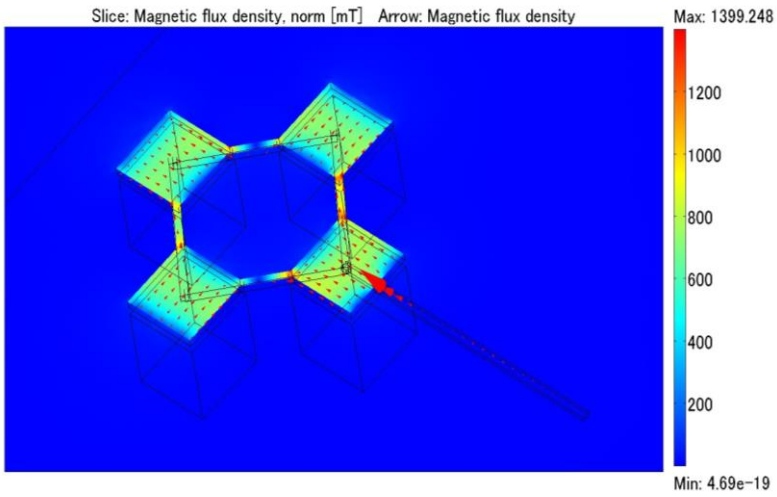

Figure 2.4 FEM results of magnetic flux density in HPD.

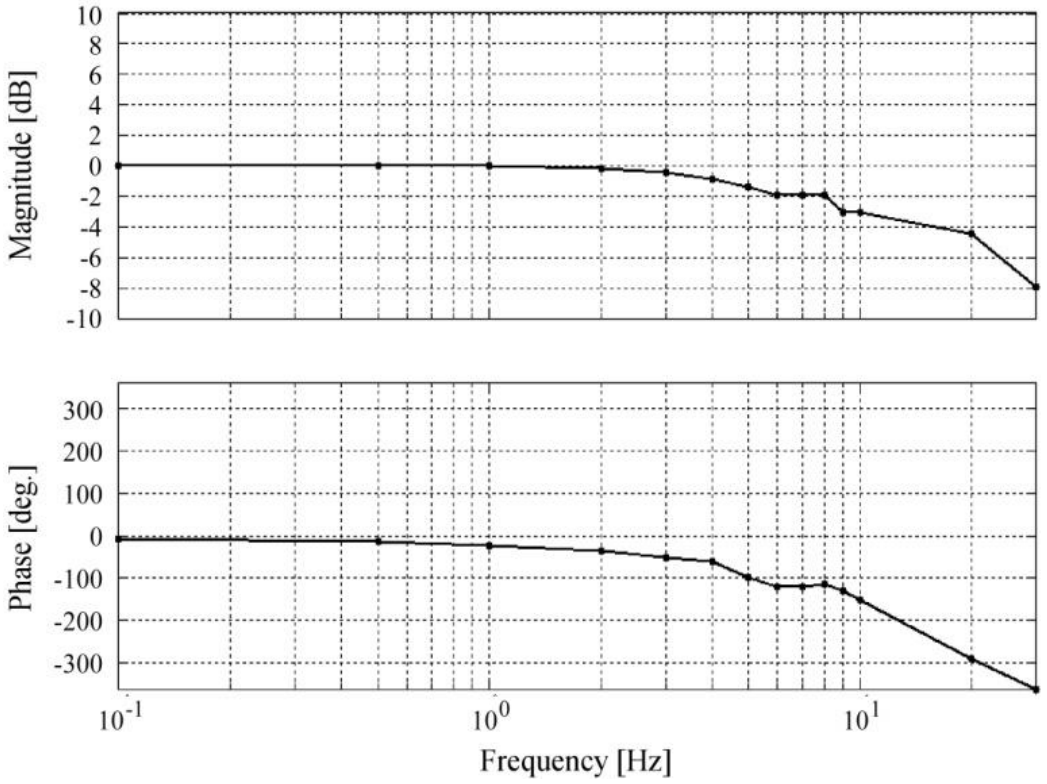

Figure 2.5 Frequency response characteristic of MMT.

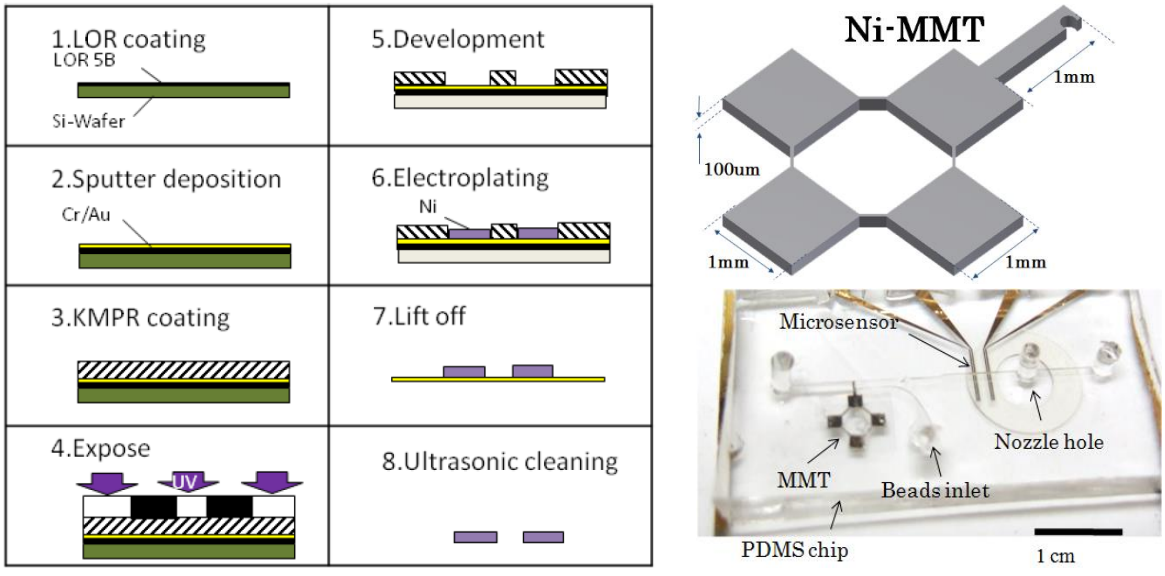

Figure 2.6 The fabrication process of Ni based MMT, and fabricated PDMS microfluidic chip.

2.2.3 Fabrication process

Figure 2.6 shows the fabrication process of Ni-MMT. The process is as flows. (1) Cr and Au are deposited (total thickness: 50 nm) on Si-wafer with sputtering technique. (2) LOR-5B (MicroChem Co. Japan) is spin-coated (200 rpm-30 sec) on the Si-wafer as a sacrifice layer and baked (180 centigrade) in an oven for 30 min. (3) SU-8 (MicroChem Co. Japan) photoresist is coated (100 μm) and replicated the shape of MMT via photolithography. (4) In the final part, the developed SU-8 patterns are soaked to metal-ion water to complete electroplating. Formed Ni-MMT is peeled off by precise operation. The microfluidic chip is fabricated by use PDMS, MMT is sandwiched inside of the microfluidic channel. Figure 2.6 also shows the fabricated MMT and microfluidic chip with MMT inside.

2.3 System Setup and Experimental Results

2.3.1 System setup

Figure 2.7 shows the driving concept of the MMT with ultrasonic vibration. Radically displaceable piezoelectric ceramic is attached to the glass substrate under the microfluidic chip and oscillates the sliding surface of the MMT. The MMT is actuated by permanent magnets whose axis is set to the horizontal direction and the permanent magnet is placed on the 2-DOF linear stage [134]. The permanent magnets were actuated by XY stage and piezo vibrator for positioning control of MMT. Loaded microbeads were pushed up and delivered the particles one by one to the upper stream.

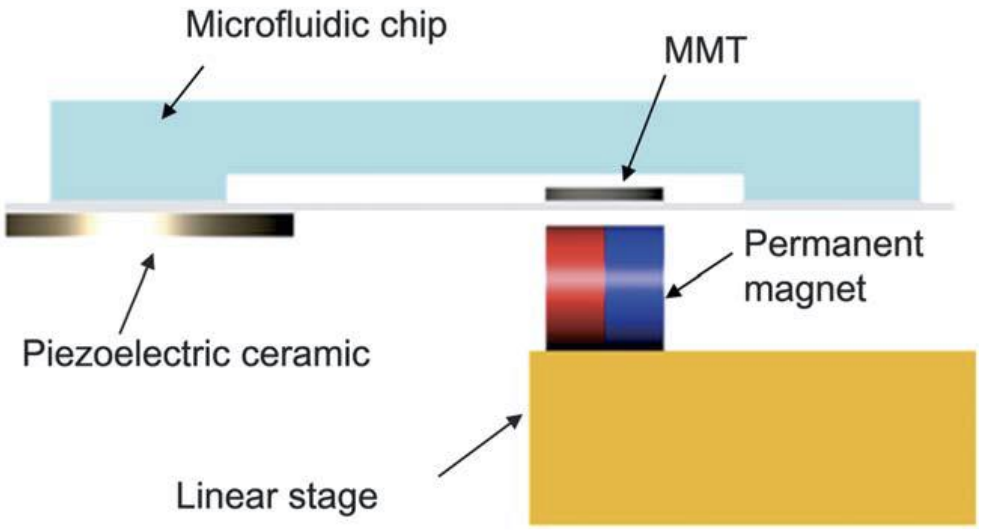

Figure 2.7 Driving concept of the MMT actuated by permanent magnet with ultrasonic vibration. Oscillating the glass substrate by the piezoelectric ceramic reduces the effective friction on the MMT [134].

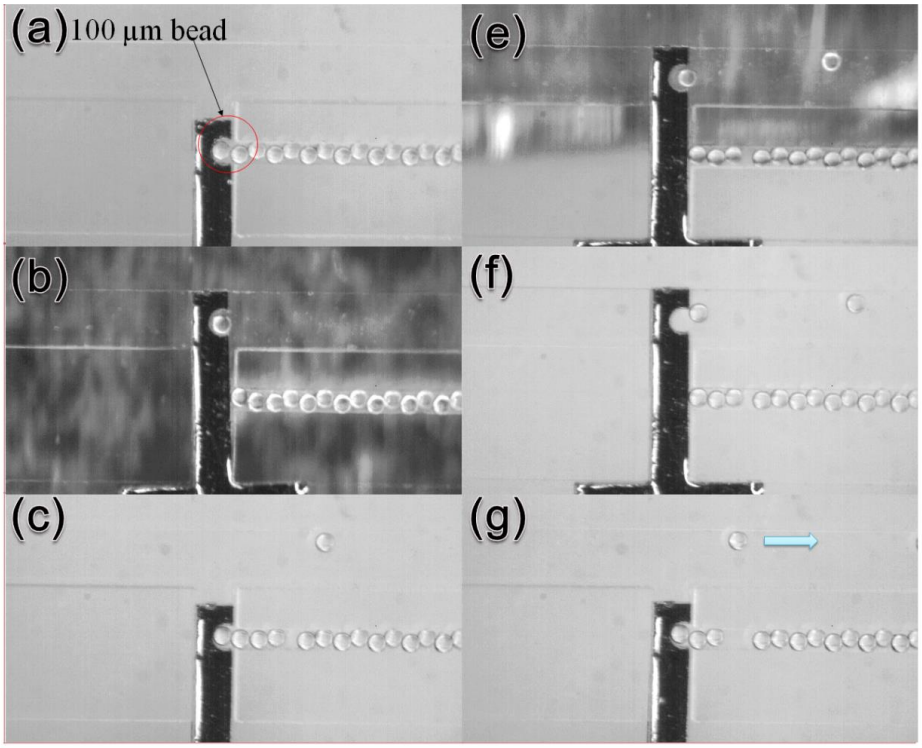

Figure 2.8 Particle loader performances. (a) A line of beads are successively approaching to Ni-MMT, and microbeads are stopped at the hook shape of MMT. (b) Ni-MMT moves up and particle moves though upper stream flow direction which is leading to the nozzle hole.

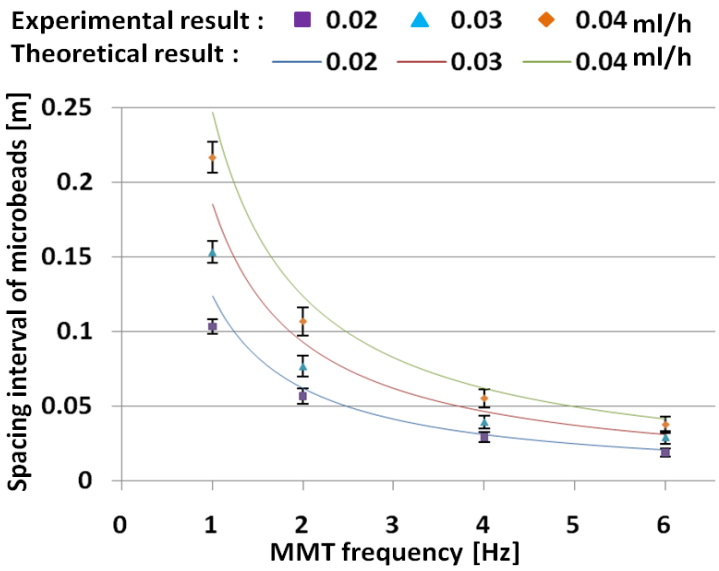

Figure 2.9 Profiles of the spacing interval of microbeads as function of the MMT frequency and flow velocity.

2.3.2 Microbeads loading results

Figure 2.8 shows the profiles of the spacing interval of microbeads as function of the MMT frequency and flow rate. It was observed that interval of micro polystyrene beads decreased by simply increasing the MMT frequency or slowing down the flow rate. For the present study, we choose the upstream flow rate from 0.02 ml/h to 0.04 ml/h, and MMT frequency is applied from 1 Hz to 6 Hz. Therefore the spacing interval between microbeads D is:

$$D = \frac{Q}{w \times h} \times \frac{1}{f} \qquad 2.1$$

where, Q is flow flux, w and h are the width and height of microchannel, and f is the MMT frequency. Loaded microbeads in the channel were pushed by the MMT into the intersection of the other channel with adjustable pace from 0.02 m to 0.25 m, and delivered to the next operation by the fluid force. Figure 2.9 shows the evaluation of the current loading system. The interval spaces of two adjacent microbeads are adjustable by varying the movement frequency

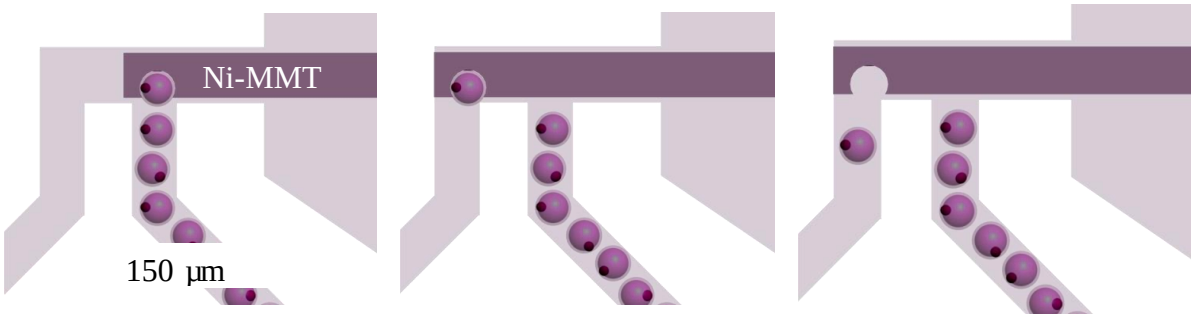

(a) (b) (c)

Figure 2.10 Oocytes loading performance. (a) Oocytes are loaded into a line, (b) Single oocyte is transport to the other microchannel. (c) Oocyte is released to the left stream.

of MMT and the flow velocity in the microchannel. And furthermore the MMT frequency is much more efficient from the changing of the flow velocity.

2.4 Preliminary Test of Oocytes Loading

As been introduced in the previous sections, the microbeads-loading has been successfully achieved. Basing on this approach, Kawahara et al succeed in on-demand loading of the microcarrier with cultured cells on [146]. In order to achieve the orderly continuous enucleation process, loading oocyte in a sequence is required. The MMT particle loader is a non-contact magnetic loader module to manipulate particles in a microfluidic channel. It is capable to load micro-particles one-by-one by using its hook shape handles while moving left and right as it is illustrated in Figure 2.10. It is controlled by magnetic actuator located outside of the microfluidic chip. Therefore, the similar approach is applied on the oocyte loading process. Figure 2.10 shows the concept of oocytes loading. The oocyte loader move left and right in terms of controlled magnet motion which is laid under a glass substrate. (a) A line of oocytes are successively approaching to Ni-MMT. (b) Oocytes are stopped at the hook shape of MMT.

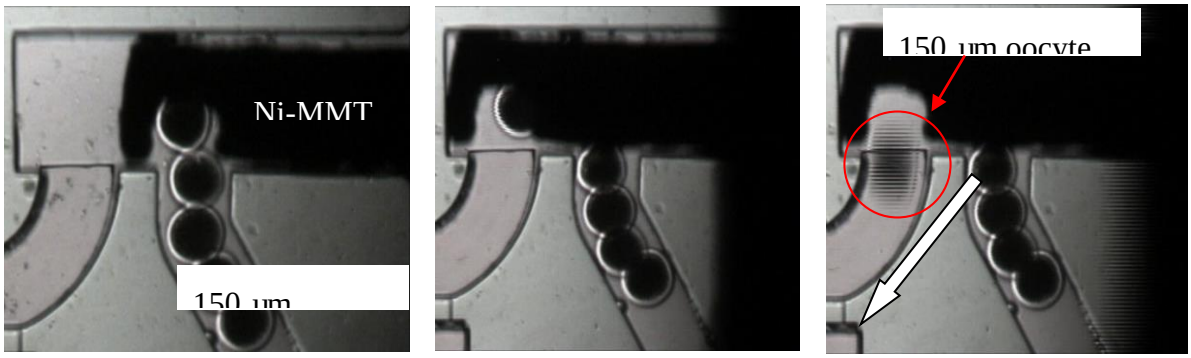

(a) (b) (c)

Figure 2.11 Oocyte loader performance. (a) Oocytes are loaded into a line, (b) Single oocyte is transport to the other microchannel. (c) An oocyte is delivered to the enucleation area. Flow velocity is 1mm/s.

(c) Ni-MMT moves left and oocyte moves though left stream flow direction which is leading to the enucleation area.

According with the concept of oocytes loading, the experiments are conducted. Figure 2.11 shows the oocytes loading results. (a) oocytes are loaded into a line, (b) single oocyte is transport to the other microchannel. (c) oocyte is delivered to the enucleation area. After loading of oocytes, the oocyte is released into the left stream. However, the oocytes shows the elastoplastic property, which means oocytes are easily deformed, therefore during the experiment, occasionally, one and half oocytes stacked into the MMT hook, and crashed by the metal MMT. During the experiment only 70 % oocytes could be successfully loaded. The success rate is unsatisfactory; a better approach for oocytes loading is desperately required for the following automatic oocyte enucleation process in the future works.

2.5 Summary

This chapter presented an on-demand microbeads delivery system in a microfluidic chip by magnetically driven microtool (MMT). The four of horizontally arranged permanent magnets and the piezoelectric vibrator are used to actuate the Ni based microtool precisely in the chip. The MMT injects the beads mechanically to flow and then into ejection operation part. Transferring microbeads one by one with the required pace to the next process has been achieved. The delivery and ejection of polystyrene beads (100 μm) with the flow velocity of from 0.02 ml/h to 0.04 ml/h and MMT frequency from 1 Hz to 6 Hz to adjust the pitch of each micro-bead has been demonstrated. The spacing interval of microbeads could be mainly adjusted by changing of MMT frequency and the flow velocity of output stream. The proposed system shows advantages of high-speed, high success ratio and disposable of microfluidic chip having MMT. This system can be a breakthrough of a high throughput of accurate and effective particle manipulations in the field of cell culturing on a single particle.

Finally, single oocytes loading has also been tested, around 60 % success rate of loading oocyte is unsatisfied, therefore more works should be studied in oocytes loading in the future. After preliminary test on oocyte loading, oocyte enucleation will be discussed in the next chapter.

Chapter 3.

On-Chip Enucleation of Bovine Oocytes

3.1 Introduction

"Dolly" is famous for being the first mammal to be successfully cloned from an adult cell [147]. Despite low success rates, several mammalian species have been successfully cloned since then [148]–[150]. Embryo manipulation is a potential technique for the genetic improvement of domestic animals and the preservation of genes of rare animals. Oocyte

enucleation is a primary technique for the cloning process. The cloning of Dolly the sheep had a low success rate; 277 eggs were used to create 29 embryos, of which only three resulted in lambs, and eventually only one lived. Peura et al. conducted a viability test of the oocyte volume during nuclear transfer and determined that the nucleocytoplasmic ratio is an important parameter for embryo development [151]. Therefore, the low success rate of cloning techniques is a bottleneck for developing this field. Conventional techniques for the enucleation process mainly include the following: manual manipulator operation, microfluidic cutting methods in a microchip, and chemical treatment methods [152]–[154]. As mentioned in the first chapter, these methods tend to have a long operation time, low success rate, contamination, and low repeatability. Additionally, such types of complicated cell manipulation processes can only be undertaken by skilled people. During the chemical treatment processes, a person unaware of toxicities may poison the cells.

Recently, researchers invented many techniques that do not require manual operation for the treatment of cells by fabricating a microrobot on a microchip. Magnetically actuated microrobots appear to be the most promising because of this method is minimally invasive to a cell, features a noncontact drive, and has a low production cost [80], [82], [155]–[157]. These methods reduced the technical skills of operation and increased the throughput and repeatability. By using the MMT we achieved μm-order positioning accuracy while maintaining a mN output force.

Enucleation by a dual arm MMT was conducted previously [158]; however, it was difficult to remove the nucleus because the oocyte is a viscoelastic material. The cutting process is a complicated model because the oocyte is soft and sticky. Once the tip of the MMT blade touched the surface of the oocyte, a resistance force generated by the oocyte decreased the position

accuracy. In addition, achieving the enucleation process was difficult because the oocyte flow was not well-controlled. This chapter will introduce a development of an enucleation system using cooperation of an MMT with fluid control. The new enucleation system contains three remarkable improvements: the oocyte enucleation process can be conducted one by one; the removal ratio in the volume is controllable, minimizing damage to the oocyte; and the nucleus can be removed with a hydrodynamic force controlled by the MMT. The methods of how to achieve these merits will be introduced sequentially in this manuscript.

3.2 Material and Methods

Figure 3.1 (a) shows the concept of the enucleation chip that we used to conduct oocyte enucleation experiments. Two large chambers with a height of 300 μm and a diameter of 5 mm were designed. The MMT with a height of 200 μm was placed in one chamber with its blade inserted in the microchannel branch. To conduct the enucleation process, the other inlet of the Y-shaped microchannel was used to inject the oocytes continually. On the other side of the inlet is a shallow withdrawal microchannel with a height of 50 μm that was used to confine the oocyte to a position to cut accurately the oocyte by a given volume. The first stage involves oocytes in a cell culture medium being injected from the inlet of the microchip. By connecting a digital pump to the outlet, the medium containing the oocytes from the inlet flowed through the microchamber towards the outlet. The tip of the MMT cutting blade was placed at the interface of the chamber and the withdrawal microchannel. The oocyte was delivered by the flow to the withdrawal microchannel, as shown in Figure 3.1 (b). Then, the tip of the MMT controls the oocyte orientation so that the nucleus comes to suction port. The delivered oocyte is obstructed at the interface because of the height limitation (50 μm) of the microchannel, as

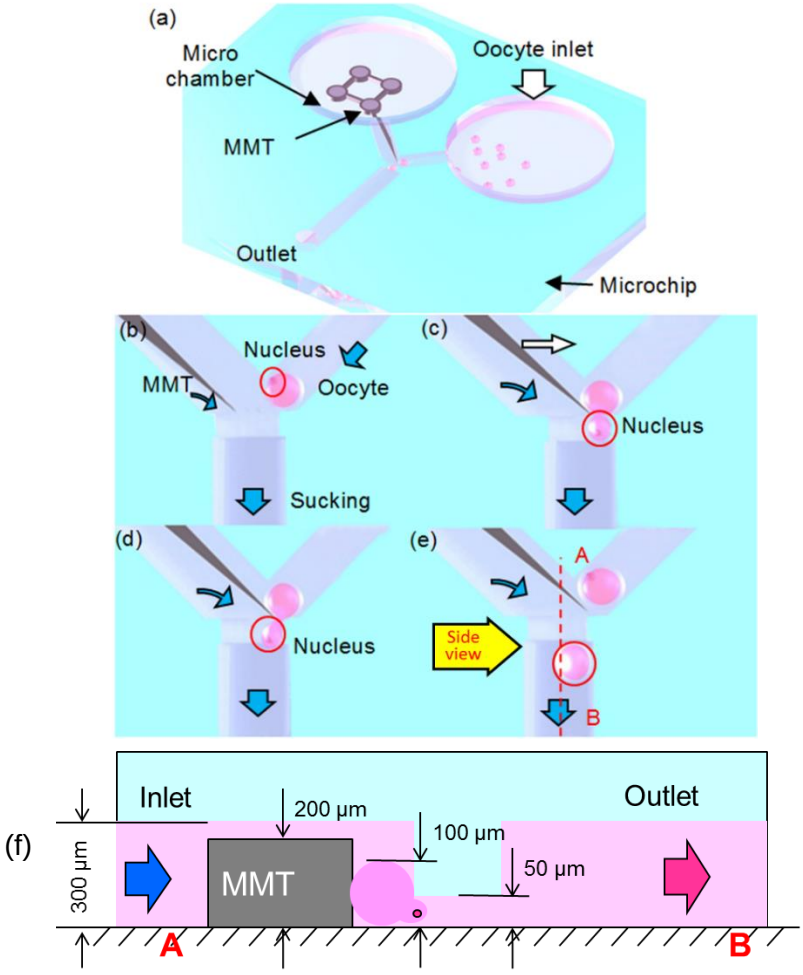

Figure 3.1 Concept of enucleation microchip. (a) Overview. (b–e) Concept of the oocyte enucleation process by the use of magnetically driven microtools (MMTs) in a microfluidic chip. Blue arrows show the flow direction. (f) Height differences in the microchannel design. The white arrow shows the movement of the MMT.

shown in Figure 3.1 (f). Then, the hydraulic pressure deformed the oocyte, allowing the lower part of the oocyte to be sucked into the withdrawal microchannel, as shown in Figure 3.1 (c). After the nucleus was in the withdrawal microchannel, the tip of the MMT was actuated to the left in order to close the interface, as shown in Figure 3.1 (d). Next, under the protection of the MMT, the initial portion of the oocyte was reserved and only the separated nucleus was flushed

away with the flow (Figure 3.1 (e)). After the nucleus separated from the oocyte, the remaining part was also sucked out and collected from the outlet. Figure 3.1 (f) shows the cross-sectional view of the microchannel; there is a height difference between the main chamber and the withdrawal microchannel. The oocyte can be stopped at the intersectional junction where the oocyte enucleation was conducted because of the height difference.

3.2.1 Fluid control by MMT

In this enucleation procedure, the nucleus is removed from the oocyte by hydraulic force. The force on a moving object due to a fluid is:

$$F_D = \frac{1}{2}\rho v^2 C_d A \tag{3.1}$$

where F_D is the force of drag, ρ is the density of the fluid, v is the speed of the object relative to the fluid, C_d is the drag coefficient, and A is the reference area. From the equation we can easily find that, the drag force is relative to the velocity of the fluid. Therefore, in order to utilize flow effectively for the oocyte enucleation process, a high-response control of the local velocity of fluid by MMT is proposed here.

It is quite intuitive to consider the flow of a fluid to be like the flow of electricity; the fluid in a hydraulic circuit behaves much like the electrons in an electrical circuit. An electric circuit analogy is used here to specify parameters of microchannel (Figure 3.2) [159]. The total volumetric flow rate Q [m^3/s] in a rectangular microchannel can be described by Hagen-Poiseuille's law [160] as

$$\mathrm{Q} = \frac{\Delta p}{R_H} \tag{3.2}$$

$$\Delta \mathrm{p} = QR_H \tag{3.3}$$

where Δp is the pressure difference [Pa] through a finite channel length L. The hydraulic resistance R_H [Pa·s^3/m] is defined as

$$R_H = \frac{8\eta L}{\pi R^4} \approx \frac{8\eta L}{\pi {r_H}^4} \tag{3.4}$$

where η is the viscosity [Pa·s] The hydraulic radius of the channel r_H [m] is a geometric constant and defined as $r_H = 2A/P$, where A is the cross-sectional area of the channel [m^2] and P is the wetted perimeter [m].

Based on the equations mentioned above, we can find that the structure of the microchannel shows great influence to the volumetric flow rate. And the area-average velocity of the fluid U [m s^{-1}] [161]:

$$U = \frac{Q}{wh} = \frac{\Delta p}{whR_H} = \frac{\Delta p \pi w^3 h^3}{8\eta L(w+h)^4} \tag{3.5}$$

where w and h are width and height of the microchannel, respectively. By changing the position of the MMT, the microchannel structure at the both sides are relatively modified, therefore the fluid distribution is positively controlled by the MMT. By employing this fluid control by MMT, the oocytes can be delivered to the suction port one by one. Considering the oocyte is regularly 100 μm in diameter, the oocyte inlet microchannel is 150 μm in width, and length is set to 300 μm. Because the height of the MMT is 200 μm, the chamber height is 300 μm and 300 μm in width, and to confine the oocyte at the sucking port. In order to have enough space on letting the MMT to conduct all process, MMT working like a rheostatic controller governed the distribution of flow, Q_2 and Q_3 letting oocyte loading to the operation location and cutting the nucleus off from the oocyte by increasing the hydraulic pressure.

For the preliminary test, the experiments have been conducted by putting fluorescent microbeads (Φ: 2 μm) in the microfluidic chip to prove the effectiveness of the MMT

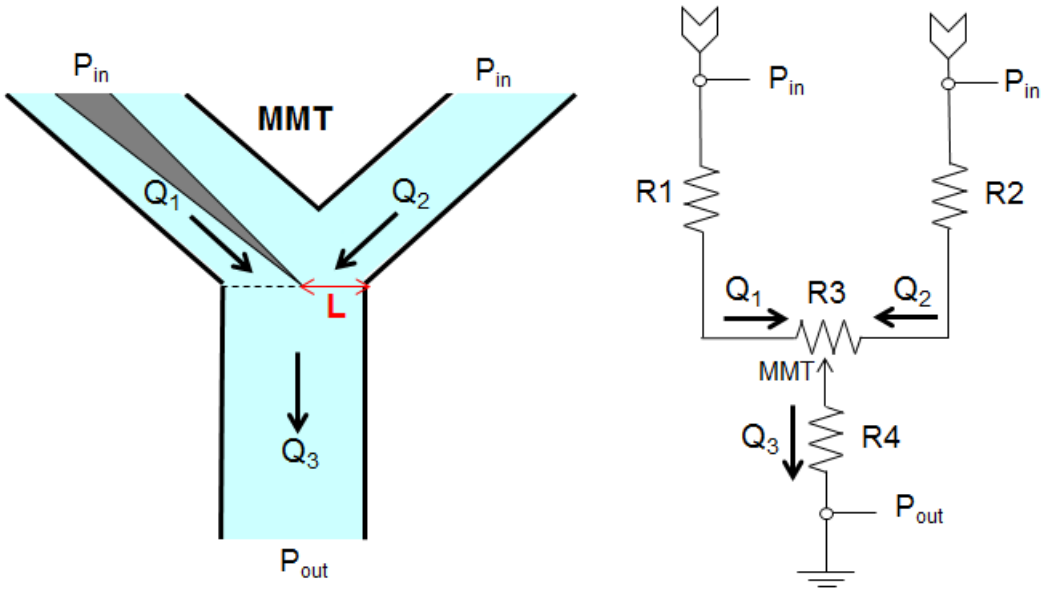

Figure 3.2 Electric circuit analogy of the enucleation chip.

movement to the velocity of fluid. Figure 3.3 shows the fluid velocity changes according with the position changes of MMT. In Fig. 3.3 (a) when MMT is close to the right side corner of the withdrawal microchannel, the velocity of fluid at left is higher than the right side of MMT, In Fig. 3.3 (b), when MMT moved to the left side the velocity of fluid in the microchannel is changed accordingly; velocity of fluid at right side became higher. Three representative points were selected to assess the velocity distribution in the microchannel. The pressure distribution on the oocyte can be derived from the velocity distribution. Points A and B show the distribution of velocity at both sides of the MMT at the suction port, while point C is used to observe velocity changes in the suction channel. The width of our microchannel is 200 μm and we selected the distance of *L* from 0 μm to 200 μm. Figure 3.3 (c) shows that the experimental result as well as the theoretical result for the fluid velocity change by the MMT position at each point. When the position of the MMT was right edge of the channel (L = 0 μm), the flow from right side channel

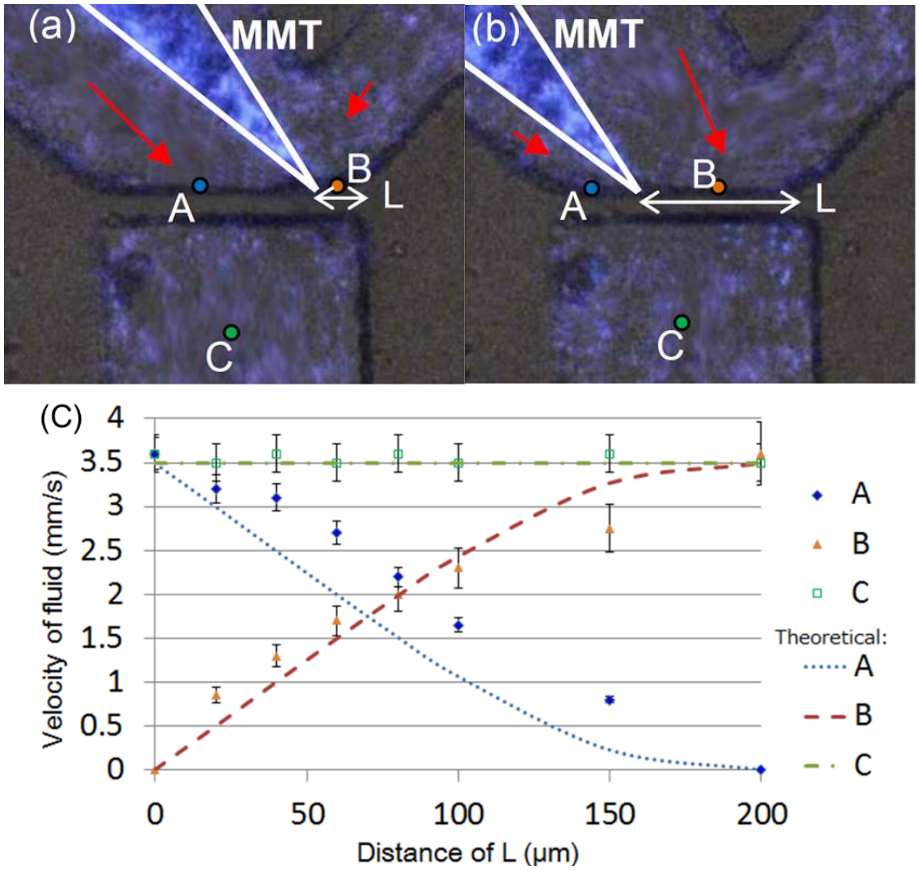

Figure 3.3 Theoretical and experimental values of the fluid velocity changes at three points in the channel. The velocity of the outflow is set to 3.5 mm/s. (a) In case that the MMT is near the right-side corner, (b) In case that the MMT is the left-side corner.

was stopped while the flow from left side was stopped when the position of MMT moved to the left edge (L = 200 μm). During the fabrication process, the size of the microchannel and the MMT may slightly different from the design (±10 μm). Therefore, even there are some difference between the experimental values to the theoretical values, however, the experimental values were reasonably corresponding to the theoretical values, and proved that the flow distribution in the channel can be controlled by MMT position like adjustable valve. As a result, we can adjust the surface traction force (F_D) affected on the oocyte to conduct the oocyte enucleation process letting oocyte split by the hydraulic force, and flushed away by the flow.

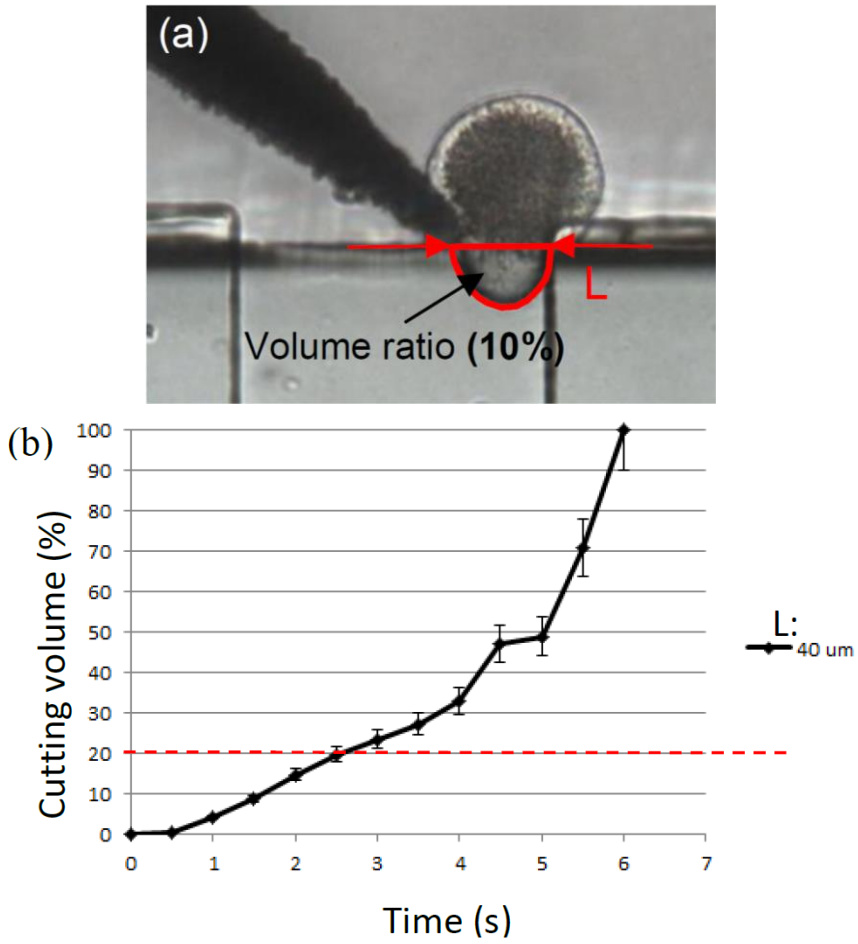

Figure 3.4 Correlations of the volume sucked into the outlet microchannel with respect to the time under the fixed position of the MMT. The velocity of the outflow is set to 3.5 mm/s. (a) The definition of volume ratio, (b) the experimental result.

3.2.2 Cutting volume estimation

In order to achieve precise cutting off of the nucleus from the oocyte with less damage, the effect of removal volume of oocyte is significant. It is very important to remove the nucleus as small as possible for the development of nuclear transfer embryos [162]. The MMT can control the volume of sucked oocyte by closing the channel after a certain amount of time. In order to find out the correlation between sucking time and oocyte volume sucked to the channel, experiments were conducted.

In the experiment, the out velocity (point C in Figure 3.3) was fixed, to avoid the interference from the pump. The PDMS chip with its outlet was connected to the syringe pump by using a teflon tube. The relationship between the oocyte volumes sucked into the outlet microchannel and the suction time was obtained. The distance of MMT tip to right edge of withdraw microchannel, L in Figure 3.4, is variable, the velocity of sucked volume changed accordingly. In our experiment, the MMT position was fixed at 40 μm distance from the right edge of the channel, the oocyte with nucleus part had enough space to be sucked into the withdraw microchannel. The sucked volume of the oocyte was measured by the oocyte area in the channel and the height of the channel (Figure 3.4 (a)). Figure 3.4 (b) shows the experimental result of volume ratio of sucked volume into the channel and the original oocyte volume over time. The graph shows that the error bar at each data point is very small. Especially the sucked volume into the channel in less than 3 seconds was very consistent and the variation was less than 5 %. This represents that the volume control over time using MMT and fluid force is highly accurate and it leads to precise enucleation process.

3.2.3 Cutting of oocyte by hydraulic force

Cutting an oocyte using two MMTs is difficult because of alignment of two cutting-edge perfectly is demanding [158]. Therefore, a new cutting method employing only one MMT is proposed here. The oocyte was squeezed by MMT towards the wall of microchannel, and then let the nucleus part cut off by the fluidic force. A 3D structure was modeled using COMSOL Multiphysics 4.1 to analyze the distribution of the surface traction on the oocyte; meanwhile the flow condition in the microchannel also could be observed clearly. MMT angle and exit

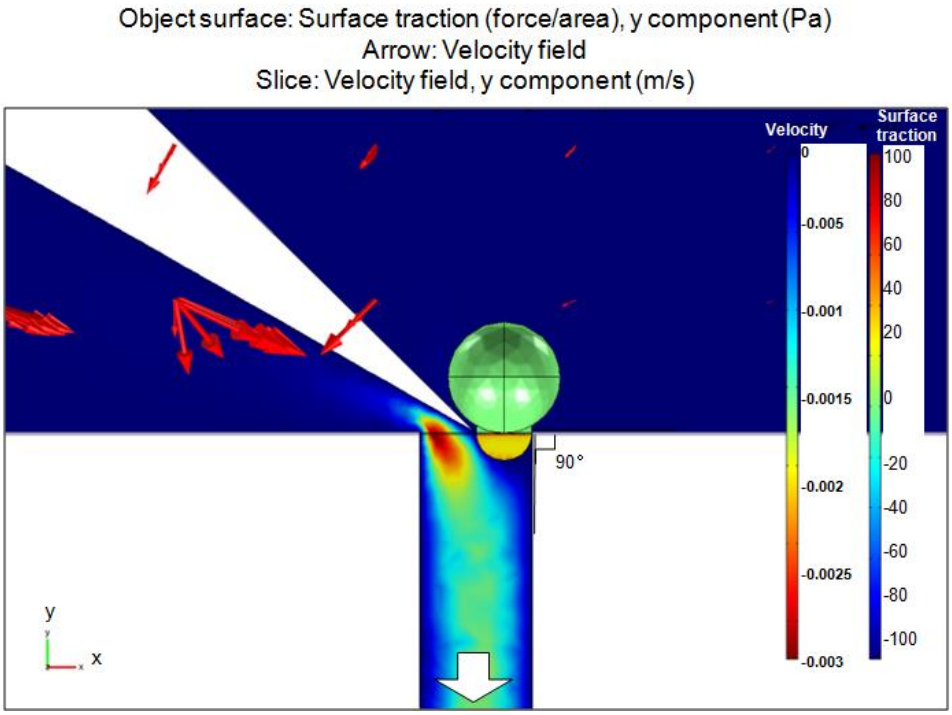

Figure 3.5 FEM results of the velocity distribution and the surface traction of oocytes in the Y-direction. Object surface: y component of surface traction (force/area) (Pa). Arrow: Velocity field, Slice: y component of velocity field (m/s).

velocity are set to 150 degree and 3.5 mm/s, respectively. Figure 3.5 shows the COMSOL simulation result; from this figure, the surface traction on the oocyte is completely different based on the velocity differences at different areas. The lower part of an oocyte which entered the withdrawal microchannel suffers a high traction force with maximum value of 72.2 Pa by hydraulic pressure on Y direction, meanwhile the part which is not being sucked into the microchannel is almost 0 Pa protected by the MMT from the impact of the medium.

3.2.4 Fabrication of hybrid MMT and microfluidic chip

A microfluidic chip consists of a PDMS microchannel and is bonded to a glass substrate. A PDMS microchannel was produced by replica molding using a master mold fabricated

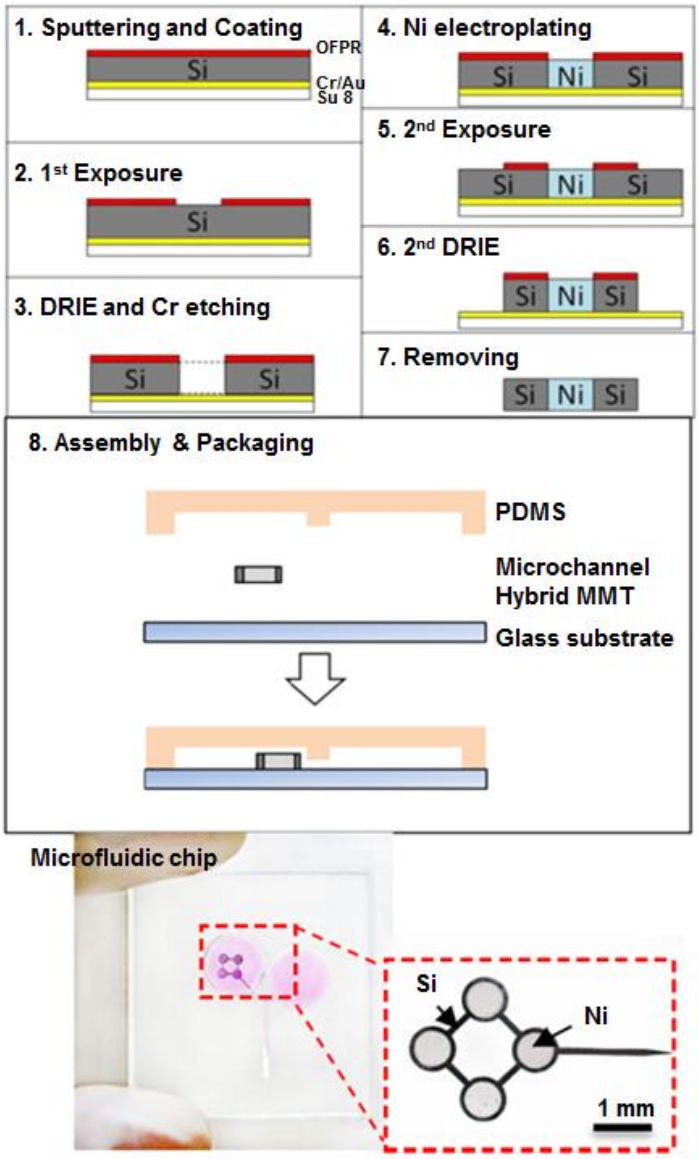

Figure 3.6 Fabrication process of the MMT and the fabricated chip with a magnified figure of the MMT.

by photolithography. Ultraviolet light was exposed through a photomask to produce a microchannel pattern using a mask aligner (LA410, Nanometrich Technology Inc., Tokyo, Japan). The substrate was then developed and rinsed. SU-8 film (DuPont Co., Wilmington, DE, USA) and the two-step exposure is employed to produce the height difference microchannel in

the microfluidic chip. The two-step exposure was performed to fabricate a precise uneven channel for cell confining. The main channel and withdrawal microchannel had heights of 300 μm and 50 μm, respectively.

Nickel (Ni) is a ferromagnetic body and it can be magnetically attracted by permanent magnet, but it is easy to bend during handling due to its ductility and very thin thickness. As a result, it is difficult to maintain the flatness of Ni which is very important to control the flow of the channel. Therefore we employed a hybrid type of MMT composed of Ni and silicon (Si), which is rigid and bio-compatible material. The Ni-Si MMT fabrication process is shown in Figure 3.6. At first, the Cr-Au was sputtered on the silicon wafer (thickness = 200 μm). Then a thick negative photoresist (SU-8, Tokyo Ohka Kogyo Co.) coated and exposed on the silicon substrate as a support layer. Meanwhile on the other side of the silicon wafer, the photoresist OFPR (Tokyo Ohka Kogyo Co.) was coated on the substrate. After the exposure on the OFPR side, the OFPR pattern was developed. Next, deep reactive-ion etching was conducted from the OFPR side, and silicon is etched to a depth of 200 μm until the Cr/Au layer. After the wet etching of the Cr, the Au surface was exposed. Then the Nickel was grown on the Au surface by the electroplating (= 200 μm). After the Nickel has accumulated in the holes on the silicon substrate, we again conducted the OFPR coating, exposure and DRIE processes to form the MMT shape. At last, removing the photoresist and Au layer, the hybrid type of MMT could finally be collected.

In order to prevent contamination after 2-3 hours experiments, one microfluidic chip is low cost just 0.2 dollars and is disposable. However the MMT could be cleaned and reused over and over again.

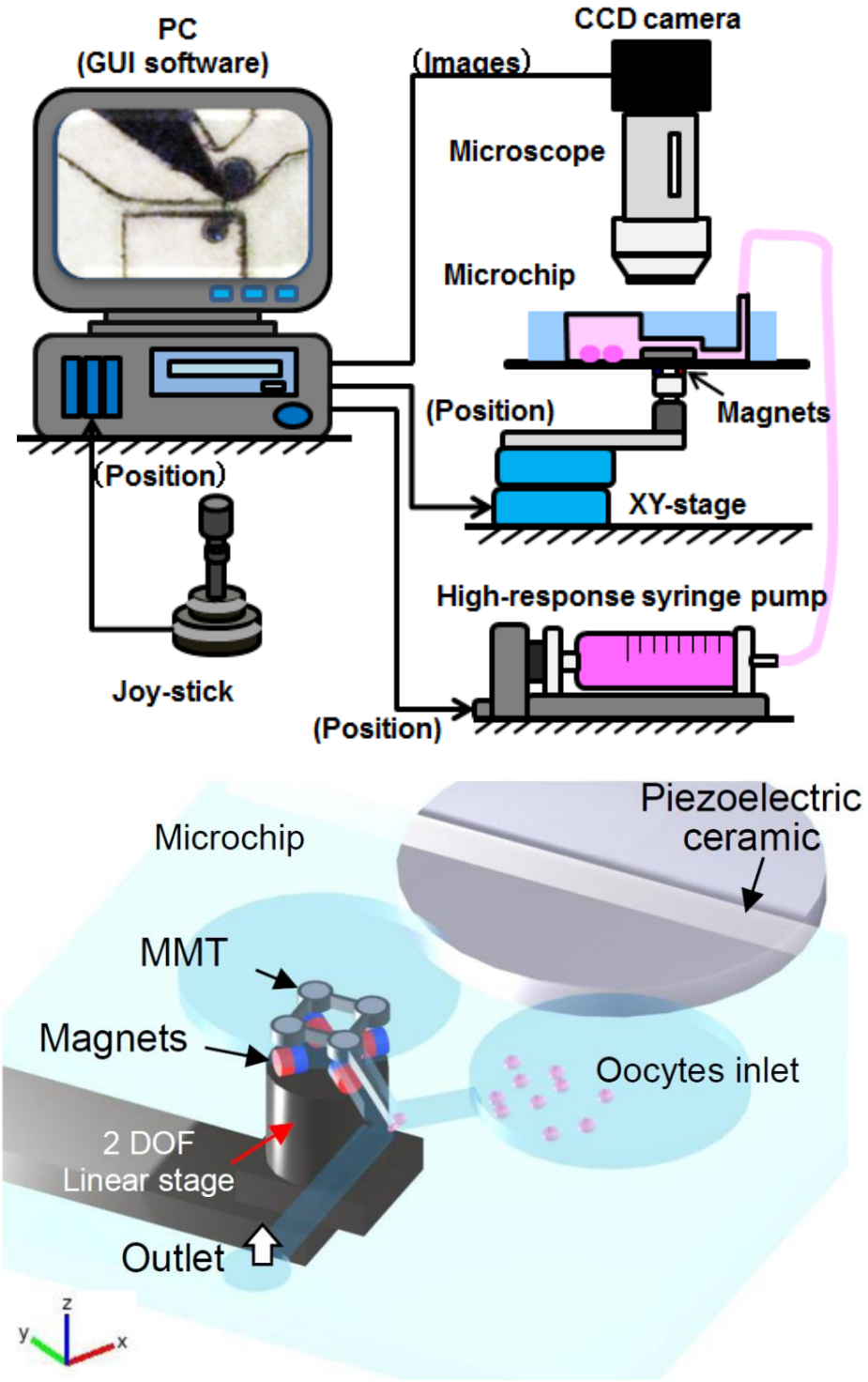

Figure 3.7 Components of experimental system: (a) Experimental setup for the enucleation of oocytes including the linear stage for magnet actuation, a microfluidic chip, and a piezoceramic for generating vibrations on the microfluidic chip. (b) System architect.

3.3 Oocyte Enucleation Experiments

3.3.1. Experimental setup

Figure 3.7 (a) shows the system components of the platform, including a linear stage for the magnet actuation, a microscope with a CCD camera, a joystick, a high-response pump, and a microfluidic chip. The microscope with the CCD camera sends the captured image data to the PC and the stage movement is controlled by the joystick. A high-response syringe pump connected to the microchip is used to control the velocity in the microchannel. Figure 3.7 (b) shows the overview of the microchip setup, including the driving concept of the MMT using HPD with ultrasonic vibration [134]. The MMT is actuated by HPD and the four neodymium (Nd2Fe14B) (diameter: 1.0 mm, grade: N40) permanent magnets, which are arranged on a swivel base set on a 2 degrees-of-freedom (DOF) linear stage [144]. The commercially available piezoelectric ceramic (W-40, MKT Taisei Co., Tokyo, Japan) has the following parameters: the size is ϕ = 42.0 × 3.5 mm; the resonance frequency is 55 kHz; and the electrostatic capacitance is 4600 pF. This was attached to the microfluidic chip and an AC of 150 Vp-p was applied at 52.5 kHz to vibrate the sliding surface of the MMTs [134]. By controlling the 2-DOF linear stage, the MMT could be actuated in the X- and Y-directions. The swivel base rotated the MMT in the X-Y plane. In summary, an MMT with 3-DOF on the X-Y plane is sufficient for performing the enucleation process.

3.3.2. Experimental process and result

Prior to the oocyte enucleation process, the bovine oocyte must be prepared in advance with hyaluronidase (0.1% of medium) for 10 min in order to remove the cumulus cells surrounding the oocytes and pronase (0.5% of Phosphate buffered saline) for 10 min to remove

the zona pellucida. Next, Hoechst 34580 is applied to stain the nucleus of the oocyte; the nucleus portion was florescent when exposed to a mercury lamp.

Figure 3.8 shows the experimental results of the bovine oocyte enucleation process. The oocyte inserted from the inlet flowed to the narrow channel. The MMT pushed the oocyte towards the wall of the microchannel so the oocyte orientation could be adjusted by letting the nucleus face towards the suctioning microchannel. The oocyte was too large to pass into the microchannel with a height of 50 μm (Figure 3.8 (a)). After the nucleus position was confirmed, the downside of the oocyte was drawn towards the withdrawal microchannel by the outward flow until the nucleus, visualized by the bright spot, was sucked in the channel (Figure 3.8 (b)). Then, the tip of the MMT held the oocyte by pressing it towards the corner of the channel (Figure 3.8 (c)). Next, the lower part of the oocyte with the nucleus was torn by hydraulic forces and was washed away with the outward flow (Figure 3.8 (d)). After the separation experiments, the remainder of the oocytes were suctioned from the outlet and immediately sent to an extraction chamber to evaluate the status of the cell membranes. Although deformation of the oocyte could happen during the separation process, Figure 3.8 (e) shows that the cell membrane of the enucleated oocyte, which is spherical, remained intact. The removed nucleus can also be observed in this figure. The nucleus was successfully removed and the oocyte shape remained circular, even after the separation. The procedure time, i.e., the duration from the oocyte reaching the narrow channel until the nucleus was removed from the oocyte, was less than 5 s and the volume removed from the oocyte is approximately 17.8% of the original volume.

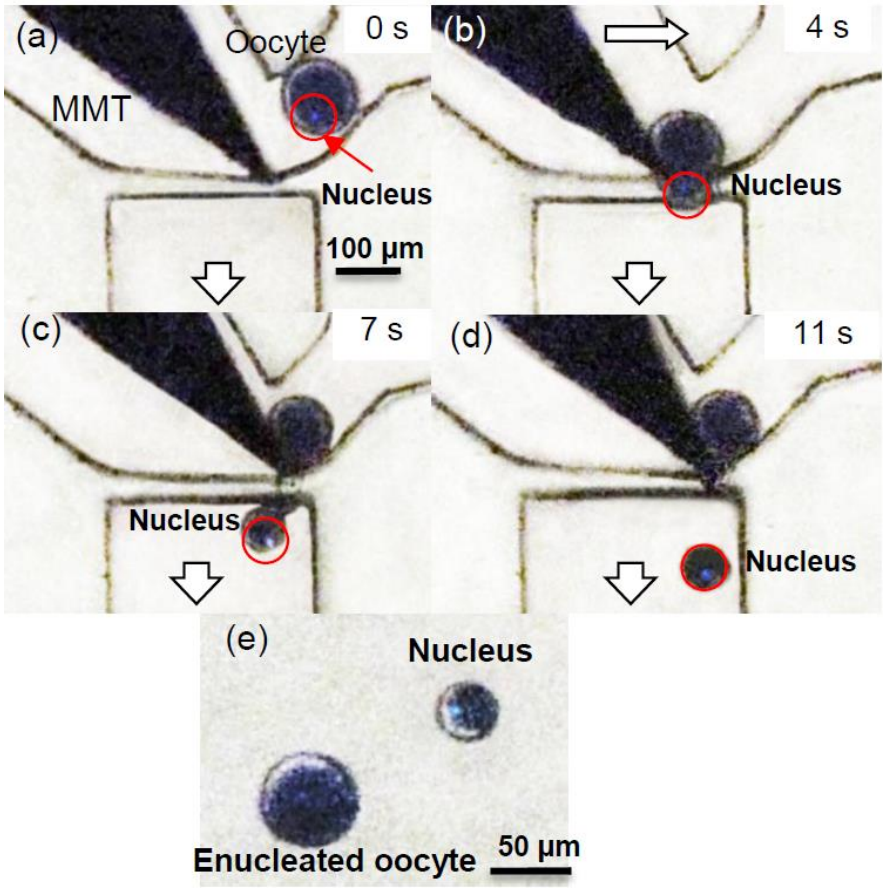

Figure 3.8 Enucleation process (a–d) Experimental results of the oocyte enucleation process. (e) Nucleus after being removed from the oocyte. The incision of the enucleated oocyte is smooth and the remaining oocyte is remains smooth; the enucleated nucleus is also shown in this figure with a removal volume of 17.8 % from the original volume.

3.3.3. Separation time and removal proportion evaluation

The dot graphs of Figure 3.9 show the evaluations of both the enucleation time and the removal proportion of oocytes based on 15 samples. Figure 3.9 (a) shows that the enucleation time was an average of 2.5 s for a single oocyte enucleation. The slowest processing time was less than 4 s. In mammalian cells, the average diameter of the nucleus is approximately 6 μm, which occupies about 10% of the total cell volume [163]. Using our approach, the removal volume of the oocyte was 20% on average; the 20% removal of the cytoplasm ratio is significant

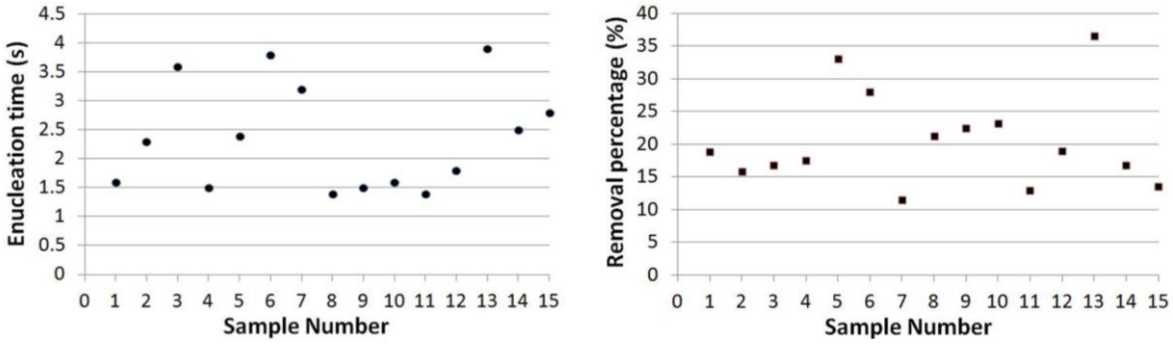

(a) (b)

Figure 3.9 System estimation. (a) Enucleation processing time for 15 samples; the average enucleation time is 2.5 s for one oocyte. (b) Removal proportion of the nucleus from the original oocyte for 15 samples; the average removal proportion is 20%.

for early cloned bovine embryos [162]. Depending on the nucleus position, the removal volume can be slightly increased, but the highest volume removed was 36%. The precise control of oocyte orientation in a few seconds assists in improving the separation accuracy, which will be further covered in our future work.

3.4 Summary

In this chapter, a new scheme that involves use of hydraulic forces controlled by a microrobot to perform an oocyte enucleation process in a microfluidic chip has been demonstrated. Using this novel design for oocyte enucleation, the nucleus was removed from the oocyte successfully. This system is advantageous for the following three reasons: (1) that oocyte enucleation can be conducted at a higher speed as compared to conventional enucleation methods; (2) that it minimizes the damage to the oocyte, and that the removal volume of the nucleus portion is small, which is important because the cytoplasmic volume affects the development of nuclear transfer embryos; and (3) that the incision of the enucleated oocyte is smooth, which may also reduce the influence of the viability on the oocyte.

Viability examinations of enucleated oocyte by proposed method has been confirmed by Ichikawa et al. [153]. The precise and faster orientation control of the oocyte needs to be studied more because it takes several seconds to minutes to properly orient the oocyte positions. Then, the next step is a fusion process using the enucleated oocyte. After oocyte enucleation process, how to transfer them to culture environment ASAP becomes to our next topic, therefore in the next chapter, the transportation methods will be proposed.

Chapter 4.

Accurate Dispensing System for Single Oocytes Using Air Ejection

4.1 Introduction

Recently, researchers have devised numerous techniques that do not require manual operation. In the previous chapter, the magnetically driven microtools (MMTs) has been introduced which has a sufficient power for a wide range of oocyte enucleation [125]–[127], [144]. Meanwhile, Ichikawa et al. are developing a microgripper that can be applied to the

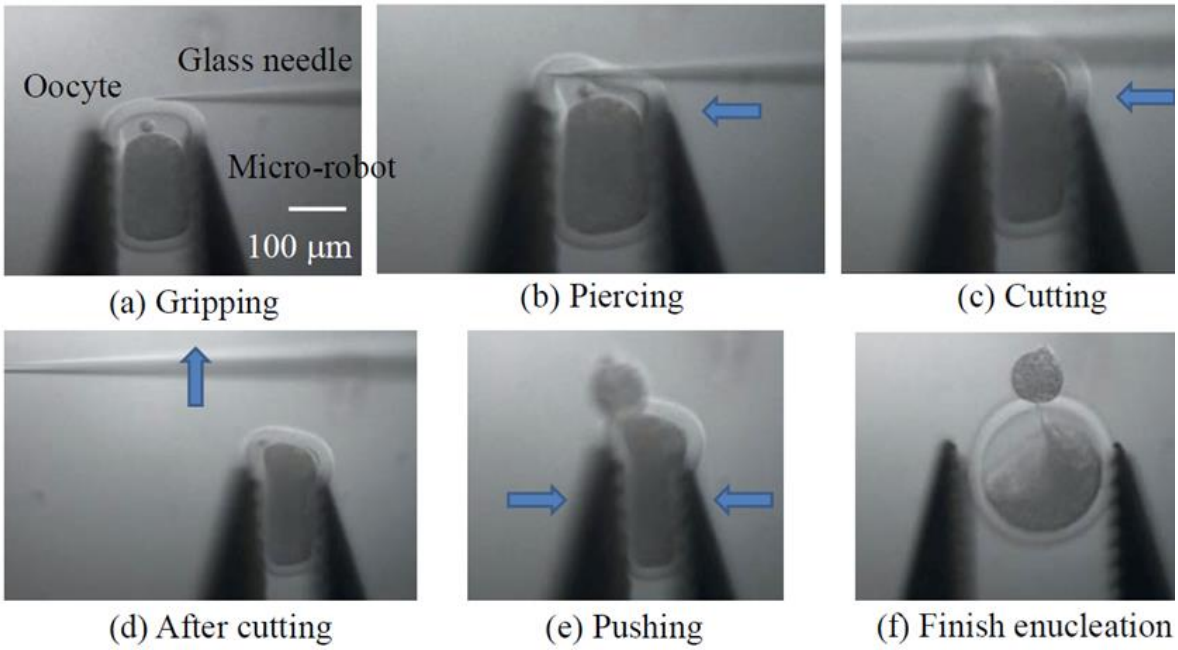

Figure 4.1 Oocytes enucleation by using microgripper [164].

oocyte enucleation process [164] (Figure 4.1).

By using such a microrobot, the enucleation process could be rapidly performed with far greater accuracy. However, following the enucleation process, the enucleated oocytes are manually collected by using an injection pipette [18] or by centrifugation [165]. Such time-consuming retrieval methods greatly affect oocyte viability and the subsequent analysis of single oocytes.

Conventionally, in order to isolate and sort different cell types, cell sorters based on flow cytometry, can sort cells in a continuous cell-laden flow, and sorted cells can be retrieved in cell suspensions [166]. Cell sorting is performed electrically, after a shot of laser light to sense the cell. Thus, such kind of system tends to be large and expensive. In the meantime, several works have succeeded in cell ejection using inkjet technology [167]–[172]. Yusof, Azmi et al. [173] have outlined a non-contact method for the controlled separation of single cells confined in a

droplet that can be printed inkjet-like onto predefined locations. This method is a suitable platform for printing single cells of various types. Mainly, the inkjet mechanism is composed of the solution tank and the nozzle part and the drive unit to generate droplets. However, such systems cannot have a module structure in order to be easily washed and are not disposable. Therefore, in cell manipulation the system encounters the risk of contamination problems. Tornay et al. [174] have proposed the cell dispensing system with the disposable microchip, which consisted with an ejection mechanism by air and a capacitance sensor. This system succeeded in the dispensing a droplet with a single latex bead. However, since this system does not have a cell loading mechanism for supplying a single cell one by one to the microchannel, the success rate of dispensing is unsatisfactory. In addition, a bunch of non-inkjet technologies like dispensing valves [175] or laser microdissection [176] are available for single cell separation and manipulation. However, transporting continuously manipulated oocytes from the microfluidic chip to the incubation atmosphere is critical for single oocyte ejection. Kawahara et al. [177] fabricated two pairs of capacitance sensors in a microfluidic chip to detect artificial beads with diameters of ~100 μm. With this method, they were able to detect polystyrene beads very well. However, their success rate reached only 50%—an unsatisfactory level for polystyrene bead ejection. And the permittivity of oocyte and culture solution were quite close, therefore, detection of oocyte became quite difficult.

A new system proposed here to improve the dispensing system of cell, the targets are to (1) develop a system by improving the sensitivity, and (2) custom-design a microchannel for single oocyte ejection. The success rate of new dispensing a single bovine oocyte is increased to 100% and that the dispensed oocytes are viable.

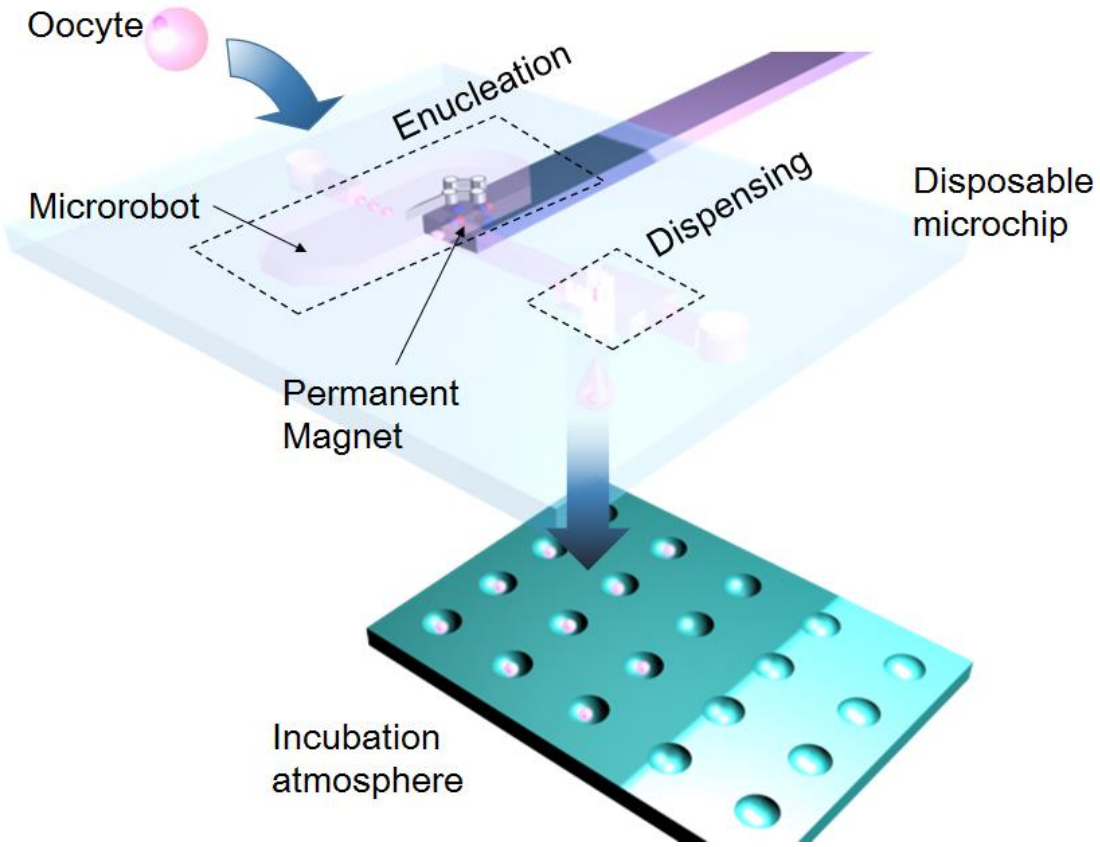

Figure 4.2 On-chip cell enucleation and dispensing system.

Figure 4.2 shows a conceptual diagram of the enucleation and dispensing system. The oocyte is injected into the microchip from the inlet, and the medium containing the oocytes from the inlet flows to the enucleation operation area. Subsequently, after the microrobots perform the enucleation process, the oocyte is delivered to the dispensing module. Finally, the oocytes are retrieved by a custom-designed culture vessel.

4.2 Methods and Concepts

Figure 4.3 shows the proposed system, which comprises a coplanar capacitive sensor and a deceleration area with a circular array of micropillars. This oocyte ejection system is

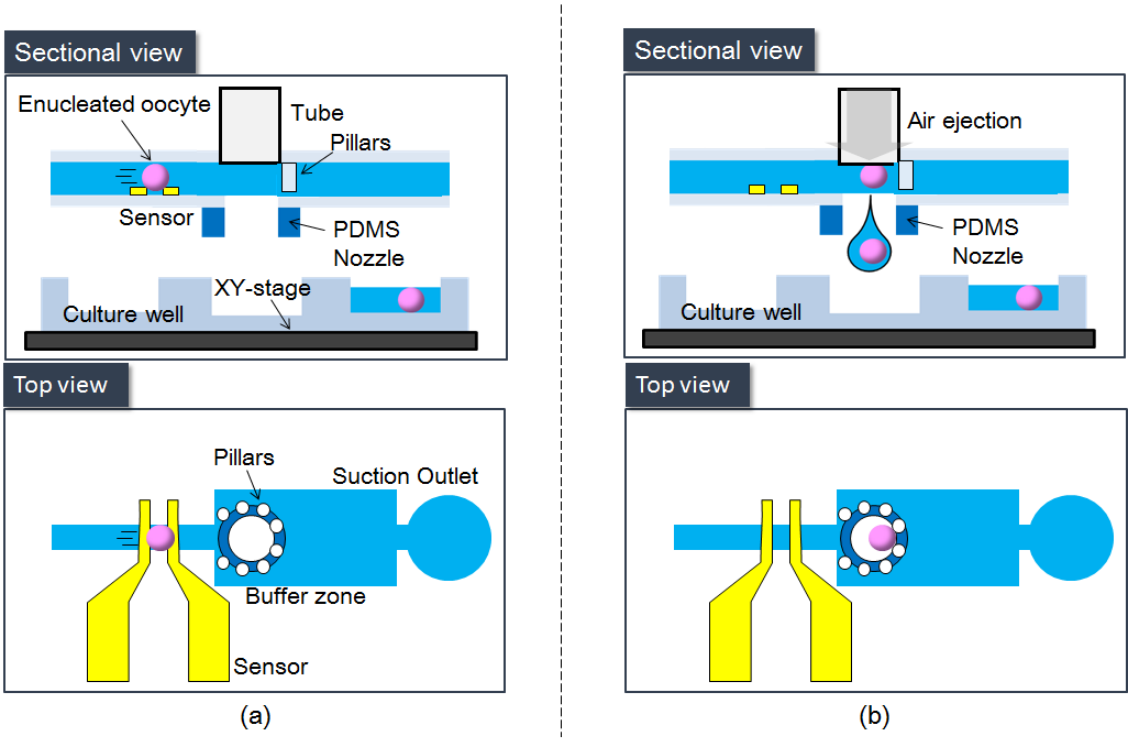

Figure 4.3 Basic concept of the on-chip oocyte dispensing system. (a) Oocyte detection. (b) Oocyte obstruction and dispensing.

fabricated from polydimethylsiloxane (PDMS); hence, any risk of contamination is avoided because such a microfluidic chip is disposable.

4.2.1 Capacitance sensors

To eject a single oocyte into each hole of the culture well, a sensor is required for accurate detection. To achieve accurate single-oocyte ejection, Previously a pair of capacitance sensors was on a microfluidic chip and placed a pair of electrodes in the microchannel so that a microsensor could be used to measure the flow velocity [177][178].

A pair of coplanar electrode sensors were fabricated on the outlet microchannel at the substrate which could work as detector using for oocyte detection. When an oocyte passed

through a pair of microsensor in the microchannel, a change in capacitance could be detected by the difference in permittivity between the oocyte and the culture medium. The microsensor sensed the change in the differential capacitance and provided an output voltage proportional to the change of capacitance. As shown in Figure 4.4, we assumed that two coplanar and semi-infinite conducting films separated by the gap distance of *2a* which were embedded within a uniform dielectric medium of permittivity ε_r, and each held at a constant potential $\pm V_o$. The capacitance of an electrode pair of finite width *w*, could be estimated by the following equation [179]

$$C = \frac{Q}{2V_0} = \frac{2\varepsilon_r \varepsilon_0 l}{\pi} \ln\left[1 + \frac{w}{a} + \sqrt{\left(1 + \frac{w}{a}\right)^2 - 1}\right] \tag{4.1}$$

where *C* is the capacitance, *Q* is the total charge on a single electrode, and V_o is constant potential held at the electrode pair, ε_0 is the vacuum permittivity, *w* is an electrode pair of finite width and *l* is the length of the electrode pair for $l >> w$. Therefore the capacitance changes by the different fluidic materials as their electric permittivity ε_r is different.

In Figure 4.4, *T* was the field penetration depth, *w* was the conducting plates of finite width, and *u* was the embedded load voltage in a dielectric liquid. In the microfluidic chip, the *T* is determined firstly, therefore the capacitance was only determined by those permittivity of different materials, and the permittivity changes causing a voltage changes is detected for sensing the oocyte passing or not.

The great advantage of the capacitance sensor is that it can rapidly sense the oocyte without a visual system. In those studies, an oocyte delivered by a culture medium was detected by measuring the impedance changes between two electrodes. The signal was then demodulated by a lock-in amplifier to yield the impedance change due to passage of the oocyte. However,

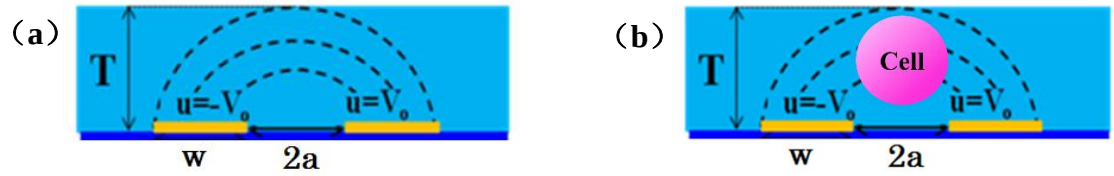

Figure 4.4 Concept view of capacitance corresponding to a pair of semi-infinite electrode. (a) Electric field, (b) electric field with oocyte in.

the noise signal of the capacitance sensors greatly interfered with the normal signal; at the same time, the sensitivity of the capacitance sensor decreased accordingly once the flow velocity increased. Therefore, the success rate of single-particle dispensing could only reach 50%. In the newly developed system, the sensitivity of the microsensor has been improved by reducing the size of the microchannel; the width and height were reduced from 800 μm and 300 μm, respectively, to 200 μm for both dimensions. Whereas the occupied oocyte volume ratio at the sensing area was merely 2.45% in the previous system, it increased to 14.7% in the new system. Therefore, the change in permittivity at the sensing area becomes more distinct. Although the sensitivity may be increased further by reducing the channel size, there is a limit because the size of an oocyte is normally around 150 to 180 μm. The maximum amplitude of oocyte detection increases by 16.7 times from 15 mV in the previous system to 250 mV in the current system. Figure 4.3 (a) shows an oocyte passing through the capacitance sensor.

4.2.2 Deceleration and obstruction mechanism

The success rate of our previous system in dispensing microbeads was low not only because of the low sensitivity of the sensor. Kawahara et al. [177] used two pairs of sensors to estimate the flow velocity in the previous system. Owing to the large variation in the estimated velocity for calculating the timing of ejection, however, their method only achieved a success rate of

50%. In the newly developed system, a deceleration chamber is established in the microchannel and 50-μm micropillars are arranged into a circular shape to block the oocyte at the dispensing nozzle. An oocyte with the zona pellucida (ZP) is normally 150 μm in diameter; therefore, the distance between each pair of micropillars is set to 50 μm to block the oocyte successfully. Figure 4.3 (b) is a sketch of an oocyte blocked by the micropillars. This mechanism works extremely well with the deceleration module in the developed system.

4.2.3 Air-flow-based inkjet mechanism

We use an air-flow-based inkjet system involving a high-speed solenoid valve with a maximum drive frequency of 500 Hz. When the solenoid valve is briefly opened, air force is applied to the microchannel (Figure 4.3 (b)). The oocyte is then ejected to the culture well [177].

In the following section, we describe the design and fabrication method for a high-accuracy single-oocyte dispensing mechanism by considering the characteristics of the system components.

4.3 Microchip Design and Fabrication

4.3.1 Microchannel design

Figure 4.5 shows the entire single-oocyte dispensing system. Figure 4.5 (a) shows the top view of the dispensing area, where D_s, D_D, D_p, and D_C are the width of the microsensor, width of the microchannel, distance from the microsensor to the center of the nozzle, and width of the deceleration microchannel, respectively. Figure 4.4 (b) shows the side view of the dispensing system, where D_N, D_i, D_W, D_T and T_N are the diameter of the nozzle, distance between the microchip and the culture well, diameter of a single vessel, distance between the sensor and the

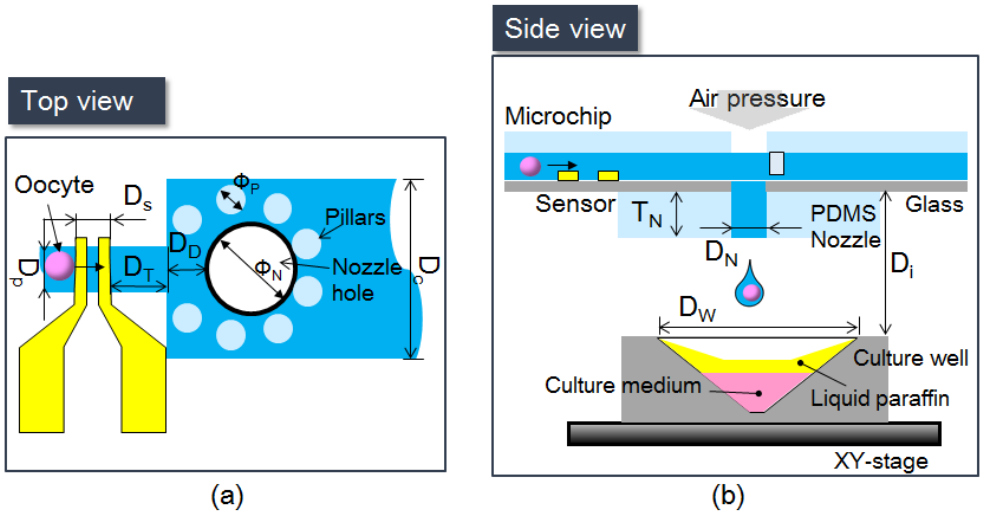

Figure 4.5 Design parameters of the dispensing system. (a) Schematic diagram of microchannel viewed from above. (b) Side view of the dispensing system.

deceleration microchamber, and thickness of the nozzle, respectively. The width of a branch of the microsensor is set to 100 μm with a distance of 100 μm between each pair of branches.

In current system, the time required for enucleation is at least 10 s for a single oocyte. Hence, our current goal is to sense and dispense one oocyte in 10 s. To this end, the length of the dispensing microchannel is set to 1 cm and the flow velocity to 1 mm/s. and distance between the microsensor and the deceleration microchamber is set to 0.5 mm. Thus, in one minutes we can dispense 6 oocytes. However, from the sensor to the dispensing nozzle, theoretically it only takes 0.63s, therefore, for the other applications this system can achieve almost 95 oocytes sensing and dispensing per minute. Because an oocyte is softer without zona pellucida (ZP) than with it, the flow velocity should differ between these two cases. As noted above, the width and height of the microchannel are set equally to 200 μm. The diameters of the nozzle and pillar are 500 and 100 μm, respectively. To block the oocyte successfully, the distance between each pillar is set to 50 μm. The oocytes, which are delivered by flow, are

detected when they pass through the sensor. After an oocyte is stopped by the pillars and the air dispenser triggered, the XY-stage with the culture well is moved to the position corresponding to the nozzle position to retrieve the oocyte.

One innovation in this study is the deceleration module. Because the parameters of the microchannel are fixed, the flow distribution in the microchannel has been analyzed by using COMSOL Multiphysics 4.3. An oocyte is elastoplastic; therefore, in the case of high flow velocity, it could be deformed and flushed through a gap between the pillars [180]. Two approaches have been used for the current oocyte enucleation process: one with ZP, and the other without it. An oocyte with ZP has a much higher Young's modulus (22.8 ± 10.4 kPa) than that without ZP [181]. The Young's modulus is difficult to measure in the latter case because the oocyte becomes soft and sticky on the surface. Here, we conducted preliminary experiments to find the optimum flow velocity.

First, we investigated the minimum flow velocity that safely stops an oocyte by micropillars without obviously deforming it. Excessive deformation of an oocyte may harm it

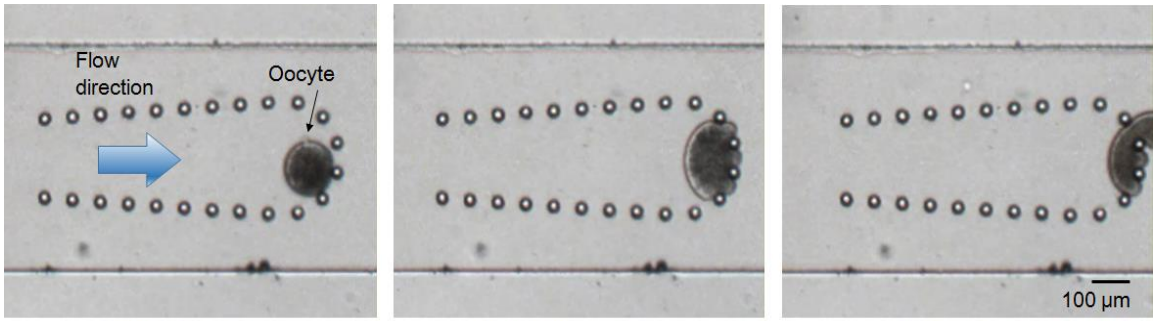

(a) V_1= 0.67 mm/s Case 1 (b) V_2= 0.74 mm/s Case 2 (c) V_3= 1.37 mm/s Case 3

Figure 4.6 Initial investigation of oocyte deformation by hydraulic pressure in microchannel.

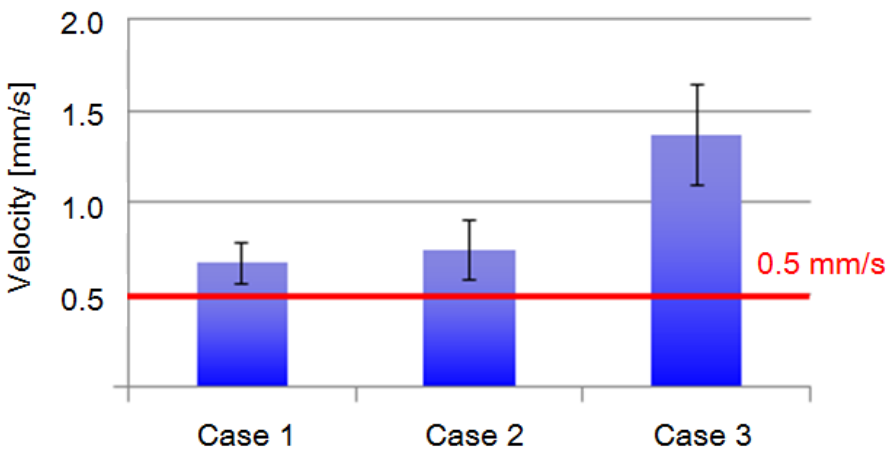

Figure 4.7 Experimental results under three different cases.

and affect its ensuing proliferation and division. Figure 4.6 shows three typical examples in a preliminary test at velocities of 0.67, 0.74, and 1.37 mm/s. In Case 1 (low flow velocity, 0.67 mm/s), an oocyte could be blocked without any obvious changes in its circular shape. When the flow velocity increased to 0.74 mm/s (Case 2), the oocyte was distinctly deformed. When the flow velocity further increased to 1.37 mm/s (Case 3), the oocyte was deformed and flushed away by the flow.

These results reveal that the maximum flow velocity must not exceed 0.6 mm/s. After analyzing 15 oocytes for each case and removing deviations in the data, a velocity of under 0.5 mm/s was set as the maximum velocity for blocking an oocyte without ZP (Figure 4.7). To determine the microchannel design for decelerating the flow velocity from 1 to 0.5 mm/s, a two-dimensional structure was modeled using COMSOL Multiphysics 4.3 to analyze the flow condition in the microchannel. The flow in the microchannel changed dramatically from the narrow channel (width: 200 μm) to the wide channel (width: 800 μm). At the intersection of the channels (x = 0.8 mm), the flow velocity decreased sharply (Figure 4.8).

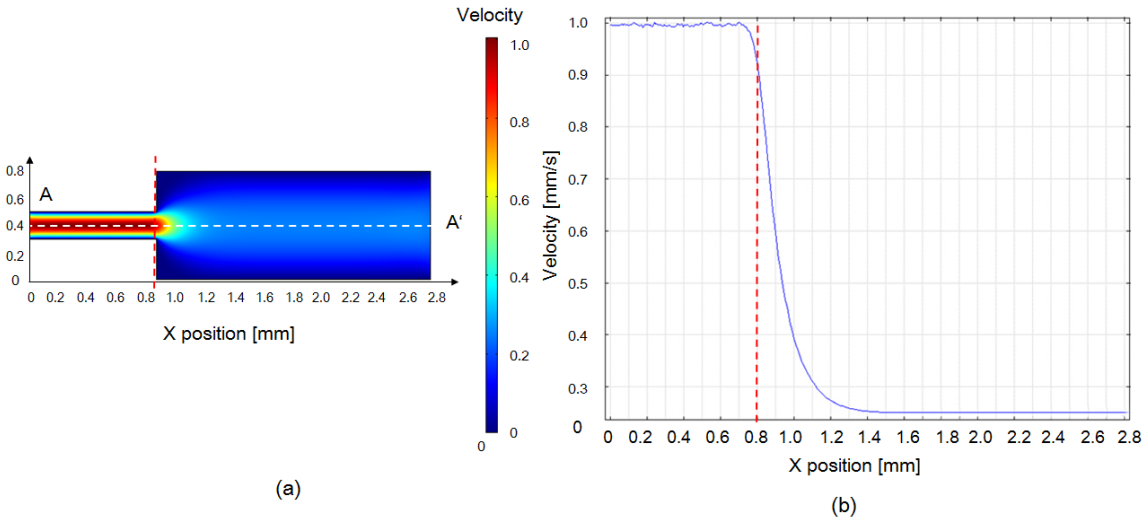

Figure 4.8 FEM results of velocity distribution in the microchannel. (a) Velocity distribution. (b) Flow velocity curve (A-A').

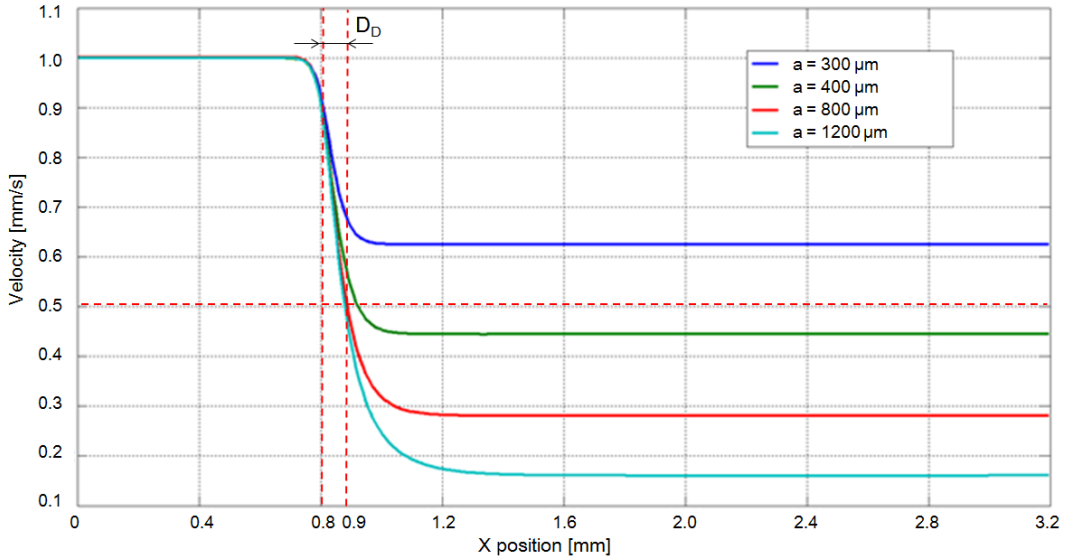

Figure 4.9 FEM results of velocity changes with microchannels of different width (a: width of deceleration channel).

The FEM simulation results suggest that to achieve a flow velocity of 0.5 mm/s, the width of the microchannel should be increased to at least 400 μm. Although the flow velocity

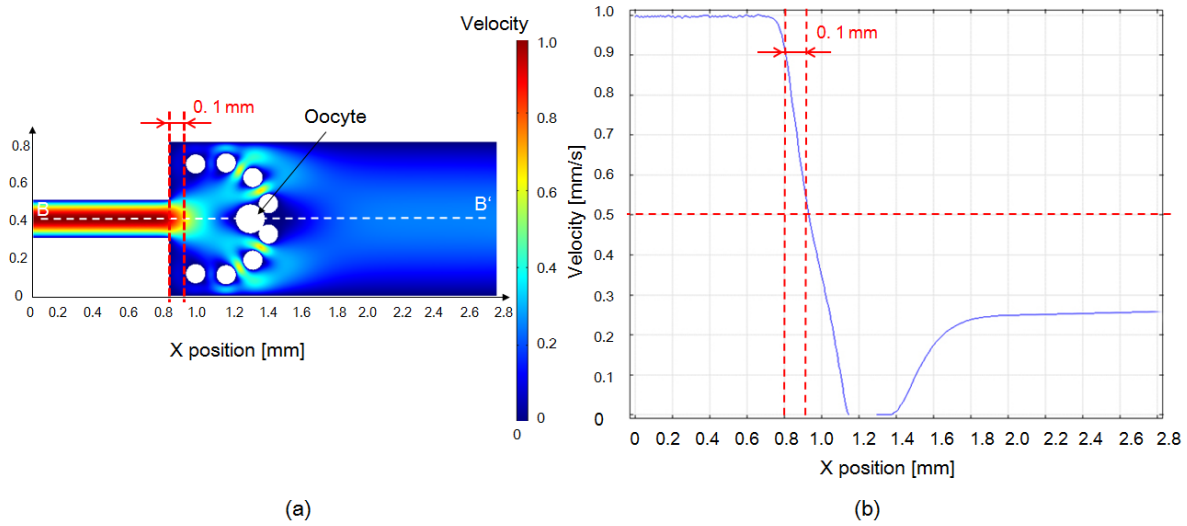

Figure 4.10 FEM results of velocity distribution in the microchannel. (a) Velocity distribution. (b) Flow velocity curve (A-A').

significantly decelerated when the width was increased to 800 μm, the rate at which the velocity decreased was not markedly different even when the width of the microchannel was increased to 1200 μm (Figure 4.9). Meanwhile, the nozzle hole should be placed with 0.1mm distance from the intersection. Therefore, in our experiments, we selected an 800-μm-wide microchannel for oocyte deceleration. Moreover, the velocity was noticeably reduced in the simulation results with the oocyte and pillars shown in Figure 4.10. The velocity decreased under 0.5 mm/s from the distance of more than 0.1 mm. Therefore, oocyte under the velocity of 0.5 mm/s makes it feasible that the pillars could block the oocyte successfully, and the pressure acting on the oocyte was released. As mentioned earlier, the stiffness of an oocyte with ZP is greater than that without ZP. Even when the flow velocity was increased to 60 mm/s, oocytes with an intact ZP were still blocked by pillars without deformation.

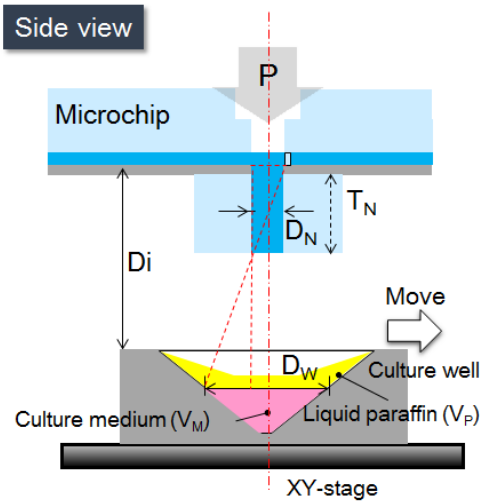

Figure 4.11 Design of nozzle and parameters of current structure.

4.3.2 Design of dispensing nozzle

In our system, we use a high-speed solenoid valve. Air pressure is applied to the microchannel when the solenoid valve is briefly opened, and a minimum pressure of 1 kPa is achieved. The surface tension of the liquid is the main force that prevents leakage, because the dispensing hole is always open. Although this suggests that a higher surface tension can generate a higher force to maintain the air-liquid interface in balance, a higher surface tension also implies that a higher air pressure is required for dispensing, which may increase the risk of unintended damages to the oocyte. For this reason, we explain how to determine the size of the dispensing hole and thickness of the nozzle. The surface tension at the nozzle hole is

$$\Delta p = \gamma\left(\frac{1}{R_1} + \frac{1}{R_2}\right) = \gamma \times \frac{4}{D_N} \tag{4.2}$$

where Δp is the maximum surface tension of the air-fluid interface, γ is the surface tension, and R_1 and R_2 are radii of curvature ($R_1 = R_2 = \frac{1}{2} D_N$). Ideally, increasing the diameter of the dispensing hole should make it easier to dispense the oocyte. However, the surface tension

should also be considered to prevent leakage. A minimum nozzle hole of 0.5 mm could be achieved with the current fabrication technique. The values of surface tension Δp are 0.58 and 0.29 kPa in cases where the diameters of the dispensing hole are 0.5 and 1 mm, respectively. The dispensing hole with a diameter of 0.5 mm is more appropriate because the dispensing air pressure is 1 kPa.

The diameter of each retrieving vessel, D_W, is 2 mm. To prevent the oocyte from being sprayed out of the vessel, the thickness of the nozzle is set to

$$\frac{D_N}{\frac{1}{2}D_W - \frac{1}{2}D_N} = \frac{T_N}{Di - T_N} \tag{4.3}$$

Table 1 Parameters of dispensing system

Parameter	Value
D_N	0.5 mm
T_N	0.7 mm
D_i	3 mm
D_W	2 mm
V_P	10 μl
V_M	3 μl
P	1 kPa

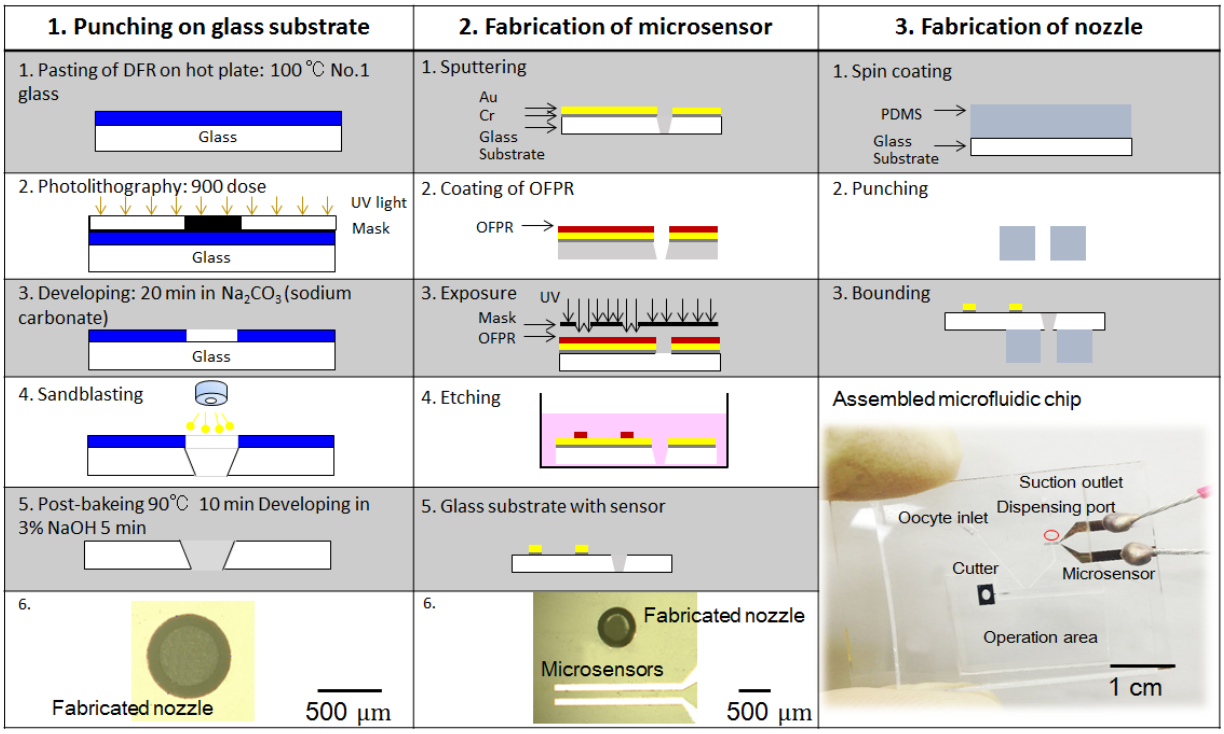

Figure 4.12 Fabrication process of microchip.

4.3.3 Fabrication of microfluidic chip

According to calculations, the minimum thickness of the nozzle should be 667 μm. In the experiment, we set the nozzle thickness to 0.7 mm (Figure 4.11). All parameters are shown in Table 1. The liquid paraffin can prevent evaporation of the culture medium and is non-toxic. The fabrication process for the microchip, which involves integrating a nozzle hole and two pairs of capacitive sensors, can be summarized as follows (Figure 4.12):

Step 1: To fabricate the dispensing hole, a positive photoresist—a 50-μm-thick dry film resist (DFR; Asahi Kasei Co., Tokyo, JAPAN)—was pasted onto the prepared 0.12-mm-thick glass substrate. After h-line (λ = 405 nm) exposure of the DFR, a hollow circle was developed by using a sodium carbonate solution for 20 min at 26 ℃. By using the sandblast technique, we fabricated a hole on the glass substrate. Finally, a NaOH solution was used to remove the

remaining photoresist. After Step 3, a 0.5 × 1 × 0.7 mm PDMS nozzle was attached to the glass substrate.

Step 2: To fabricate the capacitive sensors, layers of 30-nm-thick Cr and 300-nm-thick Au were sputtered onto the prepared glass substrate. Next, OAP (Tokyo Ohka Kogyo) was spin-coated for 30 s at 2000 rpm to bond the posi-resist onto the glass substrate and baked for 2 min at 90 ℃. Then, the positive photoresist, OFPR (Tokyo Ohka Kogyo), was spin-coated for 30 s at 2000 rpm and baked for 30 min at 90 ℃. After h-line (λ = 405 nm) exposure of the OFPR, the sensor pattern was developed by NMD-3 (Tokyo Ohka Kogyo). Subsequently, the Au and Cr layers were wet etched, and OFPR was removed by acetone. Finally, the electrode on the glass was wired with Ag paste.

Step 3: A microfluidic chip consisting of a PDMS microchannel was bonded to a glass substrate. A PDMS microchannel was produced by replica molding with a master mold fabricated by photolithography. Ultraviolet light was irradiated through a photomask to produce a microchannel pattern with a mask aligner (LA410, Nanometrich Technology Inc., Tokyo, Japan). The substrate was then developed and rinsed. We employed SU-8 film (DuPont Co., Wilmington, DE, USA) and exposure to produce the microchannel in the microfluidic chip.

Disposable microfluidic chip was used to prevent contamination after experiments that lasted 2–3 h.

4.4 Experiments

4.4.1 Experimental setup

For the setup, we used a Teflon tube to connect the microchip and silicone tube (Figure 4.13). This prevents air leakage between the microchip and the silicone tube, because the Teflon

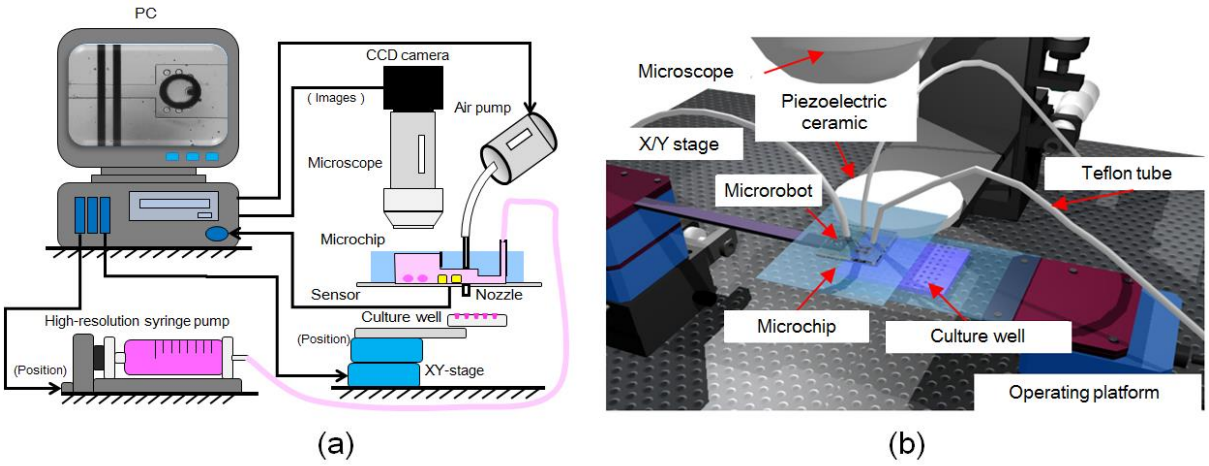

Figure 4.13 Components of the experimental system. (a) Experimental setup for dispensing oocytes, which includes a solenoid valve, chip holder, culture well, and camera. (b) Architecture of the three-dimensional rendering system.

tube is reasonably stiff and the input pressure is not excessively high (~10 kPa). The diameter of the air inlet (air hole) is 0.5 mm and the outer diameter of the Teflon tube is 1.0 mm.

The system comprised a PC, solenoid valve, chip holder, culture well, and camera. By using the camera, we could observe delivery of the oocyte to the dispensing area. The position of the culture well was controlled by a motorized XY-stage. Measurements of the sensor outputs, timing of ejection, and signals sent to the solenoid valve, in addition to position control of the culture well, were performed with a computer. For the initial detection step, we used a digital lock-in amplifier (LI 5640, NF Corporation) with the following settings for the sinusoidal waveform to the microsensor: output voltage (*Vp-p*), 0.5 V; frequency, 10 kHz; and time constant, 30 μs. We obtained the voltage value under flow with an oocyte in the microchannel. To dispense the oocytes stably, we typically used 1 kPa air pressure and a 1 ms delay, on-time signal processing to the solenoid valve. A high-resolution syringe pump connected to the microchip was used to control the flow velocity in the microchannel.

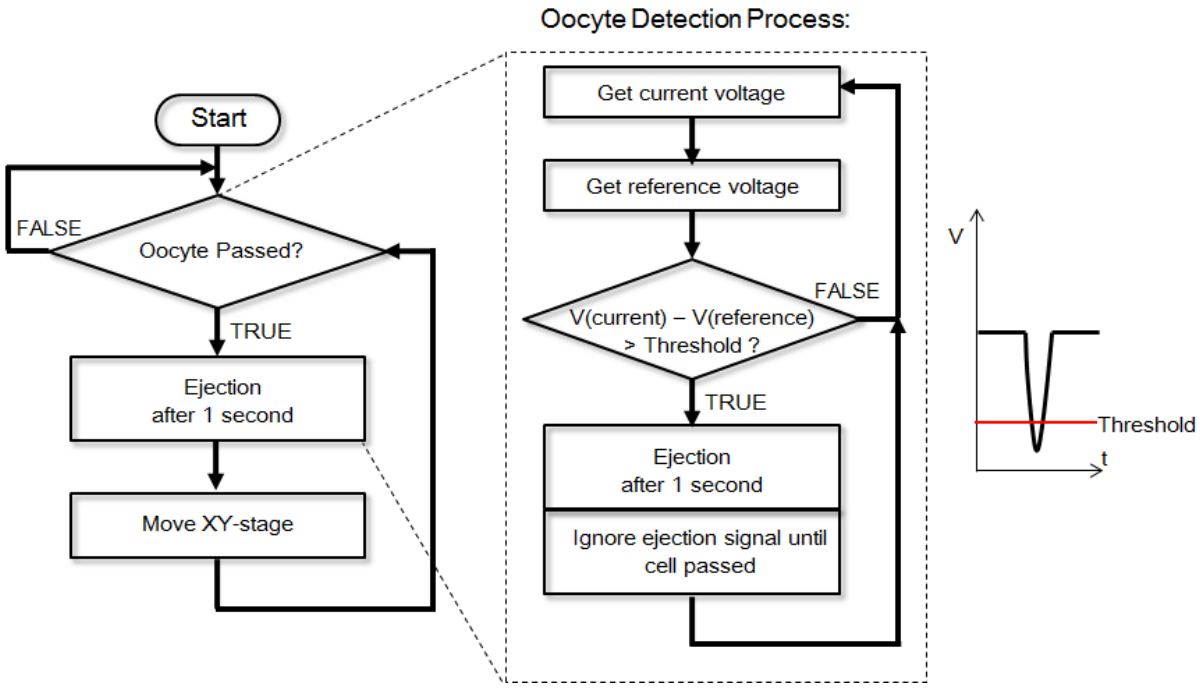

Figure 4.14 Flowchart for oocyte detection.

4.4.2 Oocyte-dispensing experiments

Figure 4.14 shows the detection, ejection, and retrieving processes. In the beginning, a signal is sent to the computer if an oocyte passes the sensor, and after a 1-s delay, the PC opens a solenoid valve and dispenses the oocyte. To determine the arrival of an oocyte, the voltage signal is continuously recorded and compared with the reference voltage. Once a wave trough is detected, the PC sends a command to open the solenoid valve, and the oocyte is dispensed to the culture well.

The oocytes were obtained from Livestock Improvement Association of Japan Inc. Tokyo, Japan. Before the experiments, bovine oocytes were prepared in advance with hyaluronidase (0.1% of TCM 199) for 10 min to remove the cumulus cells surrounding the oocytes. After this manipulation, each oocyte was delivered to the dispensing area by flow suction from the outlet

(Figure 4.15 (a)). The oocyte was then passed through the microsensor (Figure 4.15 (b)). After flowing into the deceleration microchamber, the oocyte suddenly slowed down and was blocked by the micropillars at the nozzle hole. Finally, the air pump ejected the oocyte to the culture

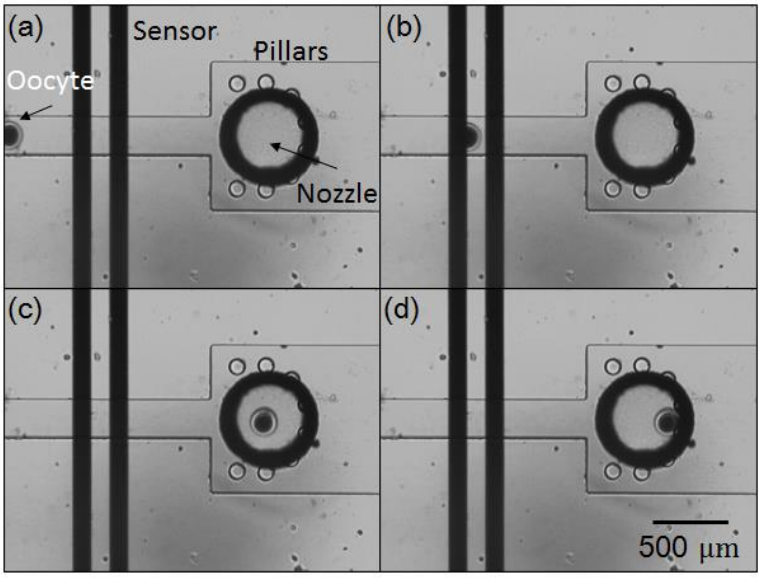

Figure 4.15 Experiment showing detection, deceleration, and obstruction (by micropillars) of an oocyte.

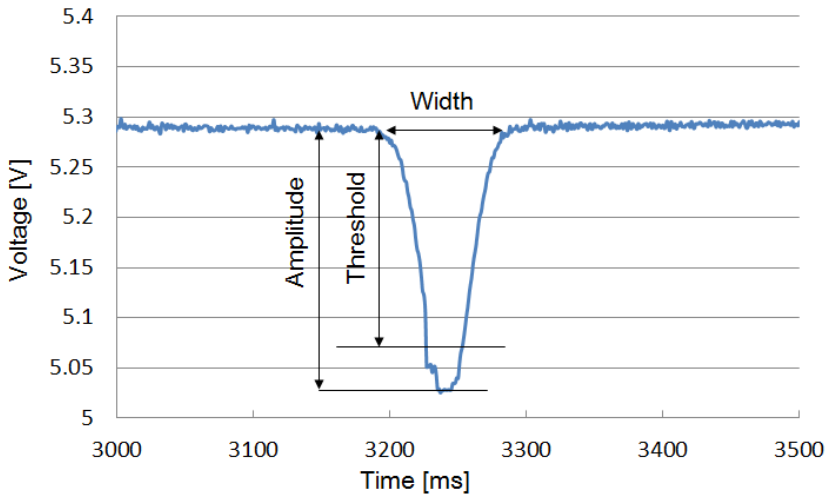

Figure 4.16 Detection of oocyte passing through the microsensor.

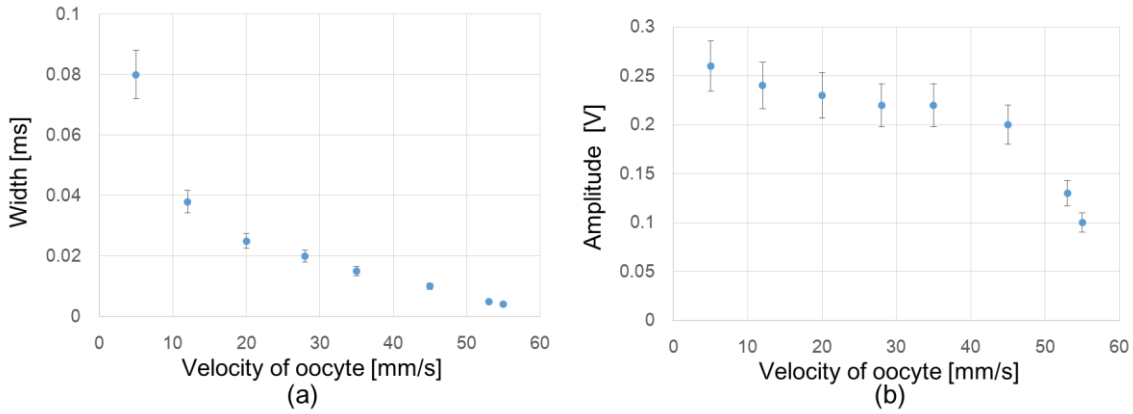

Figure 4.17 Detection of oocyte according to its velocity.

environment. To investigate the success rate, the experiments were conducted during three different days with three different PDMS chips. Totally we tried 60 oocytes for dispensing, and all of the dispensed oocytes were retrieved. Therefore, we claim that the success rate after repeating 60 dispensing experiments was 100%.

Figure 4.16 shows a typical experimental result of oocyte detection. The threshold was determined experimentally to 0.25 V. From the voltage changes in the sensor outputs, the passage of the oocyte could be detected.

In accord with Figure 4.16, the graphs in Fig. 4.16 shows the evaluated signal changes in both the width and the aptitude due to the change in flow velocity. Figure 4.17 (a) shows that the width of the detected signal decreased by increasing the flow velocity. At the same time, the amplitude of the detected signal also decreased by increasing the flow velocity. The system could detect oocytes up to a maximum velocity of 55 mm/s.

Figure 4.18 shows a representative dispensing result. In this experiment, we used a 3 cm × 3 cm culture well with vessels 4 mm in diameter (Figure 4.18 (a)). After the dispensing process,

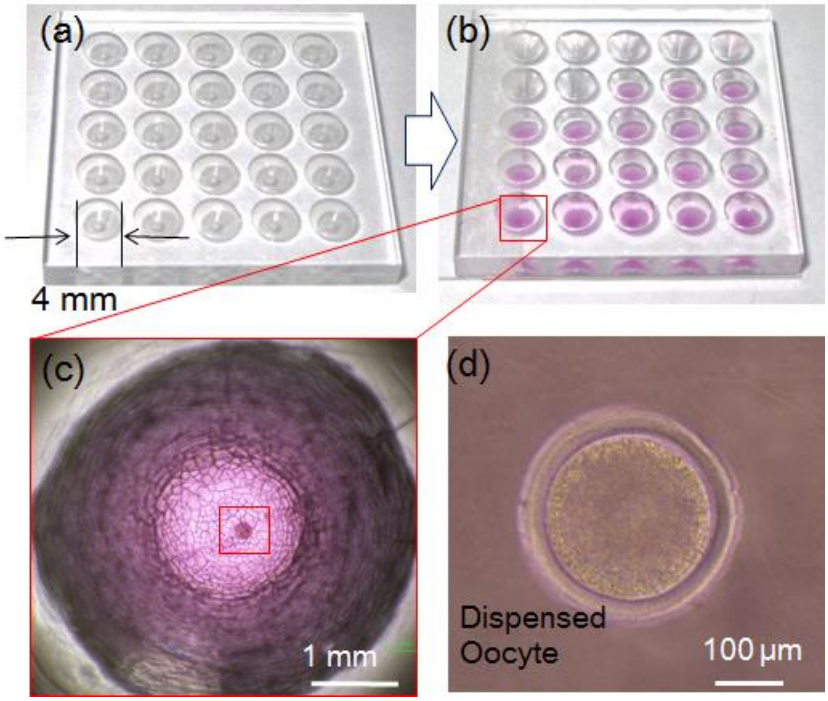

Figure 4.18 Experimental result of dispensing.

each vessel with the pink medium contained a single oocyte (Figure 4.18 (b)). The oocyte could be observed clearly in magnified views of the vessel (Figure 4.18 (c, d)).

4.4.3 Viability evaluation

Dispensed oocytes were washed with Medium 199 without FBS (Fetal bovine serum) (Gibco Co., Tokyo, Japan) twice to remove any paraffin residue; they were then washed with three droplets of 10 µM Ca ionophore (Calbiochem Co., Darmstadt, Germany), which included m-PBS (Medium 199 without FBS) prepared in a dish, by transferring them to three separate droplets each time. The latter process was carried out within 5 min to prevent degradation due to light. The oocytes were then washed with three droplets of 6-Dimethylaminopurine (6-DMAP) (Sigma Co., Tokyo, Japan), which included Medium 199 (with FBS), and incubated in

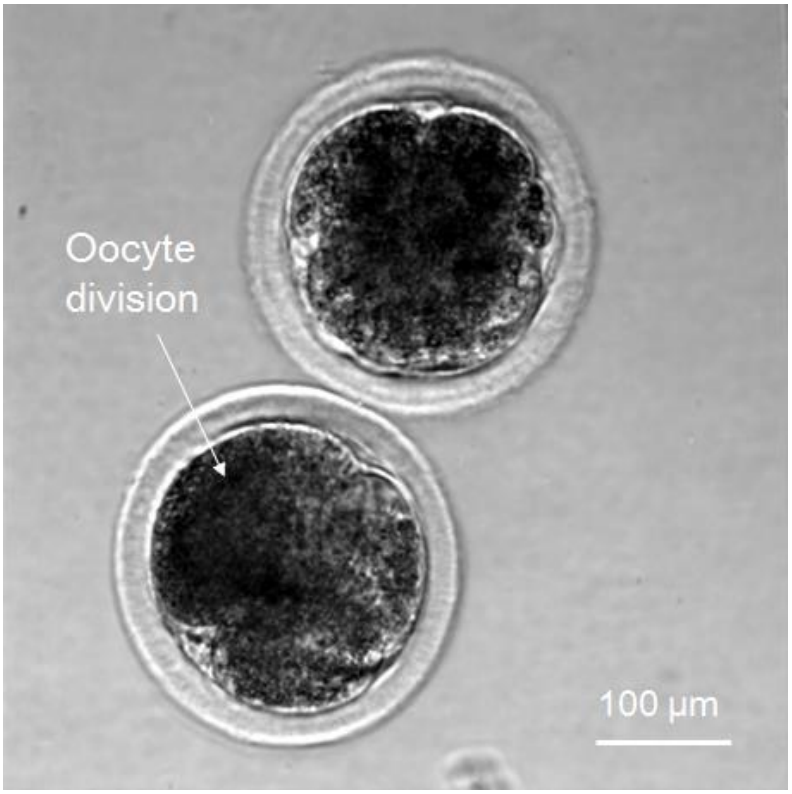

Figure 4.19 Division of dispensed oocyte in viability test.

5 ml of the same reagent for 4 h. Subsequently, the oocytes were transferred to IVD-101 (IFP Co., Yamagata, Japan) and incubated for over 20 h. Finally, we observed oocyte division (Figure 4.19). To investigate the viability rates before and after the dispensing procedure, we separated the oocytes into two groups, one was experimental group, and the other one was control group. We randomly picked 31 oocytes for the control group. These oocytes have been treated in the same way as the dispensed oocytes for the viability test. Among these 31 oocytes, we observed 22 oocytes division by using microscope. Meanwhile, 32 oocytes were selected from experimental group, 22 oocytes division have been observed by microscope. Therefore, the viability ratios of the oocytes before and after dispensing were 71% and 69%, respectively. This suggests that the dispensing process is non-harmful to oocytes.

4.5 Summary

A new scheme that involves the use of microsensors for detection and deceleration with micropillars for oocyte dispensing has been demonstrated. This system, which is specifically used to dispense single oocytes, is composed of a capacitance sensor, a deceleration module, and micropillars for stopping the oocytes. Design and fabrication strategies to increase the success rate of dispensing were also demonstrated. Through simulations and calculations, we characterized a prototype of this system. Furthermore, in preliminary experiments, we confirmed the characteristics of the system components and determined the parameters of microchip design. Subsequently, we demonstrated that by using this newly designed system, the success rate of dispensing oocytes greatly increased to 100%. Finally, through viability tests that compared the viability ratios before and after dispensing, we found that the dispensing process had no adverse effects on oocyte viability.

This system will be highly useful for cell dispensing and that similar system, in combination with the on-chip oocyte enucleation process, could usher in a new era of newly improved cloning techniques.

Chapter 5.

Three Dimensional Oocyte Orientation Control

5.1 Introduction

Cellular study demands a range of techniques for manipulations of single cells. For instance, in the early-stage of cloning, the nucleus should be removed from the oocyte with low invasion. Cutting volume shows great effects on the viability of the subsequent fertilization [151], [162], [182]. Meanwhile, in the genetic studies, the characteristics of zona pellucida (ZP) and spindle

of embryo cell, for example retardance measured by polar scope shows great influences on the quality of the oocyte for artificial insemination, stem cell research, and clinical in vitro fertilization procedures. These cellular operations target specific cellular orientation, requiring the oocytes to be noninvasively rotated in three dimensions for properly orienting target cell organelle for manipulations.

Cell orientation control in most research works and clinical applications has been conventionally performed by skilled operator. Observing by a microscope, operator uses a micropipette by repeated aspirating and releasing accordingly until the cell organelle becomes visible. Due to the low controllability, such kind of manual 3-D rotation method is a trial-and-error procedure [183]. A number of approaches have been reported in the literature for rotating single cells. Many non-contact forces can be applied to the cell manipulations, Optical tweezers use a focused laser beam to manipulate microscopic objects is an optional approach [184]–[188], However, the optical tweezers technique is limited to rotating a cell about one axis. Dielectrophoresis (DEP) uses a nonuniform electric field to exert forces on cells and has been utilized for small size cell rotation [189]–[191], however it has also been shown that the electric fields required for DEP to rotate cells can cause significant cell damage [192]. Especially for a big size cell, like oocyte it is difficult to operate, due to the diameter of oocyte is normally over 150 μm [193]. Sun et al. introduced a three-dimensional rotation of mouse embryos by using a standard holding micropipette to generate a fluidic flow to rote the oocyte [194]. However for single oocyte rotation it takes around 40 sec, and also this approach is still operating in an open space, which may easily cause contaminations to the cell environments. Previously we developed an enucleation approach, which can achieve the oocyte enucleation process without ZP [195], and even enucleation with ZP by using micro gripper by Ichikawa et al. [164].

However, both of these enucleation processes cannot achieve the oocyte orientation control. In oocyte enucleation process, the nucleus position is critical. The oocyte should be well rotated letting the nucleus facing to the cutter, for the removed volume of cytoplast is to be as small as possible since removed volume of cytoplast is critical for the consequential oocyte viability. And also in intracytoplasmic sperm injection, the polar body of the oocyte must be oriented away from the penetration side in order to prevent the damage to the oocyte. Here we introduce an on-chip oocyte orientation control method by using MMT in a closed space. By custom designed fork shaped MMT, the oocyte could be rotated in three dimensions with a high angular velocity, and with high operability.

Robots on a chip have great advantages for the treatment of biological cells instead of human handling due to its non-skill dependent, high throughput and high repeatability. Magnetic field can be a suitable power source for the on-chip robot because of its non-contact drive; low invasiveness with respect to a cell, and low production cost [80], [155]. As described in the previous chapters, magnetically driven microtools (MMTs) which can be applied to a wide range of cell manipulations. A permanent magnet possesses a magnetic field that drives an MMT with 10–100 times more force than an electromagnetic coil of the same size, effortlessly causing the output of mN-order forces. In order to reduce the effective friction of the MMT significantly, we arranged permanent magnets parallel to the driving plane, and also piezoelectric ceramics were employed on the drive plane to induce ultrasonic vibrations so that the effective friction reduced significantly [134]. As a result, we achieved 1.1 μm-order positioning accuracy while maintaining a mN output force. However it is difficult to handle the oocyte to control its posture and remove the nucleus part since the oocyte is operated in an unconfined space. Once the tip of the MMT blade touched the surface of the oocyte, as an

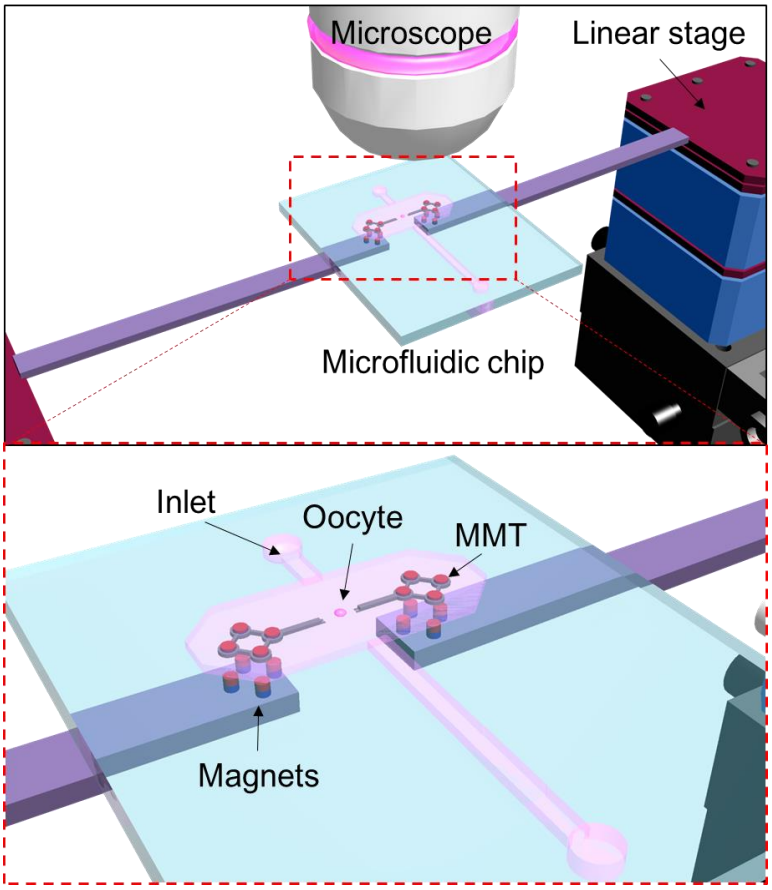

Figure 5.1 Conceptual overview of the oocyte manipulation by the MMTs in a microfluidic chip. The MMTs are actuated by permanent magnets.

oocyte is soft and sticky, a resistance force generated by the oocyte decreases the position accuracy, significantly. Currently, in ensuring the driving accuracy is not changed, both of actuation method and type of MMT have been improved, the output force is further increased from 20 mN to 44 mN, these improvement makes the new system much more robust on big cell operation like oocyte manipulation.

Herein, we describe an improved driven method for an MMT driven by vertically set permanent magnets with a precise positioning accuracy in the order of micrometres, and new driven method generates stronger output force from the permanent magnets. Figure 5.1 shows

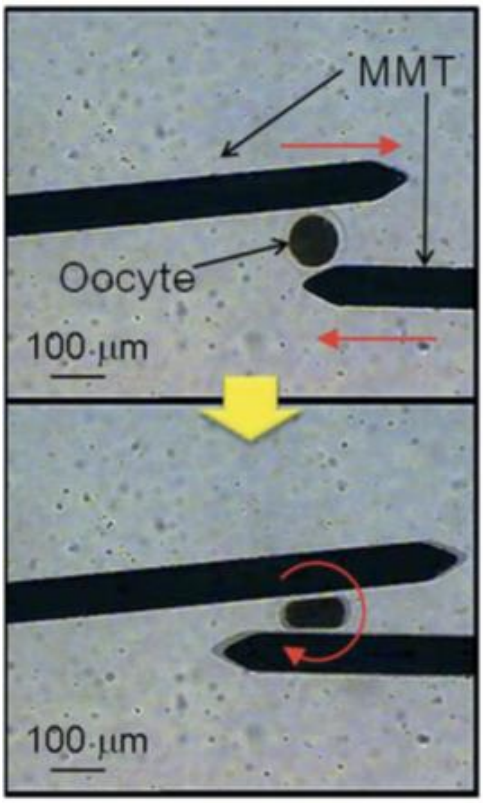

Figure 5.2 Oocyte rotation by dual-arm MMT [134].

the conceptual overview of the cell manipulation by the MMTs. The MMTs are placed in a microfluidic chip and actuated by permanent magnets set on linear stages. Then, the MMT manipulates the inserted cells under the microscope just like a micromechanical manipulator does, but the size of the microchip and the MMTs are significantly smaller, and the risk of contaminations are less than a micromechanical manipulator owing to the closed space of the microfluidic chip.

5.2 X/Y Plane Rotation of Oocyte by Using MMT

In the previous study, we have already achieved the two-dimensional rotation of oocyte,

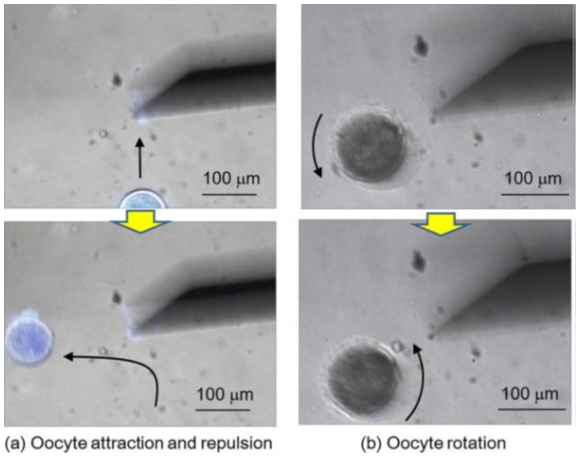

Figure 5.3 Bovine oocyte manipulation using the streamline: (a) Attraction and repulsion, (b) Rotation [196].

Hagiwara et al. using dual-arm MMT and succeeded in rotate the oocyte in X/Y plane [134] (Figure 5.2). Subsequently, Hagiwara et al. proposed another approach on rotation of oocyte in X/Y plane, by using high frequency vibration of MMT, the oocyte could be rotated without touching of the oocyte surface [196]. However, the controllability is quite low and even it is hard to estimate. And also, rotation in three dimensional is impossible by using this approach.

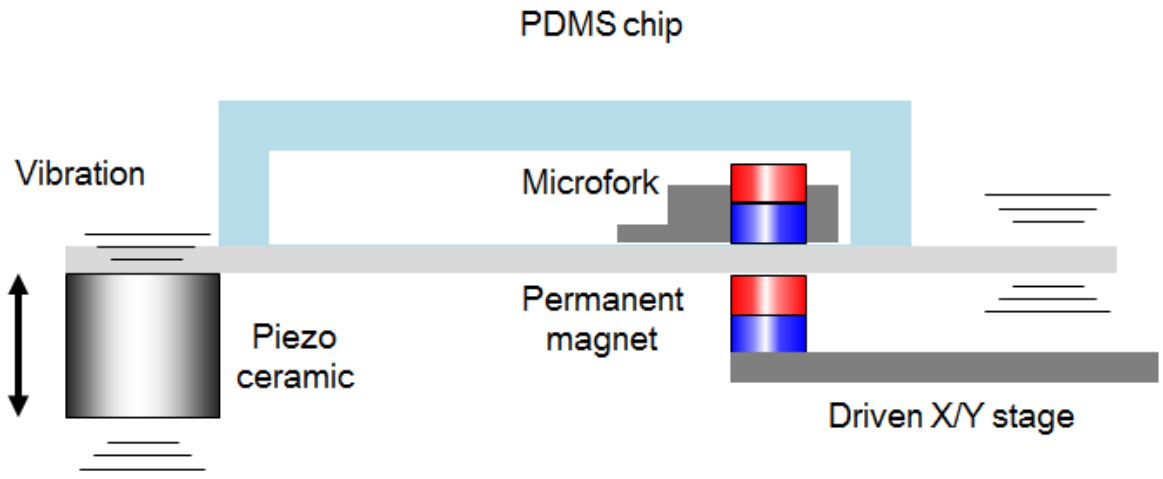

Figure 5.4 Driven concept of the MMT actuated by permanent magnet with ultrasonic vibration. Oscillating the glass substrate by the piezoelectric ceramic reduces the effective friction on the MMT.

5.3 Methods and Materials

5.3.1 Driven Concept of MMT

In order to achieve the high speed and high accuracy three dimensional rotation of the oocyte, the previous driven methods [134] are unsatisfying. Here, an improved driven method is proposed with equally high accuracy but higher output force. Figure 5.4 shows the new driving concept of the MMT with ultrasonic vibration. Radially displaceable piezoelectric ceramic is attached to the glass substrate under the microfluidic chip and oscillates the glass substrate vertically. When ultrasonic vibration ranges from ten thousand to a million times per second is applied to a surface vertically, the effective friction of the contact surface between the moving object and glass surface decreases significantly [197]–[199]. The MMT is actuated by permanent magnets whose axis is set to the horizontal direction and the permanent magnet is placed vertically on the 2-DOF linear stage.

5.3.2 Fabrication of the microfork

Figure 5.5 shows the fabrication process of microfork. At first, the photoresist OFPR (Tokyo Ohka Kogyo Co.) was coated on the substrate. After the exposure on the OFPR side, the OFPR pattern was developed. Next, deep reactive-ion etching (DRIE) was conducted from the OFPR side, and silicon is etched to a depth of 125 μm. We again conducted the OFPR coating on the opposite side of the silicon, and do the other patterning, and exposure, after DRIE process to form the MMT shape. At last, φ0.5 mm ×0.5 mm permanent magnets are assembled to shape MMT. SEM photos shows the two-time DRIE process fabricated Microfork.

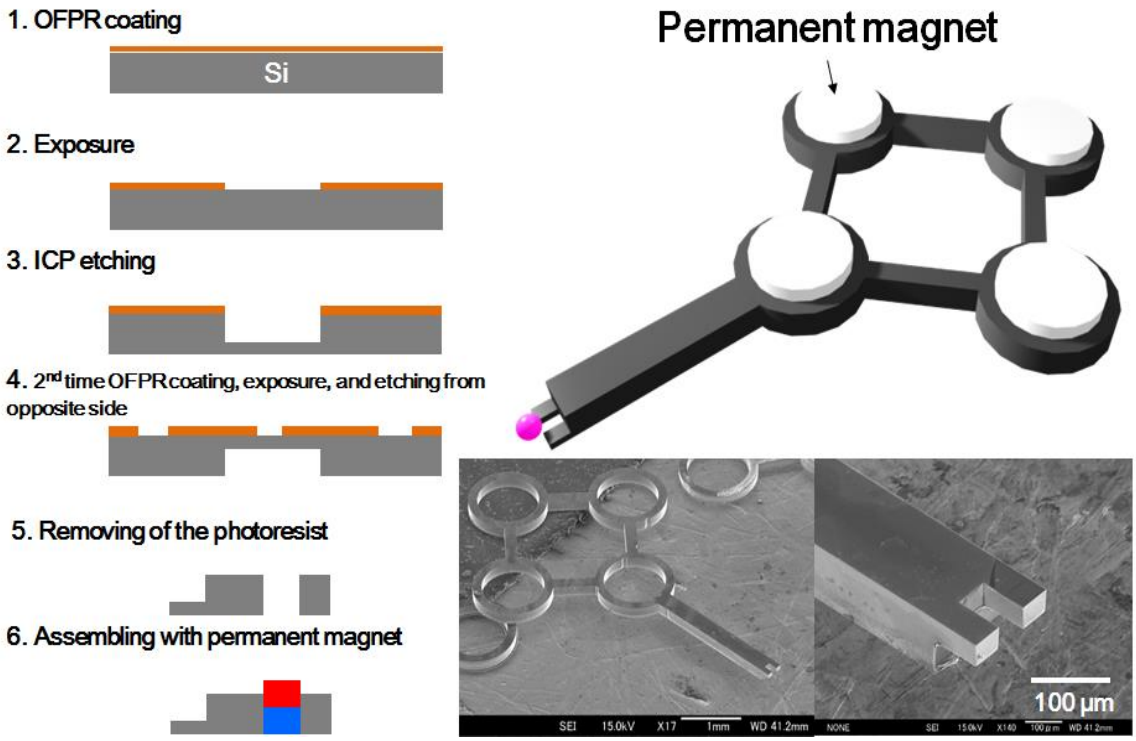

Figure 5.5 Fabrication process of the microfork.

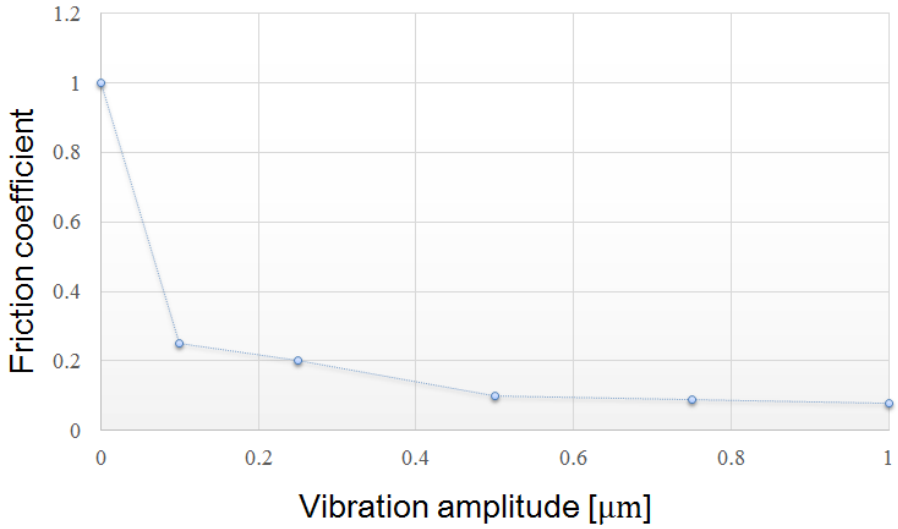

Figure 5.6 The relationship between the vibration amplitude and friction coefficient reduction (Frequency: 127 kHz, Voltage: 15 V).

5.3.3 Evaluation of the New Driven Method

An experiment was conducted in order to evaluate the effect of the vertical vibration and the reduction of the friction force. The linear stage was actuated in a circular trajectory with a constant drive velocity and the corresponding MMT positions were measured by CCD camera. Figure 5.6 shows the relationship between the vibration amplitude and friction coefficient reduction. By continuously increase the amplitude the friction coefficient reduced significantly, this phenomena could be used in the driving of the MMT. By utilizing this driven method, plenty of experiments are conducted to find the driven accuracy and output forces.

Figure 5.7 shows the positioning accuracy of the MMT with vibration by piezoelectric ceramic against the target circular trajectory. By testing various thickness of the glass, the positioning accuracy are different. The position accuracy of the MMT is quite different when

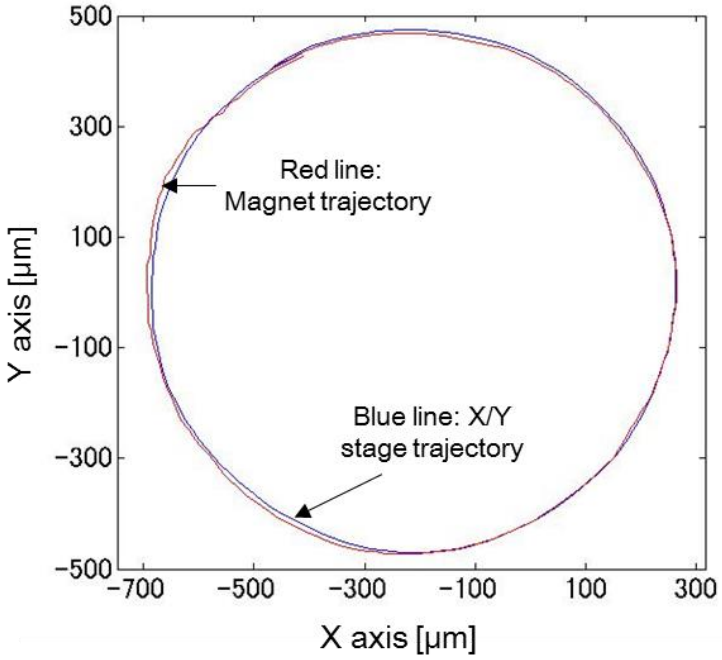

Figure 5.7 Positioning accuracy of the MMT with vertical vibration from piezoelectric ceramic. (glass thickness: 300 μm, frequency of the piezoelectric ceramics: 127 kHz, amplitude of vibration: 1 μm).

applying the vertical vibration or not. Figure 5.8 shows the results of control accuracy difference, it can be easily find out that the position accuracy increased significantly when the vertical vibration applied on the microfluidic chip. The output force of the MMT is also experimentally evaluated by the loadcell (LVS-5GA, Kyowa Electronic Instruments Co. Ltd). Figure 5.9 shows the output forces of the MMT with and without ultrasonic vibration respectively. The output force of the magnet type of MMT with ultrasonic vibration (15Vp-p, 127 kHz) increased twice as much as the previous nickel type of MMT with vibration for friction reduction. Comparing to the previous result, the output force of the current MMT is considerably higher with millinewton force. Increasing the capacity of the maximum force enables the MMT to be applied to the force

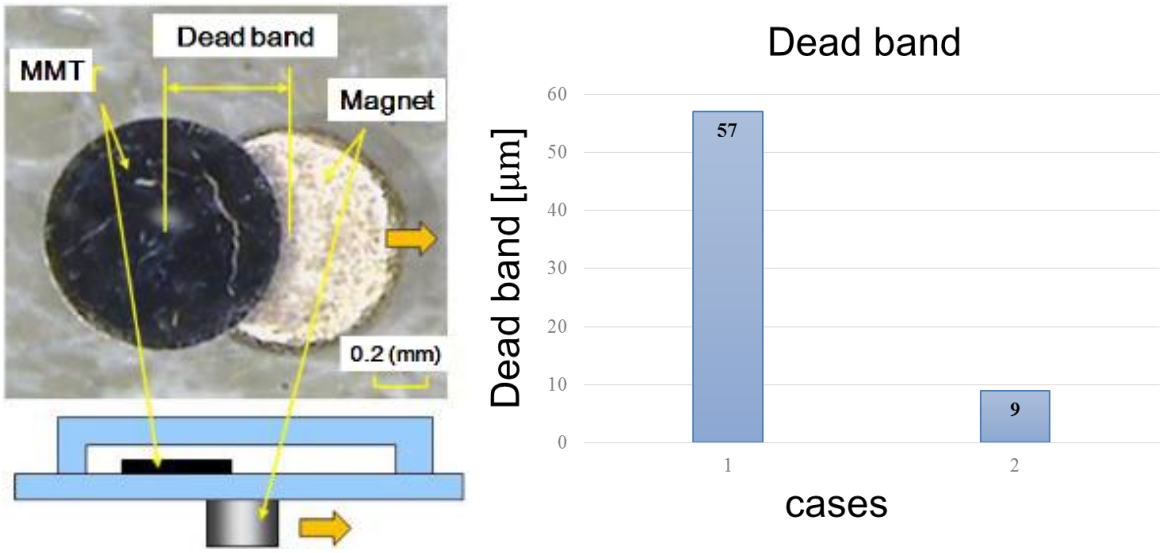

Figure 5.8 Deadband reduction. (a) Illustration of dead band, (b) Reduction of dead band. (case 1: without vibration, glass thickness: 300 µm, case case 2 with vibration, thickness 300 µm).

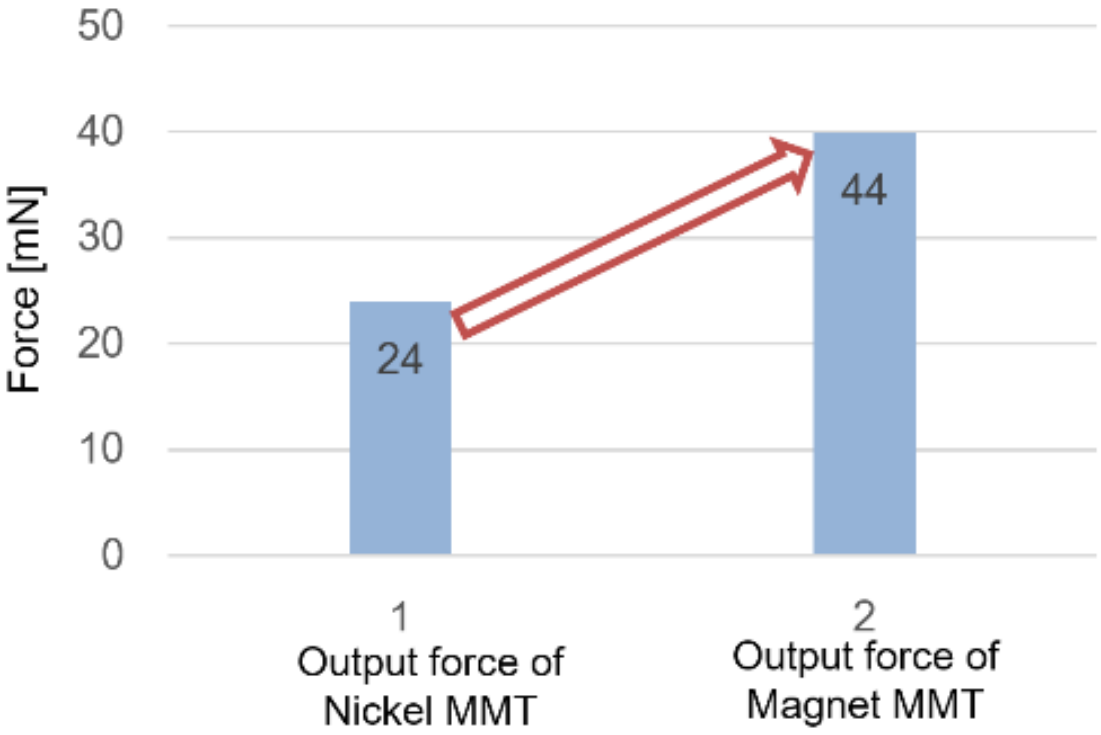

Figure 5.9 Improvement of new driven method increased the output force by 20 mN.

requirement tasks, like oocyte orientation control, and also by utilizing current setting a cell operation becomes easier, like enucleation.High power output and precise positioning accuracy allows the MMT to be employed in a wide range of applications like commercialized micromechanical manipulators. From the Figure 5.9, as can be seen, the output force increase twice and achieve to 44 mN, which means the scope of the manipulations of cell has been increased. The differences are that the size of the manipulator is tiny for the MMT and it can be actuated in a microfluidic chip. A closed environment supplies the less disturbance atmosphere to prevent cell contamination and miniaturization of the manipulator leads to the high throughput of the operations.

5.4 Three-dimensional rotation of oocyte

5.4.1 Concept and methods

Here, we propose a new rotation approach by using MMTs, by custom-designed fork shape of MMT with step structure on the tip of the MMT, 3-D rotation of oocyte becomes possible. Figure 5.10 shows the concept of the 3-D rotation of an oocyte. In order to achieve simple rotation of oocyte, we assume a pure rolling simple model shown in Figure 5.10. Due to the oocyte is an elastoplastic matter, and the operation environment is in the culture medium, the shear force cause by the fluid is hard to estimate, and both the stiffness and the surface condition of oocyte are important parameters on oocyte rotation, therefore, according to the above analysis, the most important parameter is to reduce the friction force generated at the time that MMT is touching the oocyte. Under the same load, the friction can be reduced by reducing the pushing contact area, therefore the friction force can be reduced, accordingly. Hence, in the rotation experiment, microfork structure has been customer-designed, only letting two tips

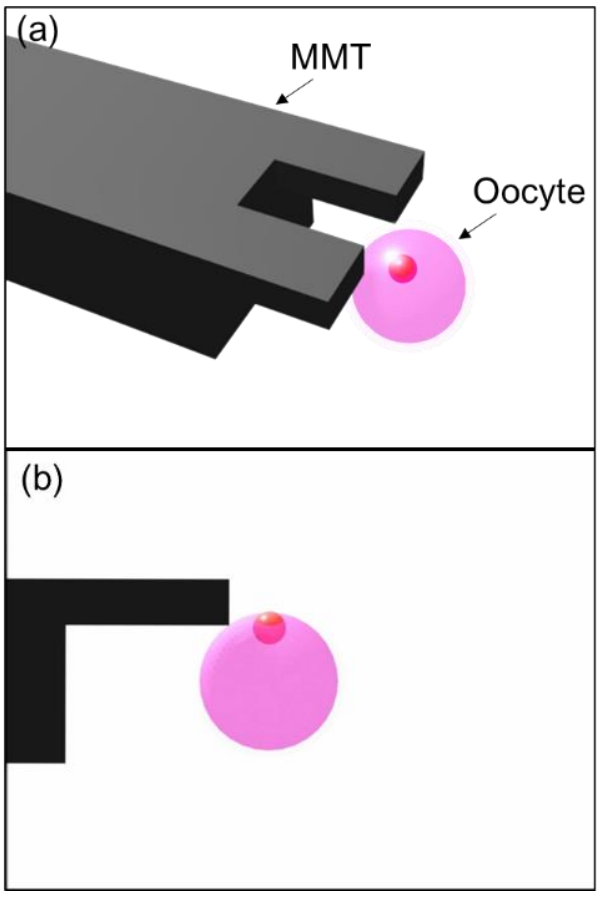

Figure 5.10 Concept of three dimensional oocyte rotation by MMT-fork, (a) overview of the oocyte rotation concept, (b) Side view of oocyte rotation.

touching the oocyte on pushing the oocyte to rotate.

Actually, in the rolling phenomena, there are two classic types, one is pure rolling, and the other is non-pure rolling. The pure rolling means there is no relative motion between contact-surface, on the contrary, the non-pure rolling has a relative motion between the contact-surface. And also, during the rotation, oocyte is soft, it can be easily deformed, therefore, two different rolling case are discussed here, 1) pure rolling, 2) rotation with oocyte deformation.

Case 1: in Figure 5.11 (a) as the sphere with a radius R does the pure rolling, assuming the

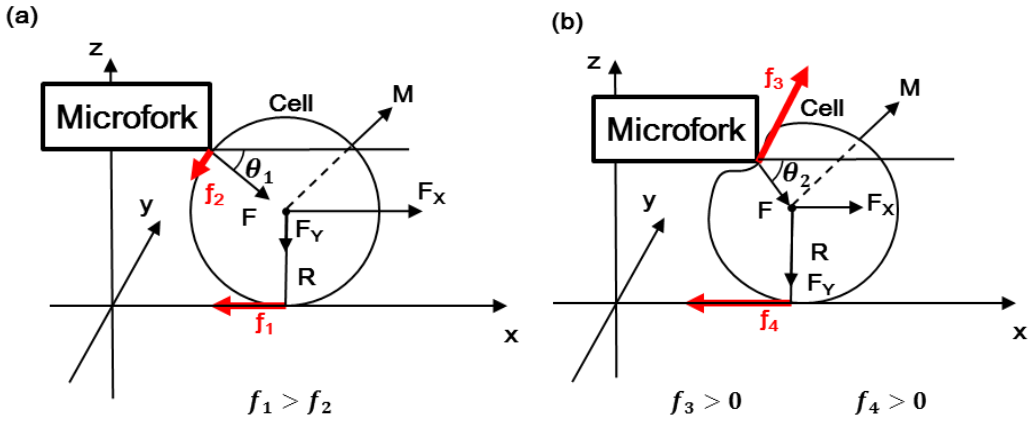

Figure 5.11 Analysis of rolling dynamics, (a) Pure rolling model, (b) rotation with oocyte deformation.

average velocity is v_c and the sphere is rotate around the rotating axis, the angular velocity is $v_c = R\omega$; by taking the derivative of the time, the relation between the axis acceleration ac and angular acceleration $\dot{\omega}$ is $a_c = R\dot{\omega}$. Therefore the kinematic condition of pure rolling are:

$$v_c = R\omega,\ a_c = R\dot{\omega} \tag{5.1}$$

Further simplify the oocyte rotation model shown in Figure 5.11, assume the resultant force is F_x, and the resultant moment is M_y, and the friction moment is $M_f = M_{stastic} + M_{rolling}$, therefore the kinematic acceleration on axle center is:

$$\ddot{x_c} = \frac{F_x + f}{m} \tag{5.2}$$

The rotation acceleration around the axis:

$$\dot{\omega_y} = \frac{M_f + M_y}{I} \tag{5.3}$$

Base on the pure-rolling condition, we can get:

$$\frac{F_x + f}{m} = \frac{M_y + M_f}{I} R \tag{5.4}$$

Where m is the mass of the object, I is the moment of inertia, R is the radius of sphere. The

condition of an object doing the pure-rolling is:

$$f_{max} \geq \left| \frac{m(M_y + M_f)R - IF_x}{mR^2 + I} \right| \tag{5.5}$$

Which means that the static friction force should be smaller than the maximum of the static friction. Therefore the friction generated by MMT should be considerably small. Microfork with two tiny tips touching on the oocyte surface, this permits that the friction force generated by MMT is considerably small when pushing the oocyte to rotate.

Case 2: at the case of oocyte rotation with deformation (Figure 5.11 (b)), oocyte pushed by the tip of MMT is deformed, hence $\theta_2 > \theta_1$, and F_y becomes greater than in case 1, which increases the friction force for the rotation by force f_3 and f_4, In this case, the performed rotation is with the same mechanism when rotating in X/Y plane by dual arm MMT [134].

Both of these two cases of oocyte rotation have been achieved, which will be introduced in the following experimental section.

5.4.2 Oocyte rotation experiments

Figure 5.12 shows the oocyte rotation in vertical direction. In the figure, the sphere object is the bovine oocyte. At the beginning the microfork close to the oocyte, in order to observe the oocyte rotation vividly a track point has been marked, and then MMT tried to get the axle of the oocyte in horizontal direction. By pushing from the side of the oocyte, the oocyte could be rotate in the vertical direction. Continuous pushing of the oocyte, it can rotate 180 degrees by utilizing MMT in just 3.4 sec. By pushing from the two opposite directions the oocyte can rotate in both clockwise and anticlockwise from the bottom up perspective side view.

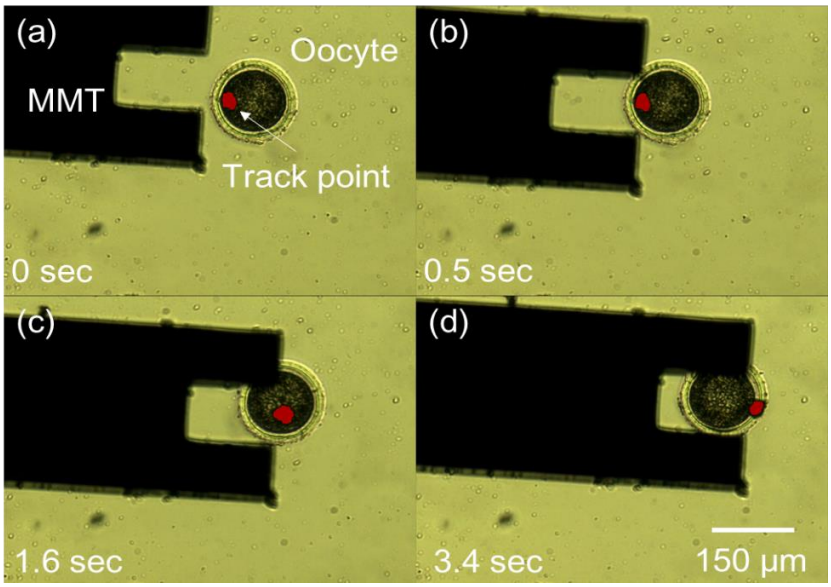

Figure 5.12 Oocyte rotation by using MMT microfork.

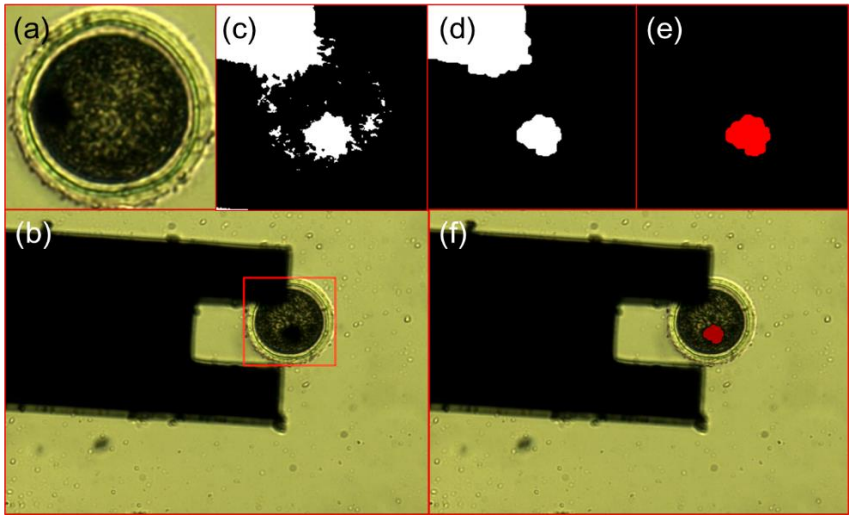

Figure 5.13 Image data processing, a) Template image for cell, b) Detected cell using template matching, c) Threshold image of cell, d) Clearing the noise using morphological operations e) Removing MMT part from the image f) Final image masked with track point.

5.4.3 Oocyte rotation evaluation

In order to do the data processing for calculation of the angular velocity of the oocyte rotation we need to detect the position of the tracking point. The steps of the algorithm can be found in

Figure 5.13. First we detect the position of the cell using template matching. The bovine oocyte image has been selected as a template for template matching, which is done in RGB image. After finding the location of the template in image we crop a slightly larger patch from the image for the rest of the algorithm. Patch is first transformed into gray scale image; thereafter in order to distinguish the tracking point on the oocyte, a threshold applied to the gray scale image and a binary image is obtained. A morphological opening operation (erosion and dilation of the binary image) is performed to remove noise and small particles that presented in the image. All other components of the embryo, such as the zona pellucida and the cytoplasm, are removed from the binary image. At this point only tracking point and the part of the MMT remain in the binary image patch. While tracking point must be somewhere close to the middle of the patch, MMT must be connected to the boundaries of it. Using connected components labelling, we first label different regions in the image. Regions which are connected to the boundary of the image is considered as part of the MMT, and thus removed from the image. Only remaining region is considered as tracking point, finally its gravitation center is taken as its position.

Figure 5.14 shows the model on how to use the X/Y plane position coordinate to estimate the Z value of Z axis in Cartesian axes. In order to calculate the oocyte rotation velocity, images are got from the top view by microscope, therefore, as the oocyte radius R can be measured from the image, generally 150 μm, according to the Cartesian coordinates values, we could derive the coordinate value of Z on the spherical surface,

$$Z = \sqrt{R^2 - (X^2 + Y^2)} \tag{6}$$

as $\vec{p} = (X_1, Y_1, Z_1)$, $\vec{q} = (X_2, Y_2, Z_2)$, the great circle distance L can be derived,

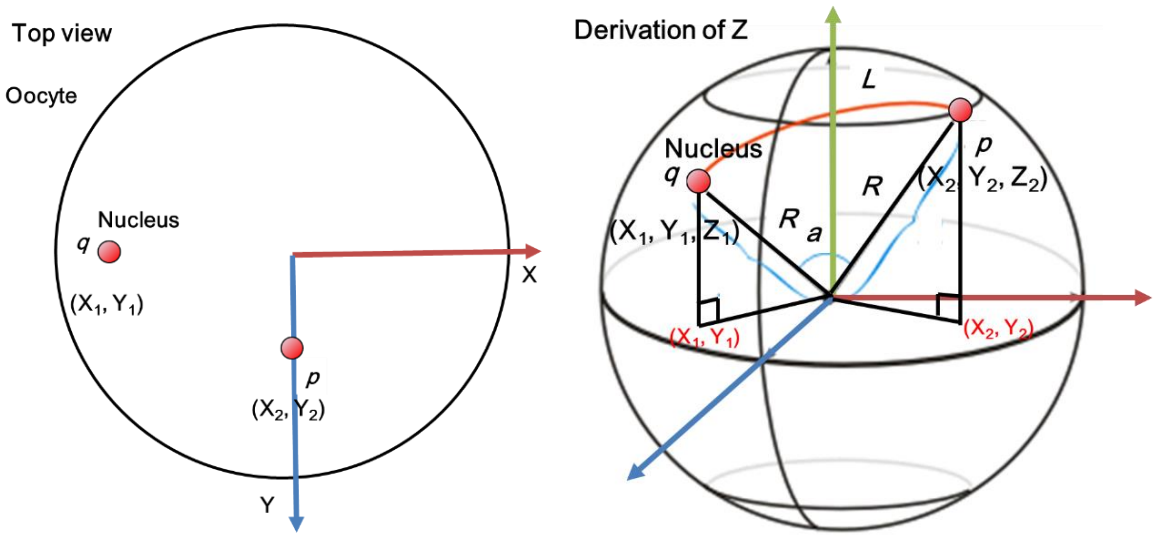

Figure 5.14 Derivation algorithm of tracking point position estimation.

$$L = \frac{\pi R}{180} arccos\left(\frac{\vec{q}\cdot\vec{p}}{|q||p|}\right) \quad (7)$$

the angular velocity of oocyte $w = L/T$, where T is the rotation time.

Figure 5.15 shows the rotation angular velocity of the oocyte can be controlled by changing the velocity of manipulated MMT at the case of pure rolling of oocyte. In current MMT system, the move speed of MMT can achieve up to 300 μm/s visibly. Basing on the moving speed of MMT, we could achieve the angular velocity of oocyte up to 3 rad/s and 2.8 rad/s in vertical orientation and horizontal orientation, respectively at the pure rolling case. And in the case two (Figure 5.15 and Figure 5.16), the rotation speed also can reach to 3 rad/ s and because the oocyte is elastoplastic, during the manipulations the MMT slightly deformed the oocyte, therefore when pushing vertical way, the oocyte slipped under the tip of the MMT. That sliding friction may happen to be what causes the small difference in the rotation velocity between vertical rotation and horizontal rotation. Additionally, the surface of the oocyte is sticky due to the cell secreted protein, which may influence rotation speed. But never the less, current system

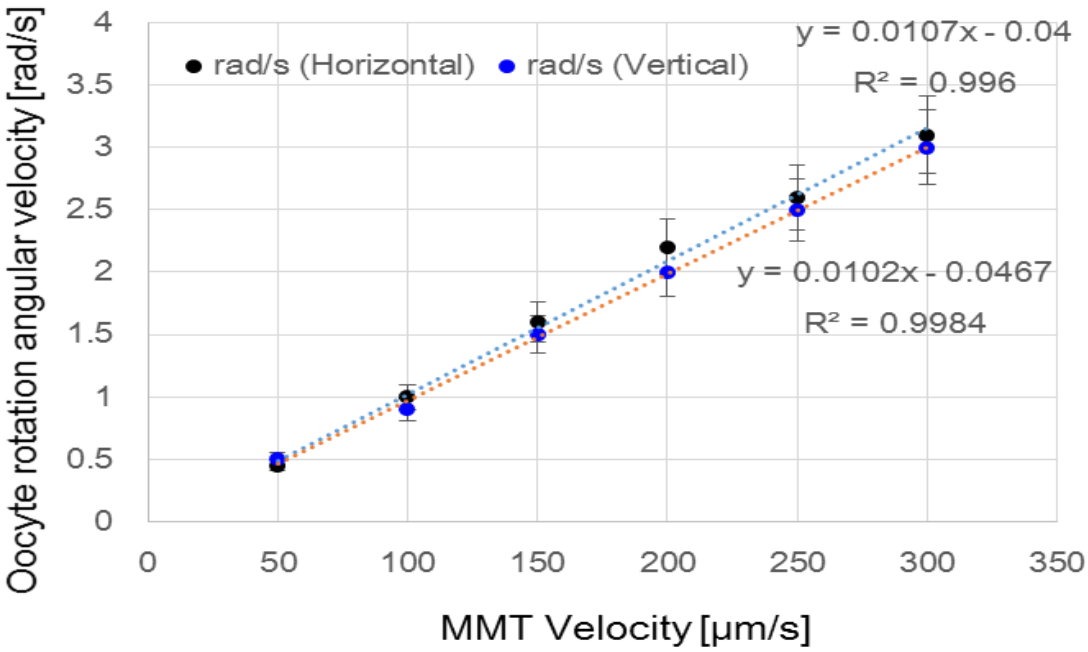

Figure 5.15 Oocyte rotation angular velocity according to the MMT velocity at the case of pure rolling.

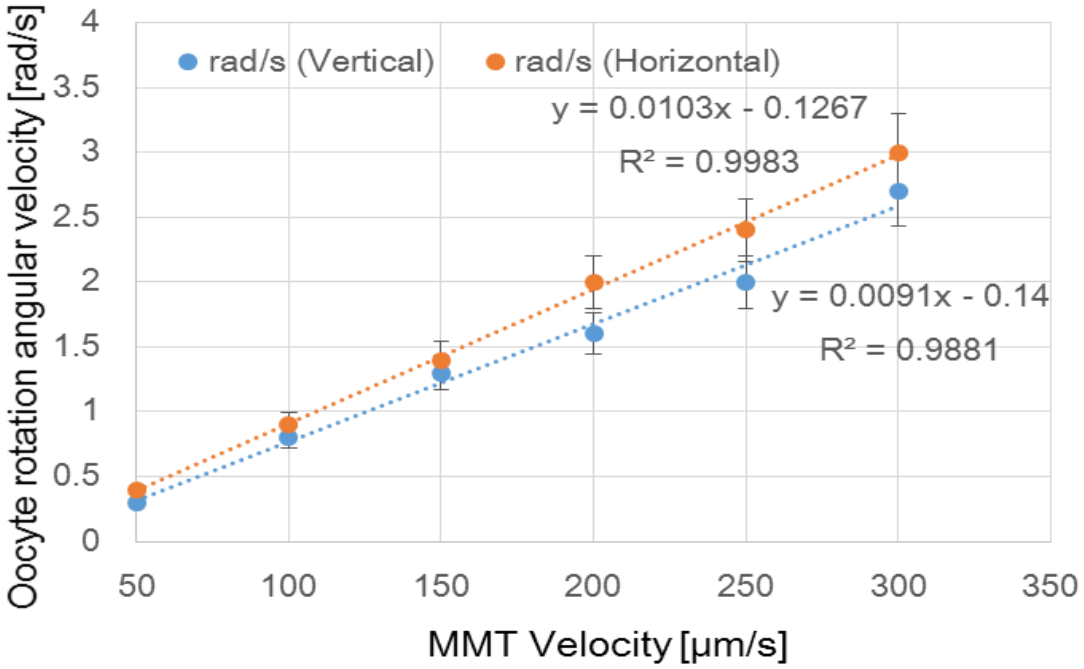

Figure 5.16 Oocyte rotation angular velocity according to the MMT velocity at the case of oocyte rotation with deformation.

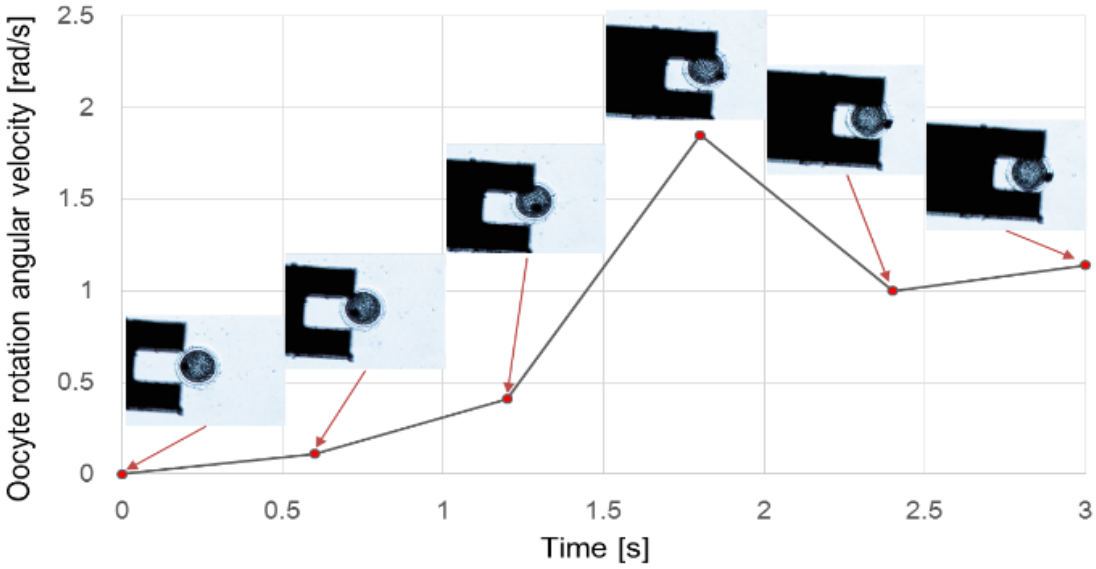

Figure 5.17 One example of oocyte rotation in vertical direction of 180 degrees, angular velocity of oocyte is convertible during the rotation.

rotate the oocyte in a high speed in less time comparing with conventional electrorotation and micropipette generated fluidic flow to rotate the oocyte. Two fitting curves have also been plotted in both Figure 5.15 and Figure 5.16 showing that the angular velocity of oocyte rotation is approximately linear to the MMT movement velocity in both directions.

Figure 5.17 shows one example of single oocyte rotation in vertical orientation. During the rotation, the angular velocity is controllable according to the moving speed of the MMT in X/Y plane.

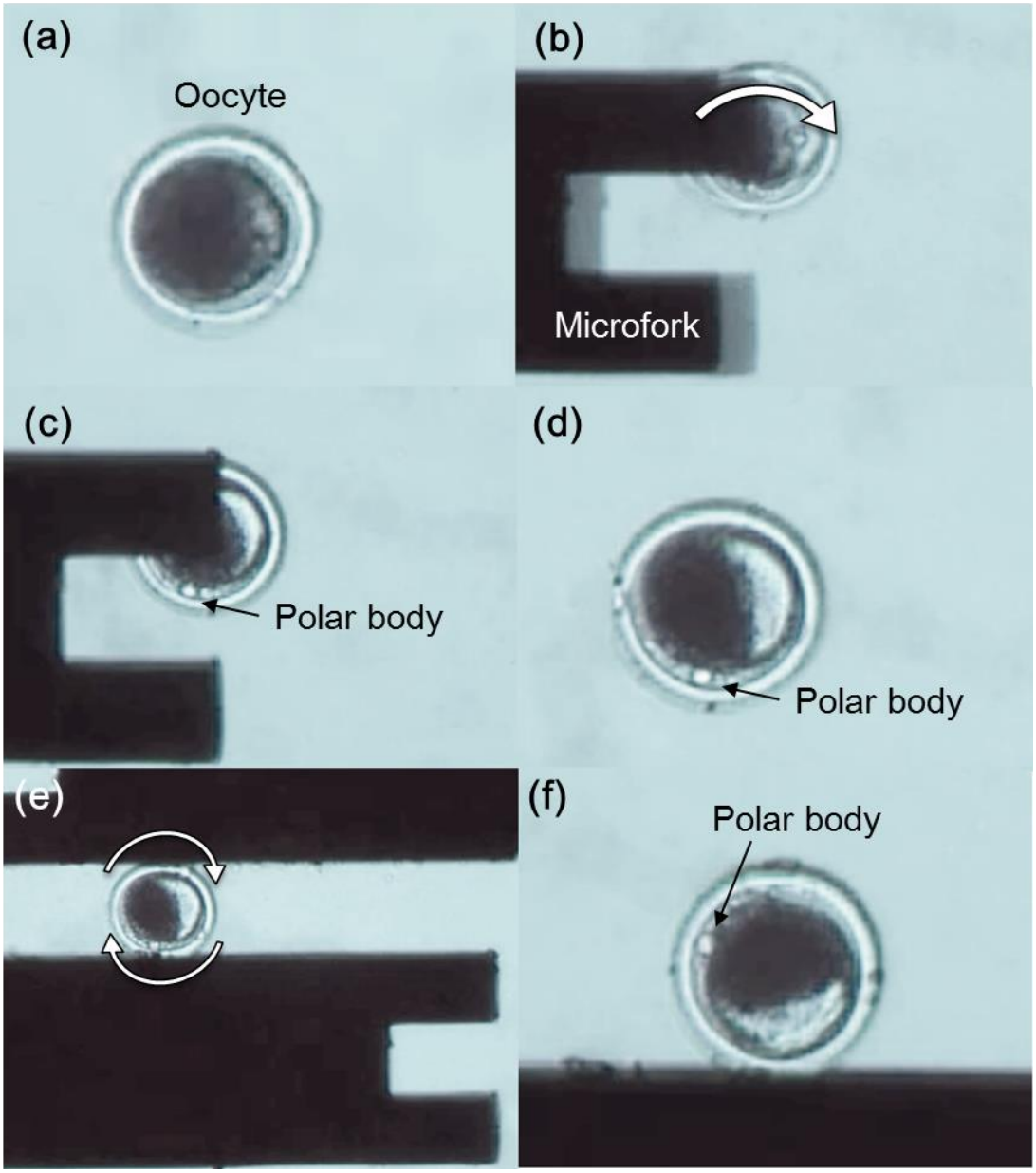

Figure 5.18 Oocyte rotation according to the polar body position. (Oocyte is 150 μm in diameter)

Figure 5.18 shows the oocyte rotation according with the polar body position, at beginning, the polar body is invisible, by vertical rotation using MMT, polar body was rotated until visible, in Figure 5.18 the polar is at the lower part of the oocyte. Then, by utilizing dual arm MMT

oocyte could be rotated in X/Y plane, here we rotated 90 degree to the left side of the oocyte.

In the current system, the minimum of MMT movement error is around 9 μm (including the image estimation error with real MMT dead band error), therefore the control accuracy of the oocyte rotation angle is declared to be 7.5 degree.

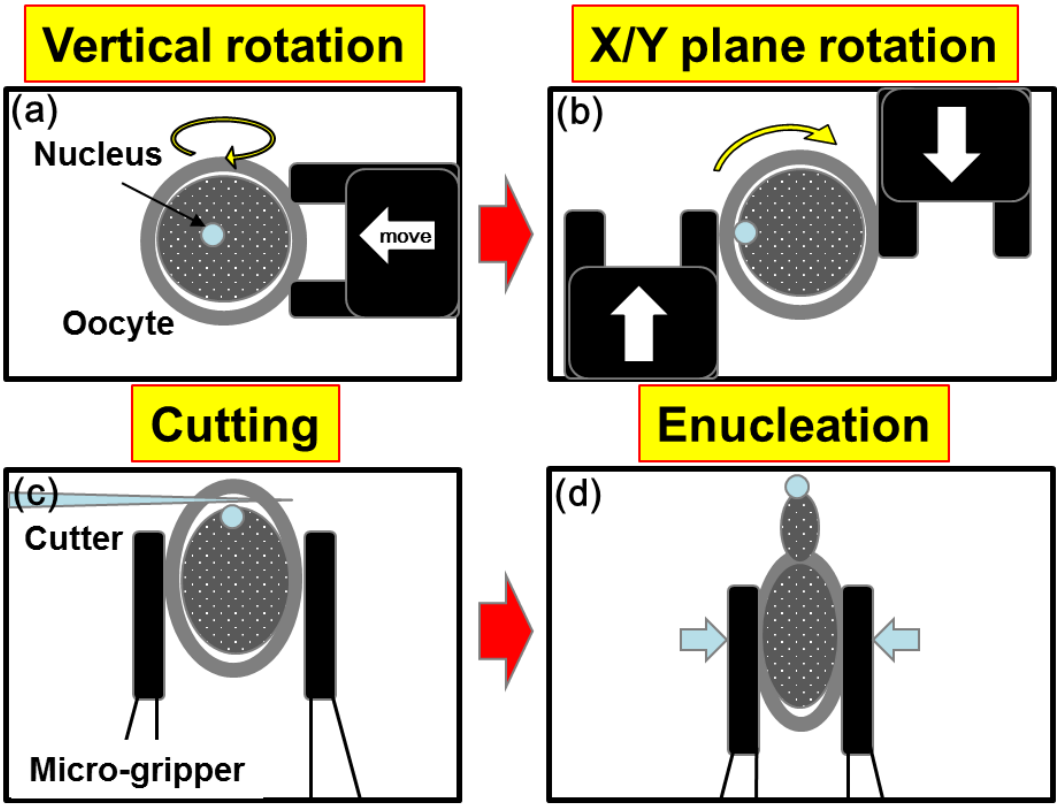

Figure 5.19 Three dimensional rotation for accurate oocyte enucleation.

5.4 Summary

In this chapter, a system for 3-D rotational control of bovine oocyte has been presented. By using customer designed MMT microfork, the oocyte orientation control could be achieved. Comparing with the conventional works, rotation control by using MMT shows great advantage in control accuracy and the rotation speed. For single oocyte rotation it is just take a few seconds. By using the visual recognition and tracking the polar body, the three dimensional rotation could be easily detected. Figure 5.19 shows that by utilizing such three dimensional rotation method, orientation of oocyte could be easily controlled, and the cutting accuracy can be improved by well-adjusted oocyte orientation and position. This system demonstrated overall out-of-plane and in-plane in a quite simple way. And by utilizing this approach, meanwhile, the cell

manipulation for cell study becomes much easier on investigating single cell characteristics and analysis mechanism properties of single cell.

Chapter 6.

Conclusions and Future Works

6.1 Summary

In this thesis, we have presented many different kinds of single oocyte manipulation methods on a microfluidic robochip. Robochip contains magnetically driven microtool (MMT), which was proposed for no contamination of cell manipulations. The novelties of using MMT are summarized as follows: 1. MMTs are fabricated precisely with photolithographic resolution in arbitrary, and MMTs can be fabricated by various process two achieve both in 2-D shape and 3-D shape for different applications. And the subsequent viability test of oocyte has also been

confirmed. 2. Magnetic force enables the noncontact actuation in a closed microfluidic chip with relatively high output forces, by utilizing hybrid type MMT assembling with the permanent magnets, the force of single MMT could obtain 44 mN forces, which shows great usage on single oocyte manipulations, like the oocyte enucleation, oocyte rotation and so on. 3. Microfluidic chip with MMT is disposable and produced at low cost for the biomedical applications. Finally, MMTs are fabricated by using MEMS process, mass production with low cost to full fill the disposability is possible.

In Chapter 2, we presented an on-demand microbeads delivery system in a microfluidic chip by magnetically driven microtool (MMT). It shows potential usage on oocytes loading. The four of horizontally arranged permanent magnets and the piezoelectric vibrator are used to actuate the Ni based microtool precisely in the chip. The MMT injects the beads mechanically to flow and then into ejection operation part. Transferring microbeads one by one with the required pace to the next process has been achieved. The delivery and ejection of polystyrene beads (100 μm) with the flow velocity of from 0.02 ml/h to 0.04 ml/h and MMT frequency from 1 Hz to 6 Hz to adjust the pitch of each micro-bead has been demonstrated. The spacing interval of microbeads could be mainly adjusted by changing of MMT frequency and the flow velocity of output stream. The proposed system shows advantages of high-speed, high success ratio and disposable of microfluidic chip having MMT. This system can be a breakthrough of a high throughput of accurate and effective particle manipulations in the field of cell culturing on a single particle. Finally, single oocytes loading has also been tested, around 60 % success rate of loading oocytes has been confirmed.

In Chapter 3, the MMT has been improved to a hybrid type fabricated by silicon with Nickel. Silicon has a higher stiffness showing the advantage on hard to be deformed or bend

over. A new scheme that involves use of hydraulic forces controlled by a microrobot to perform an oocyte enucleation process in a microfluidic chip has been demonstrated. Using this novel design for oocyte enucleation, the nucleus was removed from the oocyte successfully. This system is advantageous for the following three reasons: (1) that oocyte enucleation can be conducted at a higher speed as compared to conventional enucleation methods; (2) that it minimizes the damage to the oocyte, and that the removal volume of the nucleus portion is small, which is important because the cytoplasmic volume affects the development of nuclear transfer embryos; and (3) that the incision of the enucleated oocyte is smooth, which may also reduce the influence of the viability on the oocyte.

In Chapter 4, as the enucleation has been well studied in our group, and a new cutting approach has been achieved, therefore we then studied how to retrieve the oocytes from the microfluidic chip. A new scheme that involves the use of microsensors for detection and deceleration with micropillars for oocyte dispensing has been demonstrated. This system, which is specifically used to dispense single oocytes, is composed of a capacitance sensor, a deceleration module, and micropillars for stopping the oocytes. Design and fabrication strategies to increase the success rate of dispensing were also demonstrated. Through simulations and calculations, we characterized a prototype of this system. Furthermore, in preliminary experiments, we confirmed the characteristics of the system components and determined the parameters of microchip design. Subsequently, we demonstrated that by using this newly designed system, the success rate of dispensing oocytes greatly increased to 100%. Finally, through viability tests that compared the viability ratios before and after dispensing, we found that the dispensing process had no adverse effects on oocyte viability. This system will be highly useful for cell dispensing and that similar system, in combination with the on-chip

oocyte enucleation process, could usher in a new era of newly improved cloning techniques.

In Chapter 5, a system for 3-D rotational control of bovine oocyte has been presented. By using customer designed MMT microfork, the oocyte orientation control could be achieved. Comparing with the conventional works, rotation control by using MMT shows great advantage in control accuracy and the rotation speed. For single oocyte rotation it is just take a few seconds. By using the visual recognition and tracking the polar body, the three dimensional rotation could be easily detected. This system demonstrated overall out-of-plane and in-plane in a quite simple way. And by utilizing this approach, the enucleation and the cell manipulation for cell study becomes much easier on single cell study and analysis.

The developed MMT and custom-designed microfluidic chip can now use for many of cell manipulations, which currently commercialized mechanical manipulators conducts but the size of the manipulator is significantly smaller and the environment is more stable than a micromechanical manipulation owing to the closed space of the microfluidic chip. The proposed method, which is a microfluidic chip based robochip, is therefore a promising method for realizing high throughput sensing of the mechanical parameters of cell.

6.2 Future Works

6.2.1 Multifunctional modules integration

In order to improve the controllability of a single cell, especially for single oocyte manipulations, various manipulation functions have been discussed in this thesis. It includes oocytes loading, oocyte enucleation in high-speed, single oocytes dispensing and single oocyte orientation control. Still the oocyte loading success rate is unsatisfied, oocyte loading needs improvement in the future. And also, each system is independent, the efficiency of each system cannot be brought into fullplay, therefore unify all the modules into one system is necessary. Even every modules of cell manipulations have been achieved, however integration of all the manipulation functions into one chip is still a hard topic, for instance, position arrangement of different modules, actuation modules positioning and how to connect each modules, like after one process, how to continue the next operation process, and so on. Hence, in the future work, Integration of various modules is hard required.

6.2.2 Automated cell manipulation by MMT

All of cell manipulations presented in this thesis were operated manually through joysticks. The MMT accuracy has been improved, output force also has been improved, and hence fully automated cell manipulation will be next step by integrating vision sensor, trajectory stage control, and feedback control of drive stage. Modeling of the cell manipulation is quite important to develop automation system. Cell is not a rigid body but a soft material where large deformation can be caused and thus, handling cell is not easy task as it seems to be.

By combining chemical and robotics technologies in a microfluidic chip, cell manipulation by microrobot can be like production line of the manufacturing. Once the MMT can conduct

stable actuation at high speeds, it can perform complicated tasks for cells at high speeds similar to industrial robots because the MMT already has enough output force and accuracy to handle cells the size of dozens of micrometers with three degrees of freedom. Fluid force in the microchannels enables cells to be transferred to the MMT working area continuously, and MMTs manipulate cells according to their applications with high throughput. Then, cell manipulation can be completely non-skill dependent job.

References

[1] G. J. Leigh, “An atom is the smallest unit quantity of an element that is capable of existence whether alone or in chemical combination with other atoms of the same or other elements,” in *International Union of Pure and Applied Chemistry, Commission on the Nomenclature of Inorganic Chemistry, Nomenclature of Organic Chemistry – Recommendations 1990. Oxford: Blackwell Scientific Publications.*, 1990, p. 35.

[2] A. N. DeMaria, “A structure for deoxyribose nucleic acid.,” *Journal of the American College of Cardiology*, vol. 42, no. 2. pp. 373–374, 2003.

[3] S. Iijima, “Helical microtubules of graphitic carbon,” *Nature*, vol. 354, no. 6348, pp. 56–58, Nov. 1991.

[4] E. Norrby, “Nobel Prizes and the emerging virus concept.,” *Arch. Virol.*, vol. 153, no. 6, pp. 1109–23, Jan. 2008.

[5] N. Crickmore, D. R. Zeigler, J. Feitelson, E. Schnepf, J. Van Rie, D. Lereclus, J. Baum, and D. H. Dean, “Revision of the Nomenclature for the Bacillus thuringiensis Pesticidal Crystal Proteins,” *Microbiol. Mol. Biol. Rev.*, vol. 62, no. 3, pp. 807–813, Sep. 1998.

[6] P. B. Canham, “The minimum energy of bending as a possible explanation of the biconcave shape of the human red blood cell,” *J. Theor. Biol.*, vol. 26, no. 1, pp. 61–81, 1970.

[7] E. Erbe, “A microscopic mite Lorryia formosa,” *Agricultural Research Service*, 2005. [Online]. Available: http://en.wikipedia.org/wiki/File:Yellow_mite_(Tydeidae)_Lorryia_formosa_2_edit.jpg.

[8] I. Economidis, “An overview of the biotechnology research activities in the European Community.,” *Adv. Biochem. Eng. Biotechnol.*, vol. 46, pp. 225–234, 1992.

[9] C. Juma and V. Konde, “Industrial Applications for Biotechnology.,” *Environment*, vol. 44, p. 22, 2002.

[10] S. Liyanage and P. Gluckman, “The determinants of biotechnology innovative capability: the dynamics of knowledge and marketplace,” *International Journal of Biotechnology*, vol. 6. p. 281, 2004.

[11] C. R. Cantor, “Biotechnology in the 21st century.,” *Trends Biotechnol.*, vol. 18, pp. 6–7, 2000.

[12] J. I. Cohen, “Harnessing Biotechnology for the Poor: challenges ahead for capacity, safety and public investment,” *Journal of Human Development*, vol. 2. pp. 239–263, 2001.

[13] K. H. Campbell, J. McWhir, W. a Ritchie, and I. Wilmut, “Sheep cloned by nuclear transfer from a cultured cell line.,” *Nature*, vol. 380, no. 6569. pp. 64–6, 07-Mar-1996.

[14] National Bioethics Advisory Commission, “The science and application of cloning,” *Clones Clones Facts Fantasies about Hum. Cloning*, pp. 29–40, 1998.

[15] K. J. McCreath, J. Howcroft, K. H. Campbell, a Colman, a E. Schnieke, and a J. Kind, “Production of gene-targeted sheep by nuclear transfer from cultured somatic cells.,” *Nature*, vol. 405, no. 6790. pp. 1066–9, 29-Jun-2000.

[16] S. Iwasaki, K. H. Campbell, C. Galli, and K. Akiyama, “Production of live calves derived from embryonic stem-like cells aggregated with tetraploid embryos.,” *Biology of reproduction*, vol. 62, no. 2. pp. 470–5, Feb-2000.

[17] I. a Polejaeva, S. H. Chen, T. D. Vaught, R. L. Page, J. Mullins, S. Ball, Y. Dai, J. Boone, S. Walker, D. L. Ayares, a Colman, and K. H. Campbell, “Cloned pigs produced by nuclear transfer from adult somatic cells.,” *Nature*, vol. 407, no. 6800. pp. 86–90, 07-Sep-2000.

[18] T. Wakayama, a C. Perry, M. Zuccotti, K. R. Johnson, and R. Yanagimachi, “Full-term development of mice from enucleated oocytes injected with cumulus cell nuclei.,” *Nature*, vol. 394, no. 6691. pp. 369–74, 23-Jul-1998.

[19] K. Yanagida, H. Katayose, H. Yazawa, Y. Kimura, K. Konnai, and a Sato, “The usefulness of a piezo-micromanipulator in intracytoplasmic sperm injection in

humans.," *Human reproduction (Oxford, England)*, vol. 14, no. 2. pp. 448–53, Feb-1999.

[20] Y. Murayama, C. E. Constantinou, and S. Omata, "Micro-mechanical sensing platform for the characterization of the elastic properties of the ovum via uniaxial measurement.," *Journal of biomechanics*, vol. 37, no. 1. pp. 67–72, Jan-2004.

[21] A. A. Ramadan, K. Inoue, T. Arai, T. Takubo, and T. Tanikawa, "New Design of a Compact Parallel Micro-Nano Two-Fingered Manipulator Hand," *2007 2nd IEEE Int. Conf. Nano/Micro Eng. Mol. Syst.*, 2007.

[22] M. Ahmad and M. Nakajima, "The effects of cell sizes, environmental conditions, and growth phases on the strength of individual W303 yeast cells inside ESEM," *NanoBioscience, ...*, pp. 185–193, 2008.

[23] Y. Shen, M. Nakajima, S. Kojima, M. Homma, M. Kojima, and T. Fukuda, "Single cell adhesion force measurement for cell viability identification using an AFM cantilever-based micro putter," *Meas. Sci. Technol.*, vol. 22, no. 11, p. 115802, 2011.

[24] M. R. Ahmad, M. Nakajima, S. Kojima, M. Homma, and T. Fukuda, "Nanoindentation methods to measure viscoelastic properties of single cells using sharp, flat, and buckling tips inside ESEM.," *IEEE transactions on nanobioscience*, vol. 9, no. 1. pp. 12–23, Mar-2010.

[25] F. Kremer, "Fundamentals of Interface & Colloid Science," *Zeitschrift für Physikalische Chemie*, vol. 199. pp. 127–127, 1997.

[26] H. A. Abramson, "ELECTROKINETIC PHENOMENA," *J. Gen. Physiol.*, vol. 16, pp. 1–3, 1932.

[27] H. A. Pohl, "Some Effects of Nonuniform Fields on Dielectrics," *J. Appl. Phys.*, vol. 29, pp. 1182–1188, 1958.

[28] H. a Pohl, "The Motion and Precipitation of Suspensoids in Divergent Electric Fields," *J. Appl. Phys.*, vol. 22, no. 7, p. 869, 1951.

[29] K. Kendall, “Electromechanics of particles,” *Powder Technology*, vol. 89. pp. 177–178, 1996.

[30] A. Irimajiri, T. Hanai, and A. Inouye, “A dielectric theory of ‘multi-stratified shell’ model with its application to a lymphoma cell.,” *J. Theor. Biol.*, vol. 78, pp. 251–269, 1979.

[31] H. Morgan and G. Nicolas G, “AC electrokinetics: colloids and nanoparticles,” *Res. Stud. Press*, vol. 2, 2003.

[32] H. A. Pohl, *Dielectrophoresis: the behavior of neutral matter in nonuniform electric fields*. Cambridge: Cambridge University Press, 1978.

[33] H. Morgan and N. Green, “Dielectrophoretic manipulation of rod-shaped viral particles,” *J. Electrostat.*, 1997.

[34] N. Green, H. Morgan, and J. Milner, “Manipulation and trapping of sub-micron bioparticles using dielectrophoresis,” *J. Biochem. Biophys. …*, 1997.

[35] C. H. Kua, Y. C. Lam, I. Rodriguez, C. Yang, and K. Youcef-Toumi, “Dynamic cell fractionation and transportation using moving dielectrophoresis.,” *Anal. Chem.*, vol. 79, no. 18, pp. 6975–6987, 2007.

[36] L. Ying, S. S. White, A. Bruckbauer, L. Meadows, Y. E. Korchev, and D. Klenerman, “Frequency and voltage dependence of the dielectrophoretic trapping of short lengths of DNA and dCTP in a nanopipette.,” *Biophys. J.*, vol. 86, no. 2, pp. 1018–1027, 2004.

[37] P. Mela, A. van den Berg, Y. Fintschenko, E. B. Cummings, B. A. Simmons, and B. J. Kirby, “The zeta potential of cyclo-olefin polymer microchannels and its effects on insulative (electrodeless) dielectrophoresis particle trapping devices.,” *Electrophoresis*, vol. 26, no. 9, pp. 1792–1799, 2005.

[38] T. Heida, W. L. Rutten, and E. Marani, “Dielectrophoretic trapping of dissociated fetal cortical rat neurons.,” *IEEE Trans. Biomed. Eng.*, vol. 48, no. 8, pp. 921–930, 2001.

[39] E. B. Cummings and A. K. Singh, “Dielectrophoretic trapping without embedded electrodes,” *Microfluid. Devices Syst. Iii*, vol. 4177, pp. 164–173 ¥r292, 2000.

[40] B. H. Lapizco-Encinas, R. V Davalos, B. A. Simmons, E. B. Cummings, and Y. Fintschenko, "An insulator-based (electrodeless) dielectrophoretic concentrator for microbes in water.," *J. Microbiol. Methods*, vol. 62, no. 3, pp. 317–326, 2005.

[41] S. Fiedler, S. G. Shirley, T. Schnelle, and G. Fuhr, "Dielectrophoretic sorting of particles and cells in a microsystem.," *Anal. Chem.*, vol. 70, no. 9, pp. 1909–1915, 1998.

[42] K. Ahn, C. Kerbage, T. P. Hunt, R. M. Westervelt, D. R. Link, and D. a. Weitz, "Dielectrophoretic manipulation of drops for high-speed microfluidic sorting devices," *Appl. Phys. Lett.*, vol. 88, no. 2, p. 024104, 2006.

[43] X. Hu, P. H. Bessette, J. Qian, C. D. Meinhart, P. S. Daugherty, and H. T. Soh, "Marker-specific sorting of rare cells using dielectrophoresis.," *Proc. Natl. Acad. Sci. U. S. A.*, vol. 102, no. 44, pp. 15757–15761, 2005.

[44] I.-F. Cheng, H.-C. Chang, D. Hou, and H.-C. Chang, "An integrated dielectrophoretic chip for continuous bioparticle filtering, focusing, sorting, trapping, and detecting.," *Biomicrofluidics*, vol. 1, no. 2, p. 21503, 2007.

[45] B. M. Taff and J. Voldman, "A scalable addressable positive-dielectrophoretic cell-sorting array.," *Anal. Chem.*, vol. 77, no. 24, pp. 7976–7983, 2005.

[46] J. A. Price, J. P. Burt, and R. Pethig, "Applications of a new optical technique for measuring the dielectrophoretic behaviour of micro-organisms.," *Biochim. Biophys. Acta*, vol. 964, no. 2, pp. 221–230, 1988.

[47] C. L. Asbury and G. van den Engh, "Trapping of DNA in nonuniform oscillating electric fields.," *Biophys. J.*, vol. 74, no. 2 Pt 1, pp. 1024–1030, 1998.

[48] M. Dürr, J. Kentsch, T. Müller, T. Schnelle, and M. Stelzle, "Microdevices for manipulation and accumulation of micro- and nanoparticles by dielectrophoresis.," *Electrophoresis*, vol. 24, pp. 722–731, 2003.

[49] J. P. H. Burt, G. H. Markx, Y. Huang, X.-B. Wang, and R. Pethig, "Selective dielectrophoretic confinement of bioparticles in potential energy wells," *Journal of Physics D: Applied Physics*, vol. 26, no. 8. pp. 1278–1285, 1999.

[50] A. Ashkin, J. M. Dziedzic, J. E. Bjorkholm, and S. Chu, “Observation of a single-beam gradient force optical trap for dielectric particles.,” *Opt. Lett.*, vol. 11, no. 5, p. 288, 1986.

[51] A. Ashkin and J. M. Dziedzic, “Optical trapping and manipulation of viruses and bacteria.,” *Science*, vol. 235, no. 4795, pp. 1517–1520, 1987.

[52] A. Cable, S. Chu, A. Ashkin, and J. Bjorkholm, “Experimental Observation of Optically Trapped Atoms,” *Physical Review Letters*, vol. 57, no. 3. pp. 314–317, 1986.

[53] J. Glückstad and P. C. Mogensen, “Dynamic array generation and pattern formation for optical tweezers,” *Optics Communications*, vol. 175. pp. 75–81, 2000.

[54] R. L. Eriksen, P. C. Mogensen, and J. Glückstad, “Multiple-beam optical tweezers generated by the generalized phase-contrast method.,” *Opt. Lett.*, vol. 27, no. 4, pp. 267–269, 2002.

[55] F. Arai, K. Yoshikawa, T. Sakami, and T. Fukuda, “Synchronized laser micromanipulation of multiple targets along each trajectory by single laser,” *Appl. Phys. Lett.*, vol. 85, no. 19, pp. 4301–4303, 2004.

[56] K. Onda and F. Arai, “Multi-beam bilateral teleoperation of holographic optical tweezers,” *Optics express*, vol. 20, no. 4. pp. 3633–41, 13-Feb-2012.

[57] C. Bouchiat, M. D. Wang, J. Allemand, T. Strick, S. M. Block, and V. Croquette, “Estimating the persistence length of a worm-like chain molecule from force-extension measurements.,” *Biophys. J.*, vol. 76, no. 1 Pt 1, pp. 409–413, 1999.

[58] C. Bustamante, J. C. Macosko, and G. J. Wuite, “Grabbing the cat by the tail: manipulating molecules one by one.,” *Nat. Rev. Mol. Cell Biol.*, vol. 1, no. 2, pp. 130–136, 2000.

[59] A. Ishijima and T. Yanagida, “Single molecule nanobioscience.,” *Trends Biochem. Sci.*, vol. 26, no. 7, pp. 438–444, 2001.

[60] Y. Kimura and P. R. Bianco, “Single molecule studies of DNA binding proteins using optical tweezers.,” *Analyst*, vol. 131, no. 8, pp. 868–874, 2006.

[61] F. Arai, A. Ichikawa, M. Ogawa, T. Fukuda, K. Horio, and K. Itoigawa, “High-speed separation system of randomly suspended single living cells by laser trap and dielectrophoresis.,” *Electrophoresis*, vol. 22, no. 2, pp. 283–288, 2001.

[62] F. Arai, C. Ng, H. Maruyama, A. Ichikawa, H. El-Shimy, and T. Fukuda, “On chip single-cell separation and immobilization using optical tweezers and thermosensitive hydrogel.,” *Lab Chip*, vol. 5, no. 12, pp. 1399–1403, 2005.

[63] E. Eriksson, K. Sott, F. Lundqvist, M. Sveningsson, J. Scrimgeour, D. Hanstorp, M. Goksör, and A. Granéli, “A microfluidic device for reversible environmental changes around single cells using optical tweezers for cell selection and positioning,” *Lab a Chip - Miniaturisation Chem. Biol.*, vol. 10, no. 5, pp. 617–625, 2010.

[64] M. Werner, F. Merenda, J. Piguet, R.-P. Salathé, and H. Vogel, “Microfluidic array cytometer based on refractive optical tweezers for parallel trapping, imaging and sorting of individual cells.,” *Lab Chip*, vol. 11, no. 14, pp. 2432–2439, 2011.

[65] T. Takahata, F. Arai, K. Kotani, T. Masuda, H. Maruyama, and A. Honda, “Nanomanipulation of single influenza virus using dielectrophoretic concentration and optical tweezers for single virus infection to a specific cell on a microfluidic chip,” *Microfluidics and Nanofluidics*, vol. 10, no. 5. pp. 1109–1117, 2011.

[66] P. Y. Chiou, A. T. Ohta, and M. C. Wu, “Massively parallel manipulation of single cells and microparticles using optical images.,” *Nature*, vol. 436, no. 7049. pp. 370–2, 21-Jul-2005.

[67] W. Liang, S. Wang, Z. Dong, G.-B. Lee, and W. J. Li, “Optical Spectrum and Electric Field Waveform Dependent Optically-Induced Dielectrophoretic (ODEP) Micro-Manipulation,” *Micromachines*, vol. 3, no. 4, pp. 492–508, May 2012.

[68] J. Shi, X. Mao, D. Ahmed, A. Colletti, and T. J. Huang, “Focusing microparticles in a microfluidic channel with standing surface acoustic waves (SSAW).,” *Lab Chip*, vol. 8, no. 2, pp. 221–223, 2008.

[69] J. Shi, H. Huang, Z. Stratton, Y. Huang, and T. J. Huang, “Continuous particle separation in a microfluidic channel via standing surface acoustic waves (SSAW).,” *Lab Chip*, vol. 9, no. 23, pp. 3354–3359, 2009.

[70] T. Franke, A. R. Abate, D. A. Weitz, and A. Wixforth, “Surface acoustic wave (SAW) directed droplet flow in microfluidics for PDMS devices.,” *Lab Chip*, vol. 9, no. 18, pp. 2625–2627, 2009.

[71] C. D. Wood, J. E. Cunningham, R. O’Rorke, C. Wälti, E. H. Linfield, a. G. Davies, and S. D. Evans, “Formation and manipulation of two-dimensional arrays of micron-scale particles in microfluidic systems by surface acoustic waves,” *Appl. Phys. Lett.*, vol. 94, no. 5, p. 054101, 2009.

[72] C. D. Wood, S. D. Evans, J. E. Cunningham, R. O’Rorke, C. Wälti, and a G. Davies, “Alignment of particles in microfluidic systems using standing surface acoustic waves,” *Appl. Phys. Lett.*, vol. 92, no. 4, p. 044104, 2008.

[73] T. Franke, S. Braunmüller, L. Schmid, A. Wixforth, and D. A. Weitz, “Surface acoustic wave actuated cell sorting (SAWACS).,” *Lab Chip*, vol. 10, no. 6, pp. 789–794, 2010.

[74] R. Barnkob, P. Augustsson, T. Laurell, and H. Bruus, “Measuring the local pressure amplitude in microchannel acoustophoresis.,” *Lab Chip*, vol. 10, no. 5, pp. 563–570, 2010.

[75] Y. Bourquin, J. Reboud, R. Wilson, and J. M. Cooper, “Tuneable surface acoustic waves for fluid and particle manipulations on disposable chips.,” *Lab Chip*, vol. 10, no. 15, pp. 1898–1901, 2010.

[76] L. Y. Yeo and J. R. Friend, “Ultrafast microfluidics using surface acoustic waves.,” *Biomicrofluidics*, vol. 3, no. 1, p. 12002, 2009.

[77] P. R. Rogers, J. R. Friend, and L. Y. Yeo, “Exploitation of surface acoustic waves to drive size-dependent microparticle concentration within a droplet.,” *Lab Chip*, vol. 10, no. 21, pp. 2979–2985, 2010.

[78] J. Shi, D. Ahmed, X. Mao, S.-C. S. Lin, A. Lawit, and T. J. Huang, “Acoustic tweezers: patterning cells and microparticles using standing surface acoustic waves (SSAW).,” *Lab Chip*, vol. 9, no. 20, pp. 2890–2895, 2009.

[79] L. Masini, M. Cecchini, S. Girardo, R. Cingolani, D. Pisignano, and F. Beltram, “Surface-acoustic-wave counterflow micropumps for on-chip liquid motion control in two-dimensional microchannel arrays.,” *Lab Chip*, vol. 10, no. 15, pp. 1997–2000, 2010.

[80] M. Barbic, J. J. Mock, A. P. Gray, and S. Schultz, “Electromagnetic micromotor for microfluidics applications,” *Appl. Phys. Lett.*, vol. 79, no. 9, p. 1399, 2001.

[81] O. Cugat, J. Delamare, and G. Reyne, “Magnetic micro-actuators and systems (MAGMAS),” *IEEE Trans. Magn.*, vol. 39, no. 6, 2003.

[82] G. A. Mensing, T. M. Pearce, M. D. Graham, and D. J. Beebe, “An externally driven magnetic microstirrer.,” *Philos. Trans. A. Math. Phys. Eng. Sci.*, vol. 362, no. 1818, pp. 1059–1068, 2004.

[83] E. Piat and M. Gauthier, “An electromagnetic micromanipulation system for single-cell manipulation,” *Journal of Micromechatronics*, vol. 2, no. 2. pp. 87–119, 2002.

[84] K. B. Yesin, “Modeling and Control of Untethered Biomicrorobots in a Fluidic Environment Using Electromagnetic Fields,” *The International Journal of Robotics Research*, vol. 25, no. 5–6. pp. 527–536, 2006.

[85] M. P. Kummer, J. J. Abbott, B. E. Kratochvil, R. Borer, A. Sengul, and B. J. Nelson, “OctoMag: An Electromagnetic System for 5-DOF Wireless Micromanipulation,” *IEEE Trans. Robot.*, vol. 26, no. 6, 2010.

[86] L. Zhang, J. J. Abbott, L. Dong, B. E. Kratochvil, D. Bell, and B. J. Nelson, “Artificial bacterial flagella: Fabrication and magnetic control,” *Appl. Phys. Lett.*, vol. 94, no. 6, p. 064107, 2009.

[87] L. Arcese, M. Fruchard, F. Beyeler, A. Ferreira, and B. J. Nelson, “Adaptive backstepping and MEMS force sensor for an MRI-guided microrobot in the vasculature,” *2011 IEEE Int. Conf. Robot. Autom.*, pp. 4121–4126, 2011.

[88] C. Pawashe, E. Diller, S. Floyd, and M. Sitti, “Assembly and disassembly of magnetic mobile micro-robots towards deterministic 2-D reconfigurable micro-systems,” *2011 IEEE Int. Conf. Robot. Autom.*, pp. 261–266, 2011.

[89] E. Diller, Z. Ye, and M. Sitti, “Rotating magnetic micro-robots for versatile non-contact fluidic manipulation of micro-objects,” *2011 IEEE/RSJ Int. Conf. Intell. Robot. Syst.*, pp. 1291–1296, 2011.

[90] M. S. Sakar, E. B. Steager, A. Cowley, V. Kumar, and G. J. Pappas, “Wireless manipulation of single cells using magnetic microtransporters,” *2011 IEEE Int. Conf. Robot. Autom.*, pp. 2668–2673, 2011.

[91] M. S. Sakar, E. B. Steager, D. H. Kim, M. J. Kim, G. J. Pappas, and V. Kumar, “Single cell manipulation using ferromagnetic composite microtransporters,” *Appl. Phys. Lett.*, vol. 96, no. 4, p. 043705, 2010.

[92] G. M. Whitesides, “The origins and the future of microfluidics.,” *Nature*, vol. 442, no. 7101, pp. 368–373, 2006.

[93] H. A. Nieuwstadt, R. Seda, D. S. Li, J. B. Fowlkes, and J. L. Bull, “Microfluidic particle sorting utilizing inertial lift force.,” *Biomed. Microdevices*, vol. 13, no. 1, pp. 97–105, 2011.

[94] D. R. Gossett, W. M. Weaver, A. J. Mach, S. C. Hur, H. T. K. Tse, W. Lee, H. Amini, and D. Di Carlo, “Label-free cell separation and sorting in microfluidic systems.,” *Anal. Bioanal. Chem.*, vol. 397, no. 8, pp. 3249–3267, 2010.

[95] S. Ookawara, K. Ogawa, R. Higashi, and D. Street, “Feasibility study on concentration of slurry and classification of contained particles by microchannel,” *Chemical Engineering Journal*, vol. 101, no. 1–3. pp. 171–178, 2004.

[96] Z. Wu, B. Willing, J. Bjerketorp, J. K. Jansson, and K. Hjort, “Soft inertial microfluidics for high throughput separation of bacteria from human blood cells.,” *Lab Chip*, vol. 9, no. 9, pp. 1193–1199, 2009.

[97] N. Pamme, “Continuous flow separations in microfluidic devices.,” *Lab Chip*, vol. 7, no. 12, pp. 1644–1659, 2007.

[98] L. R. Huang, E. C. Cox, R. H. Austin, and J. C. Sturm, “Continuous particle separation through deterministic lateral displacement.,” *Science*, vol. 304, no. 5673, pp. 987–990, 2004.

[99] A. A. S. Bhagat, H. W. Hou, L. D. Li, C. T. Lim, and J. Han, “Pinched flow coupled shear-modulated inertial microfluidics for high-throughput rare blood cell separation.,” *Lab Chip*, vol. 11, no. 11, pp. 1870–1878, 2011.

[100] R. A. Vijayendran, K. M. Motsegood, D. J. Beebe, and D. E. Leckband, “Evaluation of a Three-Dimensional Micromixer in a,” *Society*, no. 2, pp. 1824–1828, 2003.

[101] A. D. Stroock, S. K. W. Dertinger, A. Ajdari, I. Mezic, H. A. Stone, and G. M. Whitesides, “Chaotic mixer for microchannels.,” *Science*, vol. 295, no. 5555, pp. 647–651, 2002.

[102] L. J. Kricka and P. Wilding, “Microchip PCR.,” *Anal. Bioanal. Chem.*, vol. 377, no. 5, pp. 820–825, 2003.

[103] K. Mae, T. Maki, I. Hasegawa, U. Eto, Y. Mizutani, and N. Honda, “Development of a new micromixer based on split/recombination for mass production and its application to soap free emulsifier,” *Chem. Eng. J.*, vol. 101, no. 1, pp. 31–38, 2004.

[104] N. Y. Lee, M. Yamada, and M. Seki, “Development of a passive micromixer based on repeated fluid twisting and flattening, and its application to DNA purification.,” *Anal. Bioanal. Chem.*, vol. 383, no. 5, pp. 776–782, 2005.

[105] K.-L. Lao, J.-H. Wang, and G.-B. Lee, “A microfluidic platform for formation of double-emulsion droplets,” *Microfluid. Nanofluidics*, vol. 7, no. 5, pp. 709–719, Mar. 2009.

[106] T. Nakashima, Y. Mine, and M. Shimizu, “Preparation and stabilization of simple and multiple emulsions using a microporous glass membrane,” *Colloids and Surfaces B: Biointerfaces*, vol. 6, no. 4–5. pp. 261–268, 1996.

[107] T. Moritani, M. Yamada, and M. Seki, “Generation of uniform-size droplets by multistep hydrodynamic droplet division in microfluidic circuits,” *Microfluidics and Nanofluidics*, vol. 11, no. 5. pp. 601–610, 2011.

[108] S. Takeuchi, P. Garstecki, D. B. Weibel, and G. M. Whitesides, “An Axisymmetric Flow-Focusing Microfluidic Device,” *Adv. Mater.*, vol. 17, no. 8, pp. 1067–1072, 2005.

[109] S.-Y. Teh, R. Lin, L.-H. Hung, and A. P. Lee, “Droplet microfluidics.,” *Lab Chip*, vol. 8, no. 2, pp. 198–220, 2008.

[110] M. Yamada, S. Doi, H. Maenaka, M. Yasuda, and M. Seki, “Hydrodynamic control of droplet division in bifurcating microchannel and its application to particle synthesis.,” *J. Colloid Interface Sci.*, vol. 321, no. 2, pp. 401–407, 2008.

[111] K. Jang, Y. Xu, Y. Tanaka, K. Sato, K. Mawatari, T. Konno, K. Ishihara, and T. Kitamori, “Single-cell attachment and culture method using a photochemical reaction in a closed microfluidic system.,” *Biomicrofluidics*, vol. 4, no. 3, p. 32208, 2010.

[112] T. Yamashita, Y. Tanaka, N. Idota, K. Sato, K. Mawatari, and T. Kitamori, “Cultivation and recovery of vascular endothelial cells in microchannels of a separable micro-chemical chip.,” *Biomaterials*, vol. 32, no. 10, pp. 2459–2465, 2011.

[113] S. L. Stott, C.-H. Hsu, D. I. Tsukrov, M. Yu, D. T. Miyamoto, B. A. Waltman, S. M. Rothenberg, A. M. Shah, M. E. Smas, G. K. Korir, F. P. Floyd, A. J. Gilman, J. B. Lord, D. Winokur, S. Springer, D. Irimia, S. Nagrath, L. V Sequist, R. J. Lee, K. J. Isselbacher, S. Maheswaran, D. A. Haber, and M. Toner, “Isolation of circulating tumor cells using a microvortex-generating herringbone-chip.,” *Proc. Natl. Acad. Sci. U. S. A.*, vol. 107, no. 43, pp. 18392–7, Oct. 2010.

[114] C. Charcosset, I. Limayem, and H. Fessi, “The membrane emulsification process—a review,” *J. Chem. Technol. Biotechnol.*, vol. 79, no. 3, pp. 209–218, 2004.

[115] A. V Korobko, W. Jesse, and J. R. C. van der Maarel, “Encapsulation of DNA by cationic diblock copolymer vesicles.,” *Langmuir*, vol. 21, no. 1, pp. 34–42, 2005.

[116] S. M. Moghimi, A. C. Hunter, and J. C. Murray, “Nanomedicine: current status and future prospects.,” *FASEB J.*, vol. 19, no. 3, pp. 311–30, Mar. 2005.

[117] T. Kojima, Y. Takei, M. Ohtsuka, Y. Kawarasaki, T. Yamane, and H. Nakano, “PCR amplification from single DNA molecules on magnetic beads in emulsion: application

for high-throughput screening of transcription factor targets.," *Nucleic Acids Res.*, vol. 33, no. 17, p. e150, 2005.

[118] C.-W. Lai, Y.-H. Lin, and G.-B. Lee, "A microfluidic chip for formation and collection of emulsion droplets utilizing active pneumatic micro-choppers and micro-switches.," *Biomed. Microdevices*, vol. 10, no. 5, pp. 749–756, 2008.

[119] B. Zheng, J. D. Tice, and R. F. Ismagilov, "Formation of Arrayed Droplets by Soft Lithography and Two-Phase Fluid Flow, and Application in Protein Crystallization," *Adv. Mater.*, vol. 16, no. 15, pp. 1365–1368, 2004.

[120] G. R. Yi, T. Thorsen, V. N. Manoharan, M. J. Hwang, S. J. Jeon, D. J. Pine, S. R. Quake, and S. M. Yang, "Generation of Uniform Colloidal Assemblies in Soft Microfluidic Devices," *Adv. Mater.*, vol. 15, pp. 1300–1304, 2003.

[121] S.-J. Jeon, S. R. Quake, G.-R. Yi, V. N. Manoharan, D. J. Pine, S.-M. Yang, and T. Thorsen, "Generation of uniform photonic balls by template-assisted colloidal crystallization," *Synthetic Metals*, vol. 139, no. 3. pp. 803–806, 2003.

[122] D. Dendukuri, K. Tsoi, T. A. Hatton, and P. S. Doyle, "Controlled synthesis of nonspherical microparticles using microfluidics.," *Langmuir*, vol. 21, no. 6, pp. 2113–2116, 2005.

[123] T. Torii, T. Higuchi, and T. Nisisako, "Novel microreactors for functional polymer beads," *Chemical Engineering Journal*, vol. 101, no. 1–3. pp. 23–29, 2004.

[124] J. L. J. Lee and C.-J. K. C.-J. Kim, "Surface-tension-driven microactuation based on continuous electrowetting," *J. Microelectromechanical Syst.*, vol. 9, no. 2, 2000.

[125] Y. Yamanishi, L. Feng, and F. Arai, "On-demand Production of Emulsion Droplets Over a Wide Range of Sizes," *Advanced Robotics*, vol. 24, no. 14. pp. 2005–2018, 2010.

[126] Y. Yamanishi, S. Sakuma, K. Onda, and F. Arai, "Powerful actuation of magnetized microtools by focused magnetic field for particle sorting in a chip.," *Biomed. Microdevices*, vol. 12, no. 4, pp. 745–52, Aug. 2010.

[127] L. Feng, M. Hagiwara, H. Uvet, Y. Yamanish, T. Kawahara, K. Kosuge, and F. Arai, "High-speed delivery of microbeads in microchannel using magnetically driven microtool," *2011 16th Int. Solid-State Sensors, Actuators Microsystems Conf.*, pp. 1312–1315, 2011.

[128] Y. Yamanishi, S. Sakuma, Y. Kihara, and F. Arai, "Fabrication and Application of 3-D Magnetically Driven Microtools," *J. Microelectromechanical Syst.*, vol. 19, no. 2, 2010.

[129] H. Maruyama, S. Sakuma, Y. Yamanishi, and F. Arai, "Size-dependent filtration and trapping of microparticle in a microfluidic chip using centrifugal force and a graduated mechanical gap," *2009 IEEE/SICE Int. Symp. Syst. Integr.*, 2009.

[130] L. Feng, T. Kawahara, Y. Yamanishi, M. Hagiwara, and F. Arai, "On-chip production of droplets with on-demand and size control," in *International Conference on Advanced Mechatronics*, 2010, pp. 367–372.

[131] Y. Yamanishi, L. Feng, and F. Arai, "On-demand and Size-controlled Production of emulsion droplets by magnetically driven microtool," *Robot. Autom. (ICRA), 2010 IEEE Int. Conf.*, pp. 4094–4099, 2010.

[132] L. Feng, Y. Yamanishi, and F. Arai, "On-demand generation of droplet in size over a wide range by microfluidic control," in *2009 International Symposium on Micro-Nano Mechatronics and Human Science*, 2009, pp. 139–144.

[133] Y. Yamanishi, L. F. L. Feng, Y. Kihara, S. Sakuma, and F. Arai, "Formation of microdroplets utilizing hybrid magnetically driven microtool on a microfluidic chip," *Robot. Biomimetics (ROBIO), 2009 IEEE Int. Conf.*, 2009.

[134] M. Hagiwara, T. Kawahara, Y. Yamanishi, T. Masuda, L. Feng, and F. Arai, "On-chip magnetically actuated robot with ultrasonic vibration for single cell manipulations.," *Lab Chip*, vol. 11, no. 12, pp. 2049–2054, 2011.

[135] W. S. N. Trimmer, "Microrobots and micromechanical systems," *Sensors and Actuators*, vol. 19, no. 3. pp. 267–287, 1989.

[136] J. P. Desai, A. Pillarisetti, and A. D. Brooks, “Engineering approaches to biomanipulation.,” *Annu. Rev. Biomed. Eng.*, vol. 9, pp. 35–53, 2007.

[137] J. Castillo, M. Dimaki, and W. E. Svendsen, “Manipulation of biological samples using micro and nano techniques.,” *Integr. Biol. (Camb).*, vol. 1, no. 1, pp. 30–42, 2009.

[138] GE Healthcare/Amersham, *Microcarrier cell culture: Principles and methods.* 2005, p. 9.

[139] J. Elisseeff, W. McIntosh, K. Anseth, S. Riley, P. Ragan, and R. Langer, “Photoencapsulation of chondrocytes in poly(ethylene oxide)-based semi-interpenetrating networks.,” *J. Biomed. Mater. Res.*, vol. 51, no. 2, pp. 164–71, Aug. 2000.

[140] P. J. Martens, S. J. Bryant, and K. S. Anseth, “Tailoring the degradation of hydrogels formed from multivinyl poly(ethylene glycol) and poly(vinyl alcohol) macromers for cartilage tissue engineering.,” *Biomacromolecules*, vol. 4, no. 2, pp. 283–92, Jan. 2003.

[141] K. W. Chun, H. S. Yoo, J. J. Yoon, and T. G. Park, “Biodegradable PLGA microcarriers for injectable delivery of chondrocytes: effect of surface modification on cell attachment and function.,” *Biotechnol. Prog.*, vol. 20, no. 6, pp. 1797–801.

[142] T. Dvash, Y. Mayshar, H. Darr, M. McElhaney, D. Barker, O. Yanuka, K. J. Kotkow, L. L. Rubin, N. Benvenisty, and R. Eiges, “Temporal gene expression during differentiation of human embryonic stem cells and embryoid bodies.,” *Hum. Reprod.*, vol. 19, no. 12, pp. 2875–83, Dec. 2004.

[143] A. Clow, P. Gaynor, and B. Oback, “Coplanar film electrodes facilitate bovine nuclear transfer cloning.,” *Biomed. Microdevices*, vol. 11, no. 4, pp. 851–9, Aug. 2009.

[144] M. Hagiwara, T. Kawahara, Y. Yamanishi, and F. Arai, “Driving method of microtool by horizontally arranged permanent magnets for single cell manipulation,” *Appl. Phys. Lett.*, vol. 97, no. 1, p. 013701, 2010.

[145] M. Hagiwara, T. Kawahara, L. Feng, Y. Yamanishi, and F. Arai, “On-chip dual-arm microrobot driven by permanent magnets for high speed cell enucleation,” *2011 IEEE 24th Int. Conf. Micro Electro Mech. Syst.*, pp. 189–192, 2011.

[146] T. Kawahara, T. Hirano, L. Feng, H. Uvet, M. Hagiwara, Y. Yamanishi, F. Arai, and F. Lin, “High-speed single cell dispensing system,” in *Micro-NanoMechatronics and Human Science (MHS), 2011 International Symposium on*, 2011, pp. 472–474.

[147] J. Lassen, M. Gjerris, and P. Sandøe, “After Dolly--ethical limits to the use of biotechnology on farm animals.,” *Theriogenology*, vol. 65, no. 5, pp. 992–1004, 2006.

[148] J. L. Edwards, F. N. Schrick, M. D. McCracken, S. R. van Amstel, F. M. Hopkins, M. G. Welborn, and C. J. Davies, “Cloning adult farm animals: a review of the possibilities and problems associated with somatic cell nuclear transfer.,” *Am. J. Reprod. Immunol.*, vol. 50, no. 2, pp. 113–123, 2003.

[149] D. K. Vanderwall, G. L. Woods, K. I. Aston, T. D. Bunch, G. Li, L. N. Meerdo, and K. L. White, “Cloned horse pregnancies produced using adult cumulus cells.,” *Reprod. Fertil. Dev.*, vol. 16, no. 7, pp. 675–679, 2004.

[150] R. D. Schramm and A. M. Paprocki, “Strategies for the production of genetically identical monkeys by embryo splitting.,” *Reprod. Biol. Endocrinol.*, vol. 2, p. 38, 2004.

[151] T. T. Peura, I. M. Lewis, and A. O. Trounson, “The effect of recipient oocyte volume on nuclear transfer in cattle.,” *Mol. Reprod. Dev.*, vol. 50, no. 2, pp. 185–191, 1998.

[152] H.-L. Wang, Z.-L. Chang, K.-L. Li, H.-Y. Lian, D. Han, W. Cui, G.-Z. Jiao, Y.-G. Wu, M.-J. Luo, and J.-H. Tan, “Caffeine can be used for oocyte enucleation.,” *Cell. Reprogram.*, vol. 13, no. 3, pp. 225–232, 2011.

[153] A. Ichikawa, T. Tanikawa, S. Akagi, and K. Ohba, “Automatic Cell Cutting by High-Precision Microfluidic Control,” pp. 13–18, 2010.

[154] N. Costa-Borges, M. T. Paramio, G. Calderón, J. Santaló, and E. Ibáñez, “Antimitotic treatments for chemically assisted oocyte enucleation in nuclear transfer procedures.,” *Cloning Stem Cells*, vol. 11, no. 1, pp. 153–166, 2009.

[155] J. Atencia and D. J. Beebe, “Magnetically-driven biomimetic micro pumping using vortices.,” *Lab Chip*, vol. 4, no. 6, pp. 598–602, 2004.

[156] J. BIBETTE, M. FERMIGIER, R. DREYFUS, M. ROPER, H. A. STONE, and J. BAUDRY, “On the dynamics of magnetically driven elastic filaments,” *Journal of Fluid Mechanics*, vol. 554, no. -1. p. 167, 2006.

[157] L. Gao, N. J. Gottron, L. N. Virgin, and B. B. Yellen, “The synchronization of superparamagnetic beads driven by a micro-magnetic ratchet.,” *Lab Chip*, vol. 10, no. 16, pp. 2108–2114, 2010.

[158] M. Hagiwara and T. Kawahara, “Precise Control of Magnetically Driven Microtools for Enucleation of Oocytes in a Microfluidic Chip,” no. July, pp. 37–41, 2012.

[159] B. Ahn, E. P. Furlani, K. W. Oh, and K. Lee, “Design of pressure-driven microfluidic networks using electric circuit analogy,” *Lab Chip*, vol. 12, no. 3, p. 515, Feb. 2012.

[160] J. Pfitzner, “Poiseuille and his law.,” *Anaesthesia*, vol. 31, no. 2, pp. 273–275, 1976.

[161] R. J. Cornish, “Flow in a pipe of rectangular cross-section,” in *Proceedings of the Royal Society of London. Series A 120.786*, 1928, pp. 691–700.

[162] S. Hua, H. Zhang, J. M. Su, T. Zhang, F. S. Quan, J. Liu, Y. S. Wang, and Y. Zhang, “Effects of the removal of cytoplasm on the development of early cloned bovine embryos.,” *Anim. Reprod. Sci.*, vol. 126, no. 1–2, pp. 37–44, 2011.

[163] B. Alberts, A. Johnson, J. Lewis, M. Raff, K. Roberts, and P. Walter, “DNA and Chromosomes,” in *Molecular Biology of the Cell, 4th ed*, 2002, pp. 191–234.

[164] A. Ichikawa, S. Sakuma, T. Shoda, F. Arai, and S. Akagi, “ON-CHIP ENUCLEATION OF OOCYTE USING UNTETHERD MICRO-ROBOT WITH GRIPPING MECHANISM,” in *Micro-Nano Mechatronics and Human Science*, 2013, pp. 323–325.

[165] B. G. Tatham, “Enucleation by centrifugation of in vitro-matured bovine oocytes for use in nuclear transfer,” *Biol. Reprod.*, vol. 53, no. 5, pp. 1088–1094, Nov. 1995.

[166] T. Lindmo, D. C. Peters, and R. G. Sweet, *Flow Cytometry and Sorting, 2nd ed*, Wiley-Liss. New York, 1990.

[167] J. F. Dijksman and A. Pierik, “Fluid dynamical analysis of the distribution of ink jet printed biomolecules in microarray substrates for genotyping applications.,” *Biomicrofluidics*, vol. 2, no. 4, p. 44101, Jan. 2008.

[168] H. Tavana and S. Takayama, “Aqueous biphasic microprinting approach to tissue engineering.,” *Biomicrofluidics*, vol. 5, no. 1, p. 13404, Jan. 2011.

[169] T. Kim, I. Doh, and Y.-H. Cho, “On-chip three-dimensional tumor spheroid formation and pump-less perfusion culture using gravity-driven cell aggregation and balanced droplet dispensing.,” *Biomicrofluidics*, vol. 6, no. 3, p. 34107, Sep. 2012.

[170] E. . Roth, T. Xu, M. Das, C. Gregory, J. . Hickman, and T. Boland, “Inkjet printing for high-throughput cell patterning,” *Biomaterials*, vol. 25, no. 17, pp. 3707–3715, 2004.

[171] P. Calvert, “Materials science. Printing cells.,” *Science*, vol. 318, no. 5848, pp. 208–9, Oct. 2007.

[172] H. Uvet, L. Feng, S. Ohashi, M. Hagiwara, T. Kawahara, Y. Yamanishi, and F. Arai, “On-Chip Single Particle Loading and Dispensing,” in *International Conference on Robotics and Automation*, 2011, pp. 3151–3156.

[173] A. Yusof, H. Keegan, C. D. Spillane, O. M. Sheils, C. M. Martin, J. J. O’Leary, R. Zengerle, and P. Koltay, “Inkjet-like printing of single-cells.,” *Lab Chip*, vol. 11, no. 14, pp. 2447–54, Jul. 2011.

[174] R. Tornay, V. Chapuis, V. Haguet, F. Chatelain, and P. Renaud, “Electrical Detection and Ejection of Beads in a One-Cell-Per-Drop Microdispenser,” in *TRANSDUCERS 2007 - 2007 International Solid-State Sensors, Actuators and Microsystems Conference*, 2007, pp. 695–698.

[175] J. L. Drobish and L. E. Taske, “Flexible container including self-sealing dispensing valve to provide automatic shut-off and leak resistant inverted storage,” No 4,728,0061988.

[176] M. R. Emmert-Buck, R. F. Bonner, P. D. Smith, R. F. Chuaqui, Z. Zhuang, S. R. Goldstein, R. A. Weiss, and L. A. Liotta, “Laser Capture Microdissection,” *Science (80-.).*, vol. 274, no. 5289, pp. 998–1001, Nov. 1996.

[177] T. Kawahara, S. Ohashi, M. Hagiwara, Y. Yamanishi, and F. Arai, “Air-Flow-Based Single-Cell Dispensing System,” *Adv. Robot.*, vol. 26, no. 3–4, pp. 291–306, Jan. 2012.

[178] L. Feng, T. Kawahara, Y. Yamanishi, M. Hagiwara, K. Kosuge, and F. Arai, “Size Controlled and On-Demand Production of Droplets by Magnetically Driven Microtool,” *J. Robot. Mechatronics*, vol. 24, no. 1, pp. 133–140, 2012.

[179] J. Z. Chen, A. A. Darhuber, S. M. Troian, and S. Wagner, “Capacitive sensing of droplets for microfluidic devices based on thermocapillary actuation.,” *Lab Chip*, vol. 4, no. 5, pp. 473–80, Oct. 2004.

[180] R. M. Hochmuth, “Micropipette aspiration of living cells,” *J. Biomech.*, vol. 33, no. 1, pp. 15–22, 2000.

[181] Y. Murayama, J. Mizuno, H. Kamakura, Y. Fueta, H. Nakamura, K. Akaishi, K. Anzai, A. Watanabe, H. Inui, and S. Omata, “Mouse zona pellucida dynamically changes its elasticity during oocyte maturation, fertilization and early embryo development.,” *Hum. Cell*, vol. 19, no. 4, pp. 119–25, Nov. 2006.

[182] V. Zakhartchenko, “Karyoplast ‐ cytoplast volume ratio in bovine nuclear transfer embryos: Effect on developmental potential,” ... *Dev.*, vol. 338, no. February, pp. 332–338, 1997.

[183] M. Johnson, “Manipulating the mouse embryo: A laboratory manual,” *Trends in Genetics*, vol. 2. p. 298, 1986.

[184] S. Bayoudh, T. A. Nieminen, N. R. Heckenberg, and H. Rubinsztein-dunlop, “Orientation of biological cells using plane-polarized gaussian beam optical tweezers,” *J. Mod. Opt.*, vol. 50, no. 10, pp. 1581–1590, Jul. 2003.

[185] Y. Liu and M. Yu, “Investigation of inclined dual-fiber optical tweezers for 3D manipulation and force sensing.,” *Opt. Express*, vol. 17, no. 16, pp. 13624–13638, 2009.

[186] S. Sato, M. Ishigure, and H. Inaba, “Optical trapping and rotational manipulation of microscopic particles and biological cells using higher-order mode Nd:YAG laser beams,” *Electronics Letters*, vol. 27, no. 20. p. 1831, 1991.

[187] M. Ichikawa, K. Kubo, K. Yoshikawa, and Y. Kimura, “Tilt control in optical tweezers.,” *J. Biomed. Opt.*, vol. 13, no. 1, p. 010503, Jan. 2008.

[188] Y.-L. Liang, Y.-P. Huang, Y.-S. Lu, M. T. Hou, and J. A. Yeh, “Cell rotation using optoelectronic tweezers.,” *Biomicrofluidics*, vol. 4, no. 4, p. 43003, 2010.

[189] J. P. J. Park, S.-H. J. S.-H. Jung, Y.-H. K. Y.-H. Kim, B. K. B. Kim, S.-K. L. S.-K. Lee, B. J. B. Ju, and K.-I. L. K.-I. Lee, “An integrated bio cell processor for single embryo cell manipulation,” *2004 IEEE/RSJ Int. Conf. Intell. Robot. Syst. (IEEE Cat. No.04CH37566)*, vol. 1, 2004.

[190] R. Kunikata, Y. Takahashi, M. Koide, T. Itayama, T. Yasukawa, H. Shiku, and T. Matsue, “Three dimensional microelectrode array device integrating multi-channel microfluidics to realize manipulation and characterization of enzyme-immobilized polystyrene beads,” *Sensors Actuators B Chem.*, vol. 141, no. 1, pp. 256–262, 2009.

[191] M. Nishioka, S. Katsura, K. Hirano, and A. Mizuno, “Evaluation of cell characteristics by step-wise orientational rotation using optoelectrostatic micromanipulation,” *IEEE Trans. Ind. Appl.*, vol. 33, no. 5, 1997.

[192] D. S. Gray, J. L. Tan, J. Voldman, and C. S. Chen, “Dielectrophoretic registration of living cells to a microelectrode array,” *Biosens. Bioelectron.*, vol. 19, no. 12, pp. 1765–1774, Jul. 2004.

[193] L. Feng, Y. Sun, C. Ohsumi, and F. Arai, “Accurate dispensing system for single oocytes using air ejection,” *Biomicrofluidics*, vol. 7, no. 5, p. 054113, Oct. 2013.

[194] C. Leung, Z. Lu, X. Zhang, and Y. Sun, “Three-Dimensional Rotation of Mouse Embryos,” *... , IEEE Trans.*, vol. 59, no. 4, pp. 1049–1056, 2012.

[195] L. Feng, M. Hagiwara, A. Ichikawa, and F. Arai, “On-Chip Enucleation of Bovine Oocytes using Microrobot-Assisted Flow-Speed Control,” *Micromachines*, vol. 4, no. 2, pp. 272–285, 2013.

[196] M. Hagiwara, T. Kawahara, and F. Arai, “Local streamline generation by mechanical oscillation in a microfluidic chip for noncontact cell manipulations,” *Appl. Phys. Lett.*, vol. 101, no. 7, p. 074102, 2012.

[197] E. Teidelt, J. Starcevic, and V. L. Popov, “Influence of Ultrasonic Oscillation on Static and Sliding Friction,” *Tribol. Lett.*, vol. 48, no. 1, pp. 51–62, Mar. 2012.

[198] H. Storck, W. Littmann, J. Wallaschek, and M. Mracek, “The effect of friction reduction in presence of ultrasonic vibrations and its relevance to travelling wave ultrasonic motors.,” *Ultrasonics*, vol. 40, no. 1–8, pp. 379–83, May 2002.

[199] K.-F. Bohringer, K. Goldberg, M. Cohn, R. Howe, and A. Pisano, “Parallel microassembly with electrostatic force fields,” in *Proceedings. 1998 IEEE International Conference on Robotics and Automation (Cat. No.98CH36146)*, 1998, vol. 2, pp. 1204–1211.

Accomplishments

I. Journal Articles

[1] Y. Yamanishi, ***L. Feng***, and F. Arai, "On-demand Production of Emulsion Droplets Over a Wide Range of Sizes," *Adv. Robot.*, vol. 24, no. 14, pp. 2005–2018, Jan. 2010.

[2] M. Hagiwara, T. Kawahara, Y. Yamanishi, T. Masuda, ***L. Feng***, and F. Arai, "On-chip magnetically actuated robot with ultrasonic vibration for single cell manipulations.," *Lab Chip*, vol. 11, no. 12, pp. 2049–2054, 2011.

[3] ***L. Feng***, T. Kawahara, Y. Yamanishi, M. Hagiwara, K. Kosuge, and F. Arai, "Size Controlled and On-Demand Production of Droplets by Magnetically Driven Microtool," *J. Robot. Mechatronics*, vol. 24, no. 1, pp. 133–140, 2012.

[4] ***L. Feng***, M. Hagiwara, A. Ichikawa, and F. Arai, "On-Chip Enucleation of Bovine Oocytes using Microrobot-Assisted Flow-Speed Control," *Micromachines*, vol. 4, no. 2, pp. 272–285, 2013.

[5] ***L. Feng***, Y. Sun, C. Ohsumi, and F. Arai, "Accurate dispensing system for single oocytes using air ejection," *Biomicrofluidics*, vol. 7, no. 5, p. 054113, Oct. 2013.

II. International Conferences Papers

[1] ***L. Feng***, Y. Yamanishi, and F. Arai, "On-demand generation of droplet in size over a wide range by microfluidic control," in 2009 International Symposium on Micro-Nano Mechatronics and Human Science, 2009, pp. 139–144.

[2] Y. Yamanishi, ***L. Feng***, and F. Arai, "On-demand and Size-controlled Production of emulsion droplets by magnetically driven microtool," Robot. Autom. (ICRA), 2010 IEEE Int. Conf., pp. 4094–4099, 2010.

[3] ***L. Feng***, T. Kawahara, Y. Yamanishi, M. Hagiwara, and F. Arai, "On-chip production of droplets with on-demand and size control," in International Conference on Advanced Mechatronics, 2010, pp. 367–372.

[4] M. Hagiwara, T. Shiori, M. Niimi, T. Kawahara, Y. Yamanishi, ***L. Feng***, and F. Arai, "On-chip Particle Sorting into Multiple Channels by Magnetically Driven Microtools," in International Conference on Advanced Mechatronics, 2010, pp. 373–378.

[5] M. Hagiwara, T. Kawahara, ***L. Feng***, Y. Yamanishi, and F. Arai, "High Precision Magnetically Driven Microtools with Ultrasonic Vibration for Enucleation of Oocytes," in International Symposium on Micro-Nano Mechatronics and Human Science, 2010, pp. 47–52.

[6] M. Hagiwara, T. Kawahara, ***L. Feng***, Y. Yamanishi, and F. Arai, "On-chip dual-arm microrobot driven by permanent magnets for high speed cell enucleation," 2011 IEEE 24th Int. Conf. Micro Electro Mech. Syst., pp. 189–192, 2011.

[7] H. Uvet, ***L. Feng***, S. Ohashi, M. Hagiwara, T. Kawahara, Y. Yamanishi, and F. Arai, "On-Chip Single Particle Loading and Dispensing," in International Conference on Robotics and Automation, 2011, pp. 3151–3156.

[8] M. Hagiwara, T. Kawahara, ***L. Feng***, Y. Yamanishi, and F. Arai, "High performance magnetically driven microtools with ultrasonic vibration for biomedical innovations," 2011 IEEE Int. Conf. Robot. Autom., pp. 3453–3454, 2011.

[9] M. Hagiwara, T. Kawahara, ***L. Feng***, Y. Yamanishi, and F. Arai, "On-chip Enucleation of Oocyte by Magnetically Driven Microtools with Ultrasonic Vibration," in International Conference on Robotics and Automation, 2011, pp. 2680–2685.

[10] T. Kawahara, T. Hirano, ***L. Feng***, H. Uvet, M. Hagiwara, Y. Yamanishi, F. Arai, and F. Lin, "High-speed single cell dispensing system," in Micro-NanoMechatronics and Human Science (MHS), 2011 International Symposium on, 2011, pp. 472–474.

[11] ***L. Feng***, U. Huseyin, T. Kawahara, M. Hagiwara, Y. Yamanishi, and F. Arai, "On-Chip High-Speed and On-Demand Single Microbeads Loading," in International Symposium On Micro-Nano Mechatronics and Human Science, 2011, pp. 472–474.

[12]***L. Feng***, M. Hagiwara, H. Uvet, Y. Yamanish, T. Kawahara, K. Kosuge, and F. Arai, "High-speed delivery of microbeads in microchannel using magnetically driven microtool," 2011 16th Int. Solid-State Sensors, Actuators Microsystems Conf., pp. 1312–1315, 2011.

[13]***L. Feng***, M. Hagiwara, A. Ichikawa, and F. Arai, "Continuous Enucleation of Bovine Oocyte by Microrobot with Local Flow Distribution Control," in International Conference on Manipulation, Manufacturing and Measurement on the Nanoscale, 2012, pp. 944–949.

[14]***L. Feng***, M. Hagiwara, A. Ichikawa, T. Kawahara, and F. Arai, "Smooth Enucleation of Bovine Oocyte by Microrobot with Local Flow Speed Control in Microchannel," in International Conference on Intelligent Robots and Systems, 2012, pp. 944–949.

[15]***L. Feng***, M. Hagiwara, A. Ichikawa, and F. Arai, "On-chip continuous enucleation by hydraulic force control using magnetically actuated microrobot," in International Conference on Miniaturized Systems for Chemistry and Life Sciences, 2012, pp. 1270–1273.

[16]***L. Feng***, M. Hagiwara, Y. Sun, A. Ichikawa, and F. Arai, "High-speed Production and Dispensing of Enucleated Oocyte by Microrobot on a Chip," in International Symposium On Micro-Nano Mechatronics and Human Science, 2012, pp. 111–115.

III. Domestic Conference Papers

[1] ***L. Feng***, Y. Yamanishi, T. Kawahara, M. Hagiwara, K. Kosuge, and F. Arai, "Robot-on-a-chip Part 1: On-chip Generation of Droplets and Size Control," in 日本機械学会ロボティクス・メカトロニクス講演会, 2010, pp. 1P1–U04.

[2] 萩原将也, 川原知洋, ***馮林***, 山西陽子, and 新井史人, "双腕マイクロアームの高精度な非接触操作," in *第 22 回化学とマイクロ・ナノシステム研究会*, 2010, p. P.26.

[3] 萩原将也, 川原知洋, ***馮林***, 山西陽子, and 新井史人, "マイクロ流体チップ内で超高速動作する双腕マイクロロボットによる細胞操作・切断," in *第 28 回日本ロボット学会学術講演会*, 2010, pp. 2M2–7.

[4] ***L. Feng***, Y. Yamanishi, T. Kawahara, M. Hagiwara, K. Kosuge, and F. Arai, "Generation of Droplet with Feedback Control on a Chip," in *第 22 回化学とマイクロ・ナノシステム研究会*, 2010, p. P.25.

[5] ***L. Feng***, Y. Yamanishi, T. Kawahara, M. Hagiwara, K. Kosuge, and F. Arai, "On-chip Size-controllable Droplet Generation," in *第 11 回 計測自動制御学会 システムインテグレーション部門講演会*, 2011, pp. 3I2–3.

[6] ***L. Feng***, Y. Yamanishi, T. Kawahara, M. Hagiwara, K. Kosuge, and F. Arai, "On-chip Smooth Enucleation by Hydraulic Force Control Using Magnetically Driven Microtool," in ロボティクス・メカトロニクス講演会, 2012, pp. 1P1–U04.

[7] 平野 達彦, 川原 知洋, ウベット フセイン, ***馮林***, 新井 史人, “ローディング機構を有する単一細胞分注システム” in *第 12 回 計測自動制御学会 システムインテグレーション部門講演会*, 2012, pp. 1P1–U04.

IV. Patent

日本国特許出願 2012-120056, 細胞操作装置 新井史人, 市川明彦, 馮林, 萩原将也, （2012 年 5 月 25 日出願）.

V. Awards

[1] 2009-11 IEEE International Symposium on Micro-Nano Mechatronics and Human Science 2009, Best Paper Award, On-demand generation of droplet in size over a wide range by microfluidic control, Lin Feng, Yoko Yamanishi, and Fumihito Arai.

[2] 2010-05 IEEE International Conference on Advanced Mechatronics 2010, Young Fellow Prize,日本機械学会若手優秀講演フェロー賞,平成23年5月27日, On-chip production of droplets with on-demand and size control, Lin Feng, Yoko Yamanishi, Tomohiro Kawahara, Masaya Hagiwara, Kazuhiro Kosuge, and Fumihito Arai.

[3] 2011-05 IEEE International Conference on Robotics and Automation(ICRA2011), 2011, Best Video Award, May 12, 2011, High Performance Magnetically Driven Microtools with Ultrasonic Vibration for Biomedical Innovations, Masaya Hagiwara, Tomohiro Kawahara, Lin Feng, Yoko Yamanishi, and Fumihito Arai.

[4] 2011-11 IEEE International Symposium on Micro-Nano Mechatronics and Human Science 2011, Best Paper Award, High Precision Magnetically Driven Microtools with Ultrasonic Vibration for Enucleation of Oocytes, Masaya Hagiwara, Tomohiro Kawahara, Lin Feng, Yoko Yamanishi, and Fumihito Arai.